# *IN VITRO* ELECTROPHYSIOLOGIC HOST-GRAFT MODEL FOR CARDIAC STEM CELL INTEGRATION

A DISSERTATION
SUBMITTED TO THE DEPARTMENT OF BIOENGINEERING
AND THE COMMITTEE ON GRADUATE STUDIES
OF STANFORD UNIVERSITY
IN PARTIAL FULFILLMENT OF THE REQUIREMENTS
FOR THE DEGREE OF
DOCTOR OF PHILOSOPHY

Michael Quay Chen

July 2010



This dissertation is online at: http://purl.stanford.edu/vw263cv9191

I certify that I have read this dissertation and that, in my opinion, it is fully adequate in scope and quality as a dissertation for the degree of Doctor of Philosophy.

**Gregory Kovacs, Primary Adviser**

I certify that I have read this dissertation and that, in my opinion, it is fully adequate in scope and quality as a dissertation for the degree of Doctor of Philosophy.

**Christina Smolke**

I certify that I have read this dissertation and that, in my opinion, it is fully adequate in scope and quality as a dissertation for the degree of Doctor of Philosophy.

**Joseph Wu**

Approved for the Stanford University Committee on Graduate Studies.

**Patricia J. Gumport, Vice Provost Graduate Education**

*This signature page was generated electronically upon submission of this dissertation in electronic format. An original signed hard copy of the signature page is on file in University Archives.*

# Abstract

The limited ability of the human heart to regenerate has made myocardial infarction and heart failure debilitating conditions. Recently, an approach using pluri- or multi-potent stem cells to repair damaged heart tissue is being explored for its potential to regenerate tissue as a tailored, patient-specific treatment. However, the mechanisms of integration remain unclear, and many cardiac grafting procedures utilizing both embryonic and adult stem cells have been met with limited success. While current evidence suggests that grafts are likely viable in host myocardium, clinical studies have reported pro-arrhythmic side-effects following transplantation, which arise from disrupted propagation patterns. These issues may be attributed to grafts lacking cardiac differentiation, or possessing conduction properties inconsistent with the host tissue. Consequently, understanding the role of the electrical environment throughout the engraftment process is necessary, but infeasible due to a lack of proper tools. Elucidating the electrical aspects of stem cell transplantation aims to ensure proper integration of the transplanted cells to prevent aberrant electrical pathways in the heart.

In this work, a set of *in vitro* tools were developed to study the potential mechanisms underlying the risk of arrhythmia following stem cell transplantation. A planar microelectrode array was first used to investigate the possibility of conduction block if undifferentiated or non-cardiomyocyte stem cells, such as mesenchymal stem cells, are used as grafts. Conduction in murine cardiomyocytes was purposely blocked by co-culture with non-conducting murine fibroblasts, and a novel mathematical transform known as a co-occurrence matrix was developed to quantitatively analyze the uniformity of conduction. The observed sensitivity of cardiomyocyte conduction illustrated the risk of grafting non-cardiomyocyte cell types despite any potential of differentiating into muscle-like cells.

Unlike non-conducting fibroblasts, stem cell grafts are expected to electrically conduct if proper cardiac differentiation takes place. However, possible differences in the conduction properties of these grafts may still lead to arrhythmia. To perform a

controlled study of such conduction mismatch, an *in vitro* co-culture system coupled to microelectrode arrays was developed. Spatially separated cultures representing the host and the graft were allowed to gradually merge above the microelectrode array, allowing the measurement of conduction throughout the integration process. Modeled host and graft cell populations were evaluated by analyzing the co-occurrence matrix and conduction velocity for the quality and speed of conduction over time. Co-cultures between murine cardiomyocytes (host) and murine skeletal myoblasts (graft) exhibited significant differences in conduction despite synchronous electrical activity. In contrast, conduction was well matched when the same host cells were co-cultured with murine embryonic stem cells (mESC).

A model using murine cardiomyocytes (host) and differentiating human embryonic stem cells (graft) allowed the characterization of conduction properties relevant to current trans-species animal models, and demonstrate the co-culture device as a screening platform for candidate graft cells. The limited region of the graft that supported conduction exhibited differences in the co-occurrence matrix as well as conduction velocity when compared to the host region. In an effort to improve the effects of conduction mismatch, both host and graft cell populations were electrically paced over the length of time the cultures remained viable (4-5 days). Although a difference between conduction velocities between host and graft was still observed, the overall uniformity of conduction improved in paced co-cultures, implying increased cardiac differentiation.

A preliminary study of genomic changes due to paced mESCs resulted in a significant upregulation of several important cardiac genes and a significant downregulation of many embryonic genes. Further efforts are currently underway to examine gene expression with paced hESCs to optimize integration in the host-graft model, and ultimately to understand how the electrical environment influences stem cell transplantation.

To my future wife, Linda Hue.

You are the love of my life, and I cannot imagine a day without you.

# Acknowledgements

The work contained in this dissertation could not be possible without the financial help of the California Institute for Regenerative Medicine (CIRM) under contract RS1-00232-1, and by the National Science Foundation Graduate Research Fellowship.

I have many, many people to thank for all the guidance and support I have received. The period of time spent in graduate school has been nothing short of incredible, and I never been so immersed in such high quality training for dealing with scientific issues and tackling problems in engineering. I owe my greatest gratitude to my primary research advisor, Gregory Kovacs, who has not only taught me how to reach for incredibly high standards, but also how to achieve them. In addition to normal graduate level mentorship, Greg has consistently gone above and beyond to teach me about life, family values, and of course, having fun. There are few advisors that are willing to open up their homes to their students like Greg has, and I have probably learned some my most valuable lessons from him during times I've spend with his family. Despite how busy he always is and the fact that he's been away from Stanford during most of my graduate career, I always know that he will do anything for his students, and for that he will always have my greatest thanks.

Because Greg has been away from Stanford for the past three years, I couldn't possibly have achieved anything in the lab if not for our "Captain," Laurent Giovangrandi. Laurent has worked tirelessly to keep our group moving in Greg's absence, and without his support and endless patience, I would never have survived. In addition to all of his amazing technical guidance, he has taught me how to drink espressos like it is water, to use silverware rather than wasteful plastic forks, and to humbly accept that I will never beat him in an uphill bike climb.

I would like to especially thank the other members of my reading committee, Joseph Wu and Christina Smolke, and the member of my oral defense committee Ellen Kuhl and Brian Kobilka. Joseph Wu and his group was one of my primary collaborators in this work, and the truth is that none of this would be possible without

their guidance and support. Joe has been a valuable source of wisdom in the stem cell field, and I am honored to have had the chance to learn from him.

Within Joseph Wu's lab, I have had the privilege of working with several post-doctoral scholars and graduate students, and I have nothing but respect for their talents. Xiaoyan (Esther) Xie, Jin Yu, Ning Sun and Kitchener Wilson were all essential in providing me with various cell types, and in analyzing data. Culturing any cells, let alone human embryonic stem cells, is an enormously challenging task. In order to enable the research performed in this work, our personal schedules were strictly tied to that of the cells, and I am very grateful for their efforts in standing with me and making success possible.

I want to especially thank Reza Ardehali for his help during the last couple years. Reza has spent an incredible amount of time providing guidance and resources to further our knowledge in stem cell therapy. In a new collaboration with him and the Weissman Lab, the work presented here is quickly taking on new dimensions. Exciting times are definitely ahead, and I look forward to our future interactions.

Another project in collaboration with Peter Day of the Kobilka Lab taught me a great deal about cardiovascular physiology. I am constantly inspired by the depth of his knowledge, and the enthusiasm he has for science.

When I had first arrived in the Kovacs Lab, I barely knew how to strip wire or build a circuit. I had the privilege of being directly mentored by Hollis Whittington, who took a naïve graduate student, and "showed me the ropes" of actually performing experiments using very complex protocols. He deserves a lot of credit for teaching me the practical side of research, and I am still in awe today of his brilliance and forethought in his methods. Many of the devices and protocols in this lab still bear his marks. Admittedly, the thing I use the most that he left behind is the music system in our Biology Lab.

The people in the Kovacs Lab make up an extraordinary group. Omer Inan had been a constant source of encouragement through the PhD process. He never hesitated to offer up some kind words when things were taking a downward turn, and always had some great advice for how to make progress. I learned a lot about what Greg

expects from his students by watching Omer excel. Unfortunately, it also meant that he was constantly setting the bar high for the rest of us. Mozzi Etemadi is by far the most emotionally intense person I know. It would take several cups of coffee to keep up with his pace, but in the end it was always great because his brilliance meant we got things done. We have enjoyed more than a few laughs, and I will certainly miss our times together. Richard Wiard was my go-to guy whenever the rest of the electrical engineers in the lab made fun of us bioengineers. His work ethic is enough to anyone to shame, as he works a full time job while going through his PhD work. Mikael Evander only joined our group a year ago, but I already feel like he has long been part of the family. His enthusiasm for everything in and out of the lab has helped being a lot of balance to my own life. I am actually very grateful that he puts up with my constant complains about graduate school, and often drags me out of the lab for coffee or a round of golf. Keya Pandia has taught me that it is actually possible to live a healthy life as a vegetarian. When we're not discussing the pros and cons to eating meat, Keya and I often wonder why we ever wanted to go graduate school in the first place. Somehow our conclusions are always the same, and we go back to work with renewed energy and motivation. I am very thankful for our seemingly trivial chats, because without them I might have quit a long time ago. Similarly, my discussion with David Burns never ended on a down beat. His endless knowledge and wise perspective have been extremely beneficial. There are so many others in the Kovacs Lab, both past and present, which I would like to thank for their advice, encouragement, and friendship: Shilpi Roy, Burak Dura, Janice Li, Amy Droitcour, Gaylin Yee, Matthew Hills, Joy Ku, and John Meador. Our amazing secretaries Sandy Plewa in the beginning and Claire Nicholas during my final years were essential to all operations in the lab. I cannot emphasize enough how important their efforts have been. Unlike much of my own research, they have never failed to make sure everything runs smoothly and efficiently.

Somehow, my friends and family were able to put up with me and my excuses for missing so many exchanges because I had to do "research." I wish to thank them all for their understanding and support during an incredibly stressful (yet rewarding)

period of my life. My mother and sister, Hannah and Sophia, have never once discouraged my efforts. Instead, their constant love and support have enabled me to always do my best here at Stanford. I have had the special advantage of being close to our home in Fremont, and I must admit that the many home cooked meals were essential to writing good thesis chapters. Sadly, my father, John, and grandfather, Kwong Yen, both passed away without seeing me achieve this degree. Their sacrifices in raising me and teaching me about life have made me much of what I am today. This PhD is theirs as much as it is mine.

Finally, I have the impossible task to properly thank my future wife in a finite amount of print. Linda Hue has stood with me each step of the way, not simply in proof-reading paper drafts, but more importantly by giving me a reason to be a better person. Achieving a PhD is just the beginning. Through our relationship, she has strengthened my Christian faith, my commitment to family, my profound appreciation for friends, and my pursuit of living a virtuous lifestyle. Words can't express what she means to me.

# Contents

# List of Tables

# List of Figures

# 1 Introduction and Motivation

## 1.1. Stem Cells

Biological systems can be observed from many viewpoints, from the largest ecological preserve all the way down to the smallest organism. From each perspective, the complexities associated with life reveal fascinating characteristics as discoveries are made, but never fail to produce more questions than answers. Even the cell, one of the smallest known independent biological systems, operates in ways that are far from being fully understood. Despite how long cells have been studied, new findings continue to have profound influences on medicine and biology.

Using only a basic microscope, Robert Hook (1635-1702) was the first to describe a cell in his 1665 book *Micrographia*. Its importance was not fully grasped however, until much later when in 1824 Henri Dutrochet (1776-1847) suggested that a single cell may exist as a "physiological unit" capable of making up all living tissues and undergoing some unknown actions to create more cells. While observing plant cells, Barthlemy Dumortier (1797-1878) described cellular reproduction as a process of "binary fission" (cell division) in 1832. This claim was able to refute ideas that new cells arise within old ones, or that they might form spontaneously from non-cellular material [1]. The concept of cell division was groundbreaking because it was one of the first clues toward understanding how multi-cellular organisms develop and regenerate. A breakthrough made much later in the early 1900s claimed that blood cells were not only able to divide, but also able to "differentiate," or transform into types different from their parent cells. In 1963, James Til and Ernest McCulloch further discovered a cell type within murine bone marrow capable of extensively proliferating and transforming into many other types of cells [2]. They called these mysterious cells "stem cells."

Over time, the notion that a single cell may give rise to other cell types inspired the theory that all cells may originate from a single source. As new technologies became available that allowed researchers to examine mammalian development, these original stem cells were found to exist right from the beginning: after a sperm fuses with an egg. The ability for two cells to join together, appropriately divide, and subsequently form a functional body has inevitably raised deep questions. Such cells must be able to respond accurately to a multitude of cues, such as chemical signals, mechanical forces, and electric fields that guide them to their eventual fate.

During differentiation, stem cells generally follow a sequential path over many cell divisions before transforming into a specific, mature cell type. As these cells become more developed, they tend to lose much of their proliferative abilities. By adulthood, most of the remaining stem cells have reached a steady state, and operate primarily to maintain the surrounding tissue. While it is generally accepted that stem cells are also capable of transforming backwards during the development process, it is still unclear whether stem cells are capable of abruptly jumping to a parallel lineage to continue developing.

The inherent potential of stem cells to differentiate into multiple cell types makes them ideal for understanding the origin and design of multicellular organisms. Despite the difficulty in isolating particular types of stem cells, many have now been successfully extracted, most notably the human embryonic stem cell by Thomson, et al. in 1998 [3]. These discoveries have enabled new waves of innovation for virtually any organ system in the body. There is also an elusive promise that stem cells can be used as a therapy to repair tissue damage, and even extend organismal life beyond that of component cells once differentiation and integration mechanisms are fully understood.

## 1.2. Cardiac Regeneration Therapies

Adult stem cells residing in organs vary widely in their ability to proliferate and differentiate. Some organs contain stem cells that are undisputedly, and frequently, active. Hematopoietic stem cells, for example, actively replenishes blood

cells every day [4]. On the other hand, the limited regenerative capacity of the heart prompts questions about whether or not cardiac stem cells continue to exist in adults.

Heart failure affects an estimated 5 million people in the United States and is growing at a rate of 550,000 new cases each year [5,6]. Remodeling processes ultimately cumulate in the formation of non-contractile fibrous scars that do little to contribute, and often impede, normal heart function [7]. Without a viable alternative, current therapeutic modalities for heart failure rely initially on pharmaceutical agents to aid cardiac function. If this is unable to help, medical devices such as mechanical ventricular assist devices are implanted as a second line of defense, especially during late-stage heart failure. Although such devices have had phenomenal success in giving patients a reasonable quality of life, they still require a clinically invasive procedure, and provide only a portion of the total output of a fully functional heart. Alternatively, cardiac transplantation techniques are available that can address these issues. However, transplant treatments are severely restricted due to the limited availability of donor organs, complications in immunosuppressive therapy, and the long-term failure of grafted organs [8].

The ability to repair and regenerate ischemic or damaged myocardium remains a challenging task. New approaches have been divided between transplanting exogenous cells into a damaged region and finding mechanisms to enable endogenous cardiomyocytes to re-enter the cell cycle and repair damaged tissue [9]. While both approaches are being actively researched, most of the current advances are in transplanting exogenous cells through a process called cellular cardiomyoplasty (CCM) [10]. The goal of a CCM procedure is to ultimately regenerate cardiomoyctes and support angiogenesis. However, it is still unclear what the optimal graft cell type should be, and what pre-conditioning is required, if any, to ensure proper integration into host myocardium. Experimental approaches have utilized a number of different cell types, including skeletal myoblasts [11], embryonic stem cells [12], bone marrow derived mesenchymal stem cells [13], enriched hematopoietic stem cells [14], and blood and bone marrow-derived endothelial progenitor cells [15]. The use of many non-cardiomyocyte cell types remains controversial, but such cells offer advantages

such as autologous origins, the potential of muscle-like differentiation, and possible ischemic resistance [11]. While stem cell transplantation have resulted various forms of functional improvement in human and animal subjects, the *in vivo* roles of transplanted cells in the myocardium remain unclear. The resulting functional improvement claimed from these studies may not necessarily correlate with the level of integration between a stem cell graft and host myocardium. Currently, the primary proof of integration is to demonstrate the presence of mechanical and electrical coupling proteins between graft and host tissue. Unfortunately, this is limited to a molecular scale and does not consider the level of participation from graft cells during each cardiac contraction cycle. Without this understanding, transplantation of exogenous cells may actually put an already damaged heart at greater risk by creating aberrant electrical pathways.

## 1.3. Electrical Conduction in the Heart

The complex functions of the heart are ultimately aimed towards pumping oxygenated blood throughout the body. Each mechanical contraction is initiated by an electrical signal that propagates throughout the myocardium in a very specific pattern. Electrical impulses are generated spontaneously in the sinoatrial nodal region of the heart. As the electrical signal reaches each cardiac cell, the cell responds by releasing a large store of calcium ions into the muscle fibers, eliciting a contraction. This process of "excitation-contraction coupling" helps form the basis of cardiac function, and highlights the importance of proper electrical rhythm. Unfortunately, disruption of electrical pathways is a very common condition that can be brought about from reentrant circuits, leading to varying degrees of cardiac arrhythmia. Damage from myocardial infarction, for example, often results in scar tissue formation which disturbs normal conduction. Typical methods of treatment include defibrillation of the entire heart through electrical cardioversion [16], radiofrequency ablation to block off re-entrant pathways [17], or pharmaceutical treatment strategies [18].

The electrical properties that allow cardiac tissue to conduct an ionic current from one cell to another are unique and cannot be easily replaced with exogenous grafts. For similar reasons that fibrous scar tissue may disrupt normal rhythm despite forming electrical junctions with native tissue, the introduction of exogenous cells may complicate electrical pathways as well. Even if graft cells are able to differentiate into cardiac cells, the potential mismatch of properties that determine electrical conduction between host and graft cells cannot be ignored. The resulting disturbance of conduction has already been observed in human studies carried out with autologous skeletal myoblasts by Menasche, et al. [19]. In this clinical trial, four out of the ten subjects developed delayed episodes of sustained ventricular tachycardia after transplantation, and required implantation of an internal defibrillator. The implied arrhythmogenic risk involved in stem cell transplantation therefore calls for a greater understanding between the electrical conduction between grafts and host myocardium. However, even if all injected cells were to reach their desired destinations and functionally couple with host tissue, it would be impossible to thoroughly investigate conduction mismatches *in vivo* without highly invasive techniques. As a practical alternative, *in vitro* models can be used to characterize the cellular interactions that take place, and may determine the extent to which transplanted cells can differentiate into functional cardiomoyctes and positively contribute to normal rhythm.

## 1.4. *In vitro* Cell Based Assays for Electrical Characterization

Electrical conduction patterns found in the heart can be modeled *in vitro* using cultured cardiac cells and studied through a number of techniques. One of the most common methods to observe impulse propagation in a cardiac cell culture is through voltage or calcium sensitive fluorescent dyes [20]. Utilizing this procedure does not require specialized equipment beyond an imaging system to capture fluorescent intensities. Moreover, the resolution of the conduction patterns is only limited by the quality of the camera used to capture the fluorescent signal. However, such dyes

exhibit major cytotoxic properties, and therefore cannot be used for any long term electrical monitoring within the same tissue sample [21,22].

An alternative method is to culture cardiomyocytes over a planar array of microelectrodes and measure action potentials extracellularly [23]. Because the electrodes are part of a planar substrate that does not couple directly to a cell as a patch-clamp would, this technique allows for long term analysis of multicellular cultures. One of the main advantages of a microelectrode array is the ability to provide temporal and spatial information simultaneously. By noting the time that an action potential reaches each electrode, the spread of electrical activity from one point to the next can be represented as a vector to illustrate the speed and direction of electrical propagation. A microelectrode array platform can be further built upon by adding stimulation electrodes to induce depolarization [24], or by spatially separating different cell types into regions of interest to probe differential or interactive events [25].

Many cardiomyocyte properties are now understood, but the simultaneous interactions between graft and cardiac host tissue remain uncertain. Chang, et al. [26] used optical methods to examine electrical conduction in mixed co-cultures of rat ventricular myocytes and human mesenchymal stem cells. In one of the first *in vitro* studies to examine the risk of arrhythmia in stem cells transplantation, non-excitable mesenchymal stem cells were found to cause abnormal conduction patterns and predispose cultures to reentrant circuit pathways. Although much can be learned from these studies, they are limited by the fact that each cell type cannot be easily distinguished in the experimental setup, preventing further examination of the causes of reentry.

To create a more spatially defined co-culture environment, various cell types have been cultured together in numerous experimental systems. Utilizing microfabrication techniques, investigators have achieved defined co-cultures by patterning biologically-reactive molecules on the culture surface prior to cell plating. This has allowed for the creation of stripes [27,28], islands [29], and other patterns of tissue for the investigation of cellular interactions or geometrical dependencies.

Although progress has been made revealing multi-cellular processes, patterning methods were permanent and often irreversible for the duration of an experiment. These methods of co-culture also involved a modified surface that may alter cell motility and function.

## 1.5. A Model for Stem Cell Integration

A set of i*n vitro* tools are presented in this work to study the risk of arrhythmia after stem cells have been transplanted into a damaged heart. Applications are described to (1) analyze conduction in heterogeneous cultures, (2) explore the likelihood of mismatch in conduction properties between a cardiomyocyte host and candidate graft cell population, and (3) examine the role of electrical pacing on stem cell differentiation and integration.

Graft cells that have not yet differentiated into cardiomyocytes, or are from a non-cardiomyocyte lineage (such as mesenchymal stem cells), may disrupt the transfer of an electrical signal across the heart. In order to quantitatively assess i*n vitro* propagation patterns, new analysis metrics were developed based on a technique used for texture characterization known as a co-occurrence matrix. This mathematical transform was capable of evaluating murine cardiomyocyte cultures with conduction blocked using increasing proportions of murine fibroblasts. The resulting trends were also verified by analyzing a finite element model of the system. Use of the co-occurrence matrix was able to quantitatively demonstrate the degree of uniformity within electrical propagation patterns.

Assuming that all transplanted cells are able to undergo cardiac differentiation, the ability to pass an electrical signal from the host myocardium still does not ensure that conduction will not be disrupted. A microelectrode array platform was used to model electrical integration between host cardiomyocytes and stem cell grafts through a versatile laser-etched co-culture chamber. This co-culture chamber separated host and graft cells on adjacent sides of a microelectrode array using a physical barrier. The barrier was removed once both cell types had adhered to their respective regions on the surface, allowing them to merge in a controlled manner. Potential mismatches

between each cell population on opposing ends of the microelectrode array were observed by comparing differences in co-occurrence matrices and conduction velocities. Murine skeletal myoblast graft cells were first co-cultured with murine cardiomyocytes to explore possible arrhythmogenic risks in grafting cells outside of the cardiomyocyte lineage. In contrasted, murine embryonic stem cells were co-culturing with murine cardiomyocytes. Finally, a trans-species model was demonstrated with murine cardiomyocytes and human embryonic stem cells. Embryonic stem cells have held much promise for their ability to differentiate into almost any cell type, and their plasticity has been thought to overcome differences in conduction properties by simply matching electrophysiologic characteristics with host tissue. The presented co-culture device was able to model these interactions in a controlled and reproducible manner.

The lack of proper conduction in heterogeneous cultures prompted further efforts to investigate electrical mechanisms of differentiation in pluripotent stem cells within the demonstrated co-culture model. During and after the integration process, transplanted cells must have the capacity to differentiate into a mature cardiac phenotype. While it is known that chemical and mechanical environments can heavily influence cardiomyocyte differentiation [30,31], the role of the electrical environment on graft cells has not been fully explored. Electrical stimulation through microelectrodes was performed using a voltage-controlled current source on co-cultures of murine cardiomyocytes and human embryonic stem cells. The subsequent increase of cardiac differentiation drew attention to the importance of continuous electrical stimulation on graft cells, which is sometimes lacking or severely attenuated in diseased patients. This had inspired further efforts to explore cardiac gene expression in electrically paced stem cells. A murine model was first demonstrated in a preliminary study to establish the foundation for on-going studies using a human model.

Probing the electrical interactions between stem cells and modeled host cardiomyocytes addresses major questions regarding the associated risk of arrhythmia. It is the hope that the set of tools and methods outlined in this work will be able to

enable breakthroughs in stem cell electrophysiology as well as inspire new technologies to bridge the gap between *in vitro* results and clinical progress.

# 2 Background and Theory

## 2.1. Introduction

Studying stem cell integration in the heart requires a broad background in cardiac physiology as well as stem cell biology. Complications in stem cell transplantation arise from unknown interactions between host and graft tissue types, making it crucial to be familiar with their individual properties. Because mechanical contractions in the heart are initiated by electrical signaling, it is important to understand the complex electrophysiologic interactions between host and graft tissues.

Information about the heart and the processes that are involved during each contraction is presented in the first section of this chapter. The heart's electrical system is especially sensitive to tissue damage, leading to widespread problems when cardiac tissue is unable to repair itself. Stem cells engraftment at the site of injury remains one of the most promising methods for tissue regeneration. A review of regenerative strategies using stem cells is described in the second section of this chapter, and highlights the difficulty of studying stem cell transplantation *in vivo*.

*In vitro* models for studying electrical interactions between host and graft tissue are a focused, low-cost alternative to live animal testing of stem cell engraftment. Devices such as microelectrode arrays are particularly well suited to this task because of their ability to provide information on electrical conduction across multicellular cultures. The theory and application of using microelectrodes for extracellular electrical sensing as well as pacing are discussed in the final section of this chapter.

## 2.2. The Heart: An Electromechanical Pump

The heart is an electro-mechanical organ whose primary function is to supply oxygenated blood from the lungs to the tissues of the body. Structurally, the heart contains four chambers: the left and right atria, and the left and right ventricles. The atria are located superior to the ventricles, and are smaller in size. The two right chambers supply de-oxygenated (venous) blood to the lungs, while the left two chambers receive oxygenated (arterial) blood from the lungs and return it to the rest of the body.

In a single cycle, venus blood from the vena cava fills the right atrium, and is delivered to the right ventricle through the tricuspid valve. Blood in the right ventricle is pushed through the pulmonary valve and into the pulmonary circuit for oxygenation. The resulting arterial blood is brought to the left atrium, pushed through the mitral valve to the left ventricle, and finally ejected through the aortic valve back into the body's circulation network.

The process of oxygenating blood and delivering it through the aorta relies on a highly coordinated pumping action initiated by electrical signals. A group of cells located in the right atrium make up the sino-atrial (SA) node, where rhythmic electrical signals are spontaneously generated that lead to a mechanical contraction. Cardiac tissue allows electrical impulses started at the SA node to spread across both the right and left atria. The signals eventually converge to a second node at the interface between the atria and ventricles called the atrio-ventricular (AV) node. The slow conducting cells in the AV node cause a brief delay in the electrical propagation pathway before conducting the impulse through the bindle of His and on to specialized tissue called Purkinje fibers. The Purkinje fibers transmit the electrical impulse down to the inferior region of the ventricles and excite the surrounding cardiac cells. A ventricular contraction therefore begins from the apex of the heart towards the right and left atria, ejecting blood out of the heart either through pulmonary artery (right side), or the through the aorta (left side).

The generation of electrical signals used to coordinate mechanical contractions is based on changes in the density of charged ions transferred through the cell

membranes of cardiac cells. The nature of these signals is better understood when observing a single cell as it undergoes a highly coordinated process known as the cardiac action potential.

## 2.3. The Cardiac Action Potential

Cardiac cells, or cardiomyocytes, are striated muscle cells that make up the walls of the heart, known as the myocardium. One of the primary functions of cardiomyocytes is to synchronously contract, and thus pump blood through the circulation system. Each contraction is initiated by a cardiac action potential, and is

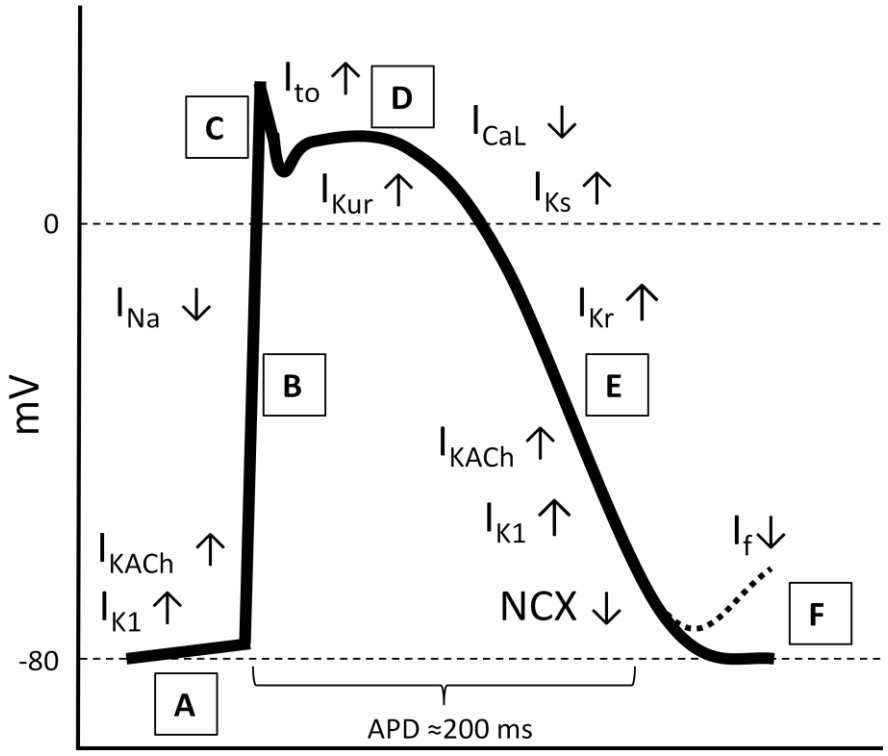


**Figure 2.1** The intracellular cardiac action potential in a ventricular myocyte. The coordinated opening and closing of various ion channels control the electrical potential difference between a cell membrane. The action potential can be categorized by the particular phase it is operating in, starting with (A) resting at a membrane potential of about -80mV, (B) phase 0 depolarization, (C) phase 1 early repolarization, (D) phase 2 plateau, (E) phase 3 final repolarization, and (F) phase 4 baseline. In a pacemaker cell with current $I_f$, phase 4 will spontaneously start depolarizing. A typical action potential duration (APD) is about 200 ms.

what gives the heart its electrical characteristics. The action potential itself is a coordinated movement of ions through specific membrane structures, primarily ion channels, which momentarily changes the potential across a cell membrane.

Under normal physiologic conditions, ion pumps maintain a higher concentration of $Na^+$ and $Ca^{2+}$ outside the cell membrane, and a higher inside concentration of $K^+$. The combined influence of intracellular and extracellular ion concentrations creates a normal resting intercellular potential of around -80mV. When an action potential is initiated, the cell membrane is impermeable to $Na^+$ and $Ca^{2+}$, but is permeable to $K^+$ through the K1 current, $I_{K1}$. An additional acetylcholine-regulated $K^+$ current $I_{KACh}$ is also used as an inward rectifier, and both $I_{K1}$ and $I_{KACh}$ drive the potential across the membrane higher. As the positive potassium ions move out of the cell, the intercellular potential slowly changes until a threshold value is reached. At this point, a large current of $Na^+$ flows through the sodium channel, designated as $I_{Na}$, and effectively depolarizes the cell membrane. After this event, $Ca^{2+}$ ions enter the cell through the L-type $Ca^{2+}$ channel ($I_{CaL}$), which maintains the depolarized state by balancing the net flow of $K^+$ out of the cell. The $K^+$ ions balance out the $Ca^{2+}$ through a series of potassium channels characterized by their time-dependent properties. These include the transient-outward ($I_{to}$) and ultra-rapid ($I_{Kur}$), and rapid ($I_{Kr}$) and slow ($I_{Ks}$)

**Table 2.1 Principle Ion-Channels and Their Primary Functions [1]**

| Ion-Channel Current | Primary Function |
|---|---|
| $I_f$ | Diastolic depolarization |
| $I_{K1}$ | Resting potential, terminal repolarization |
| $I_{KACh}$ | Mediates acetylcholine effects |
| $I_{Ks}$ | Phase 3 repolarization |
| $I_{to}$ | Early (Phase 1) repolarization |
| $I_{Kur}$ | Phase 1-2 repolarization |
| $I_{CaL}$ (L-type) | Maintenance of plateau |
| | Electromechanical coupling |
| $I_{CaT}$ (T-type) | Involved in pacemaking |
| $I_{Na}$ | Initial depolarization |
| $I_{GJ}$ | Intraceulluar conduction through gap junctions |

delayed-rectifier currents which stabilize the fluxes to give the action potential a relatively flat plateau phase. Eventually, the $I_{K1}$ and $I_{KAch}$ currents are re-activated to allow $K^+$ ions to re-enter the cell and repolarize the cell membrane. Extra $Na^+$ and $Ca^{2+}$ ions inside the cell are released back outside the cell membrane by exchanging intracellular $Na^+$ for extracellular $K^+$ through the $Na^+/K^+$ -pump, followed by exchange of $Na^+$ for $Ca^{2+}$ by the $Na^+/Ca^{2+}$ exchanger (NCX). This process is summarized in Figure 2.1 and Table 2.1 for a ventricular myocyte.

The potential across a cell membrane can be approximated by the Nernst equation, which was originally developed to determine the equilibrium reduction potential of a half-cell in an electrochemical cell. The physiological analog of the Nernst equation can be expressed by Eq. 2.1 when a cell membrane is in thermodynamic equilibrium.

$$E = \frac{RT}{zF} ln \frac{[ion\ outside\ cell]}{[ion\ inside\ cell]} \tag{2.1}$$

The Nernst equation is an expression of the potential across a cell membrane $E$ caused by a difference in ion concentration of charge $z$ inside and outside the cell. The constant $R$ is the universal gas constant (8.313 J/K-mol), $T$ is the temperature in Kelvin, and $F$ is the Faraday constant ($9.648 \times 10^4$ C/mol). One major limitation of the Nernst equation is the inability to take into account the role of other ions in the system. A more complete description of the membrane potential is provided by the Goldman-Hodgkin-Katz voltage equation, more commonly known as the Goldman equation, as shown in Eq. 2.2.

$$E = \frac{RT}{F} ln \left( \frac{\sum_i^N P_{M_i^+} [M_i^+]_{out} + \sum_j^M P_{A_j^-} [A_j^-]_{in}}{\sum_i^N P_{M_i^+} [M_i^+]_{in} + \sum_j^M P_{A_j^-} [A_j^-]_{out}} \right) \tag{2.2}$$

The Goldman equation closely resembles the Nernst equation, but incorporates the role of other ions. For $N$ positive ions and $M$ negative ions, their respective concentrations inside ($[A^-_j]$) and outside the cell membrane ($[M^+_i]$) are weighted by a permeability constant, $P$, which is a measure of the ion flux through a channel, expressed in meters per second.

The many ion channels that participate in an action potential cause the charge distributions to vary widely depending on the configuration and concentration of

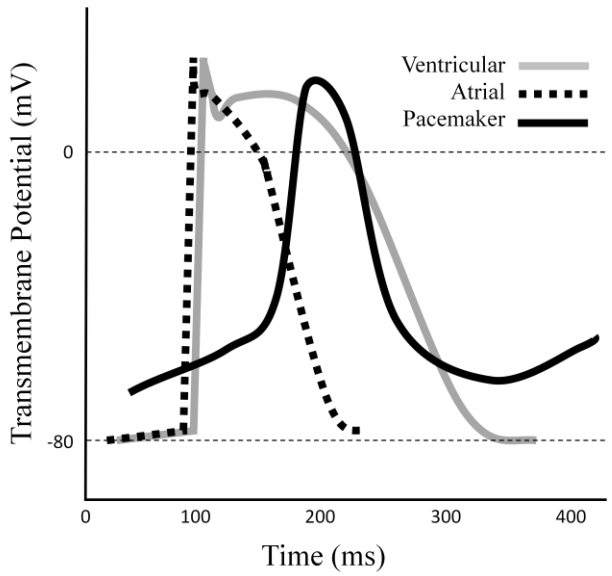


**Figure 2.2** Pacemaker AP (black) superimposed on a ventricular (gray) and atrial (dotted) AP. The pacemaker AP possesses a slower upstroke without fast sodium currents, and a much shorter plateau phase from early inactivation of inward calcium currents relative to delayed rectifier potassium currents.

channels at each cell possesses. Indeed, there are large characteristic differences between atrial, ventricular, and pacemaker cardiomyocyte action potential morphologies. Both atrial and ventricular action potentials still carry the same general shape with an initial upstroke followed by a downstroke that eventually returns to baseline values. The main difference between atrial and ventricular action potentials is that atrial potentials do not have as long a plateau phase as in a ventricular myocyte. Instead, the highly reduced plateau phases in atrial myocytes are due to a different balance between $Ca^{2+}$ and $K^{+}$ channels. It has been reported that the atrial $I_{K1}$ current may be six to ten fold smaller than ventricular $I_{K1}$ current [36]. Pacemaker cells are responsible for initialing electrical activity in the heart spontaneously, and are configured very differently than other myocytes (Figure 2.2). These cells are primarily found in the nodal regions of the heart, and are much more permeable to $K^{+}$ ions but still allow passive transfer of $Ca^{2+}$ ions. Pacemaker cells also possess a special current described as the *funny current*, $I_f$, that dampens the downstroke of the action potential, and eventually raises the potential to threshold to initiate another one.

The average baseline frequency of spontaneous depolarization is typically a function of species, but is also mediated by a variety of factors. There are many mechanisms to increase the rate of pacing, but the frequency is limited by a period of relative non-excitability called the refractory period. This period corresponds

approximately to the action potential duration (APD), and is due to ions rearranging back to baseline concentrations. Pacemaker cells exhibit longer APDs than in atrial cells, which prevents invasion by ectopic impulses, and preserves pacing dominance [37].

The time of the inactivation of the $Ca^{2+}$ and the $K^{+}$ currents influences the duration of an action potential because these currents are sensitive to the transmembrane voltage and the timing of the external stimuli. The APD is often characterized as the time required to go from the onset of the upstroke to achieving 50% or 90% repolarization to the resting potential ($APD_{50}$ or $APD_{90}$, respectively). During intense activity with higher heart rates, such as during exercise, the APD is often shorter. Qualitatively, this is explained by the need for a faster rate of contraction for greater pumping efficiency.

Experimentally, many methods are available for modulating the cardiac action potential. A simple and direct method is to block the channel of interest from passing ions. Tetrodoxin (TTX), for instance, is a guanidinium-containing molecule that effectively blocks $Na^{+}$ channels, and has been studied for anti-arrhythmic qualities [38]. Potassium channel blockers (class III anti-arrhythmics) include amiodarone, stalol, dofetilide, E-4031, and cofilium, and are used to dampen repolarization and extend the APD. Dihdropyridines (DHP) such as nifedipine or verapamil can be used to block the L-type calcium channel.

The cardiac action potential is also mediated by many different signaling molecules that indirectly influence ion channels. Membrane proteins such as acetylcholinergic, nicotinic, and adrenergic receptors rely on secondary messenger responses to initiate a signaling cascade. Through a single binding event, these receptors are capable of controlling channels, pumps, and enzymes, as well as influencing cytoskeleton contraction, transcription factors, and many other protein activities [39]. Adrenergic receptors, which are heterotrimeric GTP binding protein (G-protein) receptors, in particular play a large clinical role in affecting vasoconstriction or vasodilation through sympathetic responses. The receptors are composed of many subtypes, categorized between $\alpha$ (primarily $\alpha_1$ and $\alpha_2$) and $\beta$

(primarily $\beta_1$, $\beta_2$, and $\beta_3$) receptors that all direct different signaling cascades through agonists or antagonists such as isoproterenol and propanolol, respectively.

### *2.3.2. Cardiovascular Disease*

The primary structural proteins in cardiomyocytes used for contraction are thin actin and thick myosin protein filaments. Unlike skeletal myoblasts, which are also striated and capable of contracting, cardiomyocytes are highly resistant to fatigue due to the large number of mitochondria, which allow them to pump efficiently. Muscle contraction operates within continuous aerobic respiration through oxidative phosphorylation. However, efficiency is reduced dramatically if cardiomyocytes are forced to operate through anaerobic metabolism in a hypoxic environment. If efficiency drops low enough, the heart will not be able to supply enough blood to its coronary circulation, leading to necrosis of cardiac tissue.

Ischemia is a condition characterized by such oxygen deprivation to the heart. Circumstances that may lead to ischemia include the restriction of blood supply from atherosclerosis, tachycardia, low blood pressure, or extreme cold conditions. The heart's constant need for oxygen to continue pumping makes it particularly dangerous when oxygen is compromised. Complete restriction of oxygen to cardiac muscle for more than 20 minutes may result in irreversible damage [40].

Natural repair processes for damaged cardiac tissue does not normally include the regeneration of healthy tissue. Instead, the damaged region is often replaced with non-contractile fibrous scar tissue which does not actively participate in cardiac function [11]. This inactive region not only decreases pumping efficiency, but also has the potential to disrupt electrical pathways. Due to the many different variables involved in cardiac impulse propagation [41], even a small block in conduction can lead to re-entrant circuits in the heart. If severe enough, a re-entrant pathway may excite cardiac tissue at an inappropriate stage in the pumping cycle to functionally impair the heart.

While strategies for combating cardiovascular disease are improving, recovering patients are predisposed to complications in the future due to the limited

capacity of the heart to naturally repair itself [11]. Traditionally, heart muscle was not considered to contain any housekeeping mechanisms to repair against minor damage, and cardiomyocytes were expected to respond to physiological and pathological stress by hypertrophy rather than hyperplasia [42]. Fortunately, recent studies have reported evidence of cardiomyocytes re-entering the cell cycle and actively proliferating when damaged [43]. However, despite reporting 10-60 fold increases in mitotic figures, this was only found from a population of cells representing 0.015 to 0.08% of the total [44]. Such drastically low figures do not provide much optimism for natural regeneration.

Greater hope might be found in natural cardiac regeneration processes if these dividing cardiomyocytes could be isolated and better understood, but these cells continue to remain elusive. A clue, however, was found from a source outside the heart. During investigations in sex-mismatched heart transplant patients, researchers noticed that some male recipients of female hearts carried cardiomyocytes with a male-specific Y chromosome [45, 46]. This was a fascinating case where cells from an extracardiac source integrated into myocardium and participated in normal cardiac function. Although this is not the first case of functional chromosomal mismatch between donors, it did indicate that cells outside of the heart might be capable of regenerating cardiac tissue.

## 2.4. Tissue Regeneration

Many biological tissues undergo self-renewal processes on a regular basis, and can be observed through events such as skin regeneration or muscle building. On a larger scale, even the tips of fingers have been observed to regenerate in children [47]. Although regeneration of an entire limb is not seen in humans, it is nonetheless observed in many other species, most notably amphibians. The mechanisms involved in limb regeneration provide a useful model for studying the physiological response during tissue repair. During this process, the body orchestrates the delivery of regenerative cells (which may include dedifferentiated cells) to the proper location, where the physical, humoral, and chemical environments influence the quality of the

repair. Many studies have reported on the role of the chemical environment on regeneration, and identified many important growth factors [48] and special receptors [49] that are crucial for repair processes. The molecular profile at the site of injury has also shown similarities to human cancer signatures [50]. However, the exposure of carcinogens to amphibians during regeneration of damaged tissues resulted in normal morphogenesis and differentiation, thus hinting at an inverse relationship between susceptibility to cancer and the ability to regenerate tissue [42]. At the center of all regenerative strategies are stem cells for their ability to proliferate and differentiate into the needed cell types. This section provides an overview of their characteristics, and how they could be used as future therapies for heart failure.

### *2.4.1. Stem Cell Biology*

Stem cells are often loosely characterized by their ability to both self-renew and form one or more differentiated cell types. More formally, stem cells are cells that exhibit extensive self-renewal capacity, exist in a mitotically quiescent form, and clonally regenerate all of the different cell types that make up the tissue where they

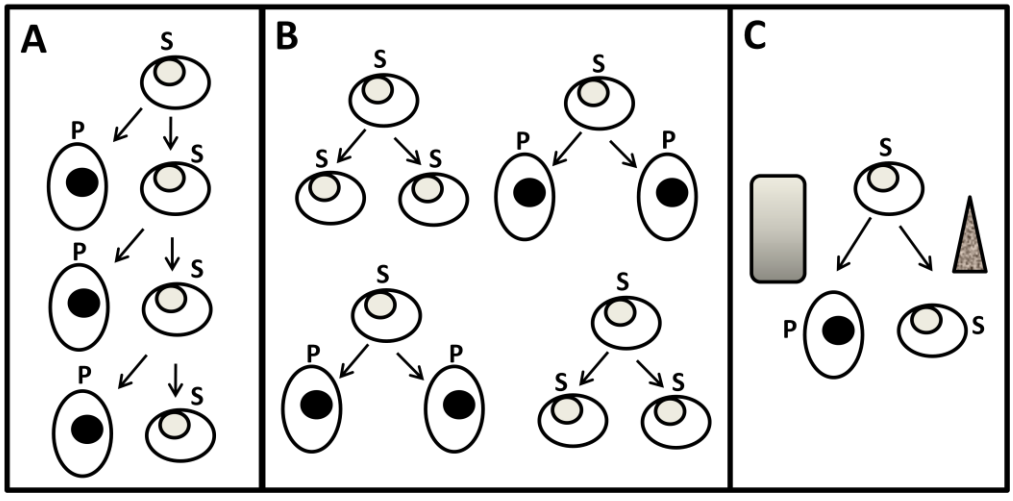


**Figure 2.3** Stem cells undergo different patterns of activity during division which cause them to remain a stem cell "S," or become a committed or restricted progenitor cell "P." Intrinsic mechanisms include (A) asymmetric division, and (B) symmetric division. (C) Non-intrinsic behavior may rely on external stimuli to direct the stem cell's next course of action. Examples of these patterns have all been observed in nature [3].

exist [3]. Still, this definition hardly describes the unknown mechanisms involved with how stem cells proliferate and differentiate. Stem cell differentiation patterns are often tissue specific, and yet are still inconsistent across with different animal models. The cues that direct a stem cell to remain a stem cell, or differentiate into another cell type remain unclear. As described in Figure 2.3, stem cells may differentiate according to intrinsic mechanisms, or by environmental factors. Intrinsic mechanisms include asymmetric division in which two daughter cells follow different lineages, or symmetric division in which two daughter cells follow the same lineage. Because asymmetric division may result in at most one remaining stem cell, this process does not allow amplification of stem cells. Symmetric divisions on the other hand may rely on stochastic events to determine the type of differentiation to take place. Environmental factors that influence stem cell actions include chemical signaling, cell coupling, mechanical forces, or electrical signaling.

Stem cells constitute a very broad class of cells, and can be categorized anatomically, functionally, or even by biomolecular markers. What makes stem cells unique is the type of cells they are capable of eventually differentiating into, an ability referred to as "plasticity." As a result, it is often easier to classify stem cells by their

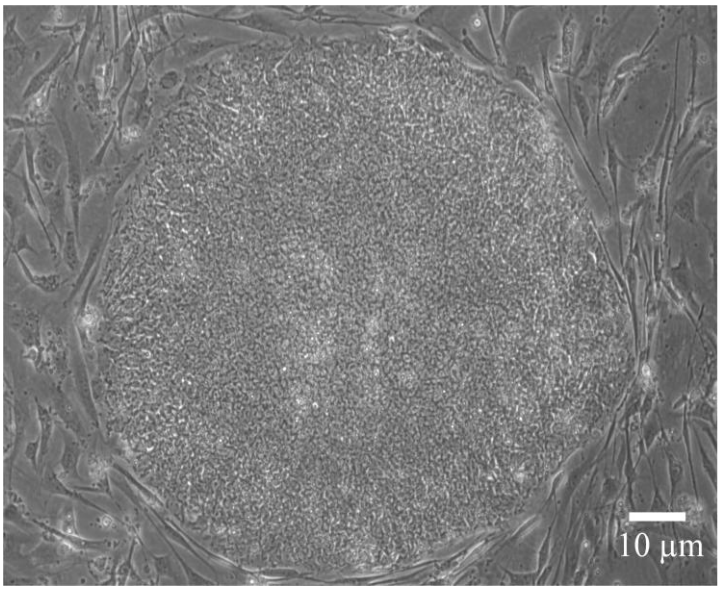


**Figure 2.4** Human embryonic stem cells isolated from a human blastocyst are able to be cultured *in vitro*. Cells are typically grown on a layer of murine fibroblast feeder layers and form large colonies.

ability to differentiate, either as those that come from the embryo (embryonic stem cells), or those in adult somatic tissue (adult stem cells). One other similarly classified type of stem cell comes from the embryo, zygote, and their immediate descendants within the first two cell divisions. These "totipotent" stem cells have the greatest plasticity with the ability to form virtually any cell type. However, these cells have not yet been stably isolated and are not considered viable candidates for cell therapy.

Embryonic stem cells (ESC; see Figure 2.4) are isolated from the blastocyst region of a fertilized embryo. They are characterized by their ability to differentiate into almost all cells that arise from the three germ layers during development, but unable to form the placenta and supporting structures. The degree to which ESCs are able to differentiate is termed as "pluripotency." The isolation of human ESCs (hESCs) by Thomson, et al. [7] in 1998 opened up tremendous opportunities for both regenerative and developmental research, but the diversity of possible cell types derived from ESCs has made it difficult to find methods to differentiate them into the precise cell type of interest *in vitro*. Given the spontaneous nature of ESCs to differentiate into almost every cell type, there is the perpetual risk of impure cultures regardless of the quality of culture methods.

Recently, a new group of embryonic-like stem cells have been engineered from human somatic cells and are called induced pluripotent stem (iPS) cells [51, 52]. Such cells are able to bypass the need for fertilized embryos to generate pluripotent cells, and offer the real possibility of a patient-specific treatment strategy. The methods used for re-programming somatic cells have also given immense insight into novel *in vivo* self-renewal strategies. While still undergoing intense characterization studies, one of the biggest problems is the extremely low yields of derived iPS cells. Recently, similar re-programming methods had been applied to human adipose tissue to derive embryonic-like cells by Sun, et al. [53]. Compared to somatic cells, adipose cells are able to yield larger quantities of iPS cells under shorter expansion times, and are easier to maintain in cultures. Utilizing adipose tissue also offers a new, more plentiful source of cells for reprogramming.

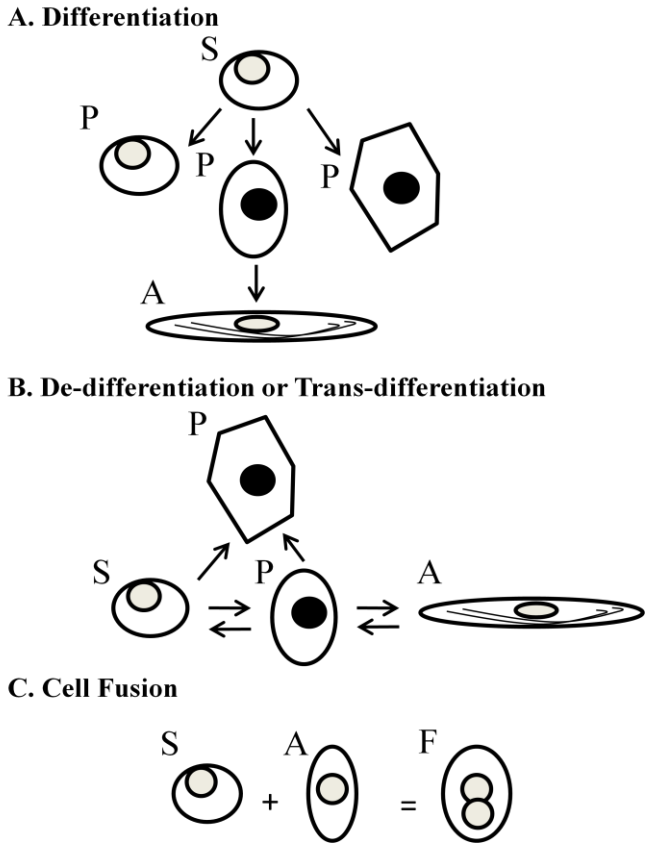


**Figure 2.5** Possible pathways for stem cells development. (A) Stem cells, "S," have the ability to both self-renew and differentiate into other cell types in a linear fashion. Adult stem cells, "P," are characterized by the type of cells they are capable of eventually differentiating into, termed "A." (B) Adult stem cells do not necessarily follow a fixed path, and may de-differentiate, or possibly trans-differentiate. (C) What may appear as plasticity may also be caused by transplanted cells fusing with host cells of a different lineage leveled "F.".

Adult stem cells, or progenitor stem cells, are found in more mature tissue, and labeled "multipotent" for their ability to produce a small range of differentiated cell lineages that are dependent on their physiological environments [54]. Stem cells with the least potential for differentiation are labeled "unipotent," such as epidermal stem cells which can only differentiate into keratinized squames. Although adult stem cells are limited in differentiation ability, there has been evidence of the ability to "de-differentiate" into an earlier lineage depending of their environment and type of stimulation they are exposed to [55, 56] (Figure 2.5). The ability of stem cells to "trans-differentiate" and go from one adult stem cell line directly to another is still under debate [57, 58].

An additional cellular process often mistaken for stem cell plasticity is cell fusion. Instead of typical differentiation processes, stem cells have been observed to fuse with native cells to produce a hybrid cell expressing both types of cell markers. It is unclear what capacity these cells are able to participate in regenerative processes,

and there is little evidence to suggest that cell fusion plays an important role in cardiac repair [59].

### *2.4.2. Stem Cell Therapy*

Repairing damaged cardiac tissue using stem cells is not yet a viable strategy due to many unknown mechanisms during the stem cell integration process. However, the possibility of a biological, patient-specific treatment for many cardiovascular conditions has continued to motivate further research. Current studies have relied on simply injecting exogenous cells into a damaged myocardium, a process called cellular cardiomyoplasty (CCM). Although such a haphazard delivery mechanism does not deliver cells to a specific region of interest, it does successfully introduce transplanted cells into the heart. Injection is often performed directly through the myocardium, intramyocardially via the endocardium, through intracoronary arteries, or through retroperfusion via the cardiac veins [60]. In early studies using rat neonatal cardiomyocytes as the donor cells into a rat host, the vast majority of transplanted cells died following injection, with only about 5% actually seeding into myocardium [61]. Many efforts are still ongoing to find more practical ways to introduce exogenous cells to the myocardium. It is of interest to note that bone-marrow stem cells have been observed to naturally target the site of myocardial injury following engraftment [42].

The mechanism of integration between a stem cell graft and host myocardium is a complex process, with the optimal cell type for this procedure still under debate. Ideally, transplanted cells must be able to differentiate into cardiomyocytes, integrate into the host tissue, and aid in normal cardiac function. Many candidate cell types have been injected into various human and animal studies, including skeletal myoblasts [15], embryonic stem cells [16], bone marrow-derived mesenchymal stem cells [17], enriched hematopoietic stem cells [18], blood and bone marrow-derived endothelial progenitor cells [19], and many others. While many of these trials had reported modestly positive outcomes for the animal or human subjects, none of the engrafted cells were able to perfectly differentiate and engraft into the heart. At best, injected cells were partially engrafted into the heart and induced angiogenesis in the

host scar tissue [13]. At worst, transplanted cells disrupted normal rhythm in the heart [23], or proliferated uncontrollably [62].

There is an urgent need to better understand the mechanisms that take place following cell transplantation. In addition to cellular interactions, the chemical, mechanical, and electrical environments all play major roles throughout the integration process and have yet to be comprehensively understood (Figure 2.6). Methods of cardiac differentiation for candidate cell grafts have not even been fully agreed upon. There is certainly no lack of references within existing literature to techniques that may encourage differentiation from various cell types. Cardiomyocyte differentiation is influenced by many factors, including the structural formation of embryoid bodies from murine and human ESCs [63, 64], addition of retinoic acid to murine ESCs [65], mechanical stretching on rat neonatal cardiomyocytes [35], co-culture of human ESCs with visceral endoderm-like cells [66], and application of a brief high-voltage DC pulse to murine embryoid bodies [67]. The range of methods used for cardiac differentiation illustrates the influential role environmental conditions play in this process. However, studying the physical conditions of stem cells is limited by a lack of robust *in vitro* tools. The electrical environment, especially, is severely understudied compared to work investigating mechanical or chemical factors in cardiac differentiation. Studying the electrical interactions between a cardiac host and

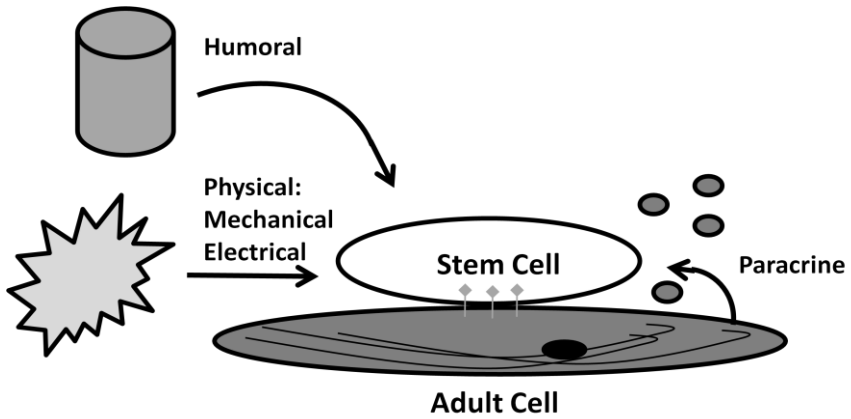


**Figure 2.6** Environmental influences on stem cell differentiation. Various cues by the local environment provide a special niche that helps to mediate stem cell growth and differentiation. Methods in guiding differentiation should consider the influence of physical space, coupling to neighboring cells, and paracrine signaling interactions.

stem cell graft *in vitro* require methods that provide information on conduction patterns, as well as metrics for quantitative analysis.

## 2.5. Real-Time Analysis of Cardiac Cultures

The electrical characteristics of living cells play an integral part in biological function. Once the science of electricity was understood by researchers, it did not take long before electrical potentials were found in animals and humans. Early experiments by Galvani, du Bois-Reymond, von Helmhotlz, and Fontanta and Bowditch in the late eighteenth and nineteenth centuries were especially groundbreaking in the emerging field of electrophysiology. Their initial studies were key to clarifying the electrical roles in muscle response, resting potentials, conduction velocity, and the "all-or-nothing" law, respectively [68].

Membrane potentials in living cells were not directly observed until much later until 1949 when Gerard and Ling developed the technique of using glass capillary microelectrodes inserted intracellularly through the cell membrane of frog muscle fibers [69, 70]. One of the most well known applications of this method was in 1952, when Hodgkin and Huxley used an intracellular microelectrode to develop quantitative models of the membrane potential from squid neurons [71]. Intracellular recordings are still in use today, and are recognized for reliably high signal to noise ratios. However, use of this method is limited to sensing potential changes across the cell membrane, and is unable to truly measure changes in ion concentration during an action potential.

The innovation of the patch clamp in the 1970's [72, 73] was a breakthrough in electrophysiology because it provided a way to not only directly study the exchange of current through a cell membrane, but also have the resolution to study individual protein channels. Instead of impaling a cell with a fine-tipped electrode, a patch-clamp consists of a micropipette whose tip is attached ("sealed") to a membrane surface. The micropipettes are filled with an ionic solution similar to that of the intracellular fluid of the cell, and a chloride-silver wire is inserted into the micropipette to serve as an electrode. The electrical signal measured by the wire is referenced to another electrode

in contact with the extracellular fluid around the cell. Depending on the way the patch clamp is applied, one can measure the aggregate current through a cell membrane during normal physiological function ("whole-cell" mode), or study the role of individual ion channels ("cell-attached" mode).

Currently, the patch clamp is a gold standard for electrophysiological studies. Nonetheless, despite how advanced patch clamping systems have become, analysis is limited to a single cell and does not allow for long term monitoring. Patch clamping also requires a highly trained technician and it is very difficult to scale up the number of samples to analyze. The data obtained from a patch clamp gives no direct information on multi-cellular interactions, which would be essential for studying stem cell integration to host cardiac tissue. Different tools are therefore necessary that are able to probe multiple cultures simultaneously. Notwithstanding the use of voltage- or calcium sensitive dyes that are cytotoxic in long term studies [25, 26], an alternative non-invasive option is to use microelectrodes to extracellularly sense transmembrane voltages from coupled cells.

### *2.5.1. Non-invasive Techniques with Microelectrodes*

The use of microelectrodes for electrical measurements of living cells began around the same time as patch clamps, first presented by Thomas, et al. [74] who created a planar array of microelectrodes to sense bioelectric activity from neonatal chick cardiomyocytes. Since then, many more designs have been fabricated in different configurations and for a vast number of applications. A very brief list of examples include the study of neurons [75], bioterror agent detection [76], environmental biosensing [77], cardiac stimulation thresholds [28], and functional analysis of stem cell derived cardiomyocytes [78].

Microelectrode arrays (MEA) measure extracellular potentials across an entire syncitium of cells. These devices do not convey as much information on particular ion channel contributions as patch clamps do, making the technique not ideal when examining individual cells. Nonetheless, the advantages of measuring extracellular signals lie in non-invasive, long-term recording, which gives special insight into the

conductivity among networks of cells. Many studies have been performed to explore the relationship between extracellular signals from a microelectrode to intracellular potentials from patch clamps [79-81]. Mathematically, the extracellular signal can be shown to be proportional to the second derivative of the intracellular action potential primarily due to the capacitive effects of the cell membrane.

In order to relate the intracellular potential with the extracellular voltage measured, Spach, et al. derived an expression based on a model cylindrical surface $S_o$ taken at time $t_o$, as shown in Eq. 2.3 [79].

$$\varphi_e(t_o, z) = \frac{a\sigma_i}{4\pi\sigma_e} \int_{-\infty}^{+\infty} \frac{\frac{\partial^2 \varphi_i}{\partial t^2}|_{Z_o}}{\sqrt{1+\left(\frac{\theta(t'-t)}{a}\right)^2}} \mathrm{dt} \tag{2.3}$$

The cell radius $a$, is over a length $z$, and the intracellular and extracellular conductance is represented by $\sigma_i$ and $\sigma_e$, respectively. By using this central equation, the extracellular potential $\varphi_e$ appears to reflect the second derivative of the intracellular action potential $\varphi_i$. However, Spach, et. al. also showed quantitative differences by varying the temperature and extracellular potassium concentration. Additional theoretical discrepancies may also lie in non-uniform coupling between the cell membrane and the planar electrode, which could present complex geometries that deviate significantly from the ideal cylindrical model. Regardless, it is clear that the intracellular action potential heavily influences the extracellular signal. A mathematical approximation of the intracellular action potential is therefore useful in understanding the data obtained from a MEA.

Initial work by Hodgkin and Huxley [71] modeled the action potential as a transmembrane current (I), which is determined by the concentrations of specific ions such as sodium, potassium, and calcium.

$$I = C_M \frac{dV}{dt} + I_i \tag{2.4}$$

This transmembrane current is expressed as a function of the membrane capacitance per unit area $C_M$ multiplied by the change in transmembrane voltage V over time, added to the capacitive and ionic components. The term $I_i$ comprises the many ion

channel currents within the cell membrane, and is expressed as the product of ion conductance g, and the transmembrane potential difference when each ion is at equilibrium. The ion currents defined for this system rely primarily on $Na^+$ in $I_{Na}$, and $K^+$ in $I_K$. Besides these two major currents, all other participating ions are combined in the leakage current term, $I_l$.

$$I_{Na} = g_{\mathrm{Na}}(\mathrm{V} - \mathrm{V_{Na}}) \tag{2.5}$$

$$I_K = g_{\mathrm{K}}(\mathrm{V} - \mathrm{V_K}) \tag{2.6}$$

$$I_l = g_{\mathrm{l}}(\mathrm{V} - \mathrm{V_l}) \tag{2.7}$$

The transmembrane potential is further defined as the difference between the ionic equilibrium potential $E_{Na}$, $E_K$, and $E_{l,}$ and the resting potential $E_r$.

$$V_{Na} = \mathrm{E_{Na}} - \mathrm{E_r} \tag{2.8}$$

$$V_K = \mathrm{E_K} - \mathrm{E_r} \tag{2.9}$$

$$V_l = \mathrm{E_l} - \mathrm{E_r} \tag{2.10}$$

Taken together, the expression in Eq. 2.4 can be expanded using time and temperature dependent variables n, m, and h derived from experimental data in Eq. 2.11. All three of these variables are in units of $[\text{time}]^{-1}$, and are dependent on voltage and temperature.

$$I = C_M \frac{dV}{dt} + g_K\, \mathrm{n}^4(\mathrm{V} - \mathrm{V_K}) + g_{Na}\, \mathrm{m}^3\mathrm{h}(\mathrm{V} - \mathrm{V_{Na}}) + g_l\, (\mathrm{V} - \mathrm{V_l}) \tag{2.11}$$

In this expanded description of the transmembrane current density, the conductance values $g_k$, $g_{Na}$, $g_l$ are constants expressed in conductance/unit area.

Expressing the action potential as function of membrane capacitance and ion channel distribution is an excellent way to describe the process within a single cell, but includes no information on its conductive properties. In addition to expressing transmembrane current with respect to time and voltage, the action potential can also be defined with respect to its spatial location, as shown by a linear core-conductor theory by Hodgkin and Huxley [71] (Eq. 2.12). This expression assumes that extracellular resistance is much smaller than intracellular resistance, currents are evenly distributed, and propagation occurs at a fixed velocity θ.

$$I = \frac{a}{2R}\frac{\partial^2 V}{\partial x^2} \tag{2.12}$$

The expression in Eq. 2.12 describes the conduction across a cell with radius *a* traveling in one dimension of length *x*. The resistance of the cellular cytoplasm is given by *R*. The original derivation of this expression was based on a nerve fiber, but can be universally applied to any type of electrically conducting cell.

If the conduction velocity is held constant, both the temporal and spatial aspects to this system can be related in Eq. 2.13, revealing the transmembrane voltage as the ordinary differential equation shown in Eq. 2.14.

$$\frac{\partial^2 V}{\partial x^2} = \frac{1}{\theta^2}\frac{\partial^2 V}{\partial t^2} \tag{2.13}$$

$$\frac{a}{2R\theta^2}\frac{\partial^2 V}{\partial t^2} = C_M\frac{dV}{dt} + g_K\,\mathrm{n}^4(\mathrm{V}-\mathrm{V_K}) + g_{Na}\,\mathrm{m}^3\mathrm{h}(\mathrm{V}-\mathrm{V_{Na}}) + g_l\,(\mathrm{V}-\mathrm{V_l}) \tag{2.14}$$

This is further simplified by defining a constant K.

$$K = \frac{2R\theta^2 C_M}{a} \tag{2.15}$$

$$\frac{\partial^2 V}{\partial t^2} = K\left\{\frac{dV}{dt} + \frac{1}{C_M}\left[g_K\,\mathrm{n}^4(\mathrm{V}-\mathrm{V_K}) + g_{Na}\,\mathrm{m}^3\mathrm{h}(\mathrm{V}-\mathrm{V_{Na}}) + g_l\,(\mathrm{V}-\mathrm{V_l})\right]\right\} \tag{2.16}$$

The expressions in Eq 2.13-2.16 identify several key variables that play important roles during the propagation of an action potential, namely the cell morphology, ion channel configuration, and conduction velocity (a function of the gap junction distribution). Experimental data on electrical conduction within a cell culture therefore contains highly relevant information on inherent cellular properties.

### *2.5.2. Mapping Conduction on Microelectrode Arrays*

Depolarization of a cardiac cell during an action potential will initiate another action potential in neighboring cells, made possible by intercellular electrical coupling proteins called gap-junctional hemichannel connexin (Cx) proteins [82]. Gap junctions are able to lower the electrical resistance between cells by allowing the transfer of ions through them. The movement of ions during an action potential in one cell shifts the electrical potential in neighboring cells at the junction, initiating another action potential and creating a wave of depolarization throughout the tissue. This depolarization wave travels through cardiac tissue and leads to coordinated mechanical contraction. One method of mapping conduction patterns is to simultaneously probe multiple points in a cell culture, which can be done using an array of microelectrodes. After an action potential is transduced through an electrode, additional analysis is necessary to characterize the action potential propagation across the surface. Understanding the properties of excitation, conduction, and propagation

will naturally provide insight to how electrical pathways are disrupted during arrhythmogenic conditions.

Conduction is often represented by a velocity vector, which indicates the speed and direction of propagation in cardiac activity. Mapping the propagation of action potentials throughout the tissue can provide a means to visualize and evaluate the development of re-entrant pathways. In some clinical examples, the propagation speed and refractory period are combined to determine the basic wavelength, and hence stability, of arrhythmias [83]. In a general scenario, if the refractory period of cells is measured as $\tau_r$ and the local propagation speed is v, then the smallest length of the reentrant path can be given by $L = v\,\tau_r$.

While L is merely the product of two variables, the system may become much more complicated depending on how the conduction velocity is calculated. In principle, one can simply measure the location of the activation front at different times with two electrodes, and then divide the distance traveled by the time interval. Unfortunately, while this approach is valid, it is highly simplified and would be inaccurate unless the spatial and temporal resolutions of the measurement system are extremely high. The heart is also not a one dimensional system and conduction patterns tend to be anisotropic. Conduction velocity calculated using two electrodes will only be correct if the electrodes are located exactly perpendicular to the activation front. For this reason, multiple electrodes are necessary that span the dimensions of interest.

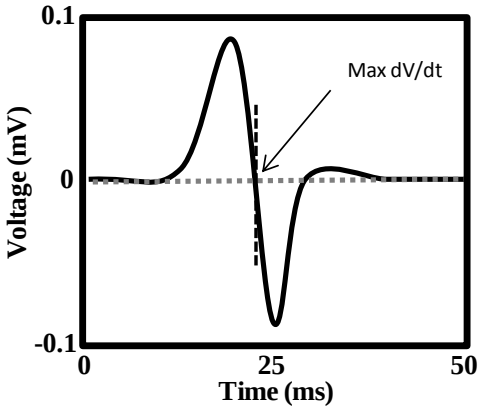


**Figure 2.7** Defining the local activation time. An extracellular action potential is characterized by a single upstoke and downstroke. The local activation time for each electrode is defined by the point of the maximum voltage derivative over time.

In order to characterize conduction over a two-dimensional surface, Bayly, et al. described a method of using a field of velocity vectors [84]. For each electrode in the array, the time

of arrival is determined by first taking the time derivative of the voltage measurement through a three-point central difference method. The time point when the first derivative is at its maximum value was defined as the "local activation time," as illustrated in Figure 2.7.

A velocity vector is assigned to each point of the field, and is defined by the velocity in the x and y directions described by the following vector.

$$\boldsymbol{v} = \left[\frac{dx}{dt}, \frac{dy}{dt}\right]^T \tag{2.17}$$

This vector is estimated by taking local activation times from each electrode and its active neighbors within a user defined window of size $\Delta x_{max}$ and $\Delta y_{max}$ and within a time interval $\Delta t_{max}$ (The values used by Bayly, et al. was $\Delta x_{max} = \Delta y_{max} = 4$ mm and $\Delta t_{max} = 16$ ms). All activation times are then fitted through a least-squares algorithm into a smooth polynomial surface defined by $t_i = T(x_i,y_i)$.

$$T(x, y) = ax^2 + by^2 + cxy + dx + ey + f \tag{2.18}$$

The polynomial function in Eq. 2.18 shows the activation time T as a function of the position, and requires a minimum of 20 points using the defined window size. The gradient of T(x,y) is referred to as the "slowness" vector, and can be solved analytically.

$$\nabla T = \left[\frac{dT}{dx}, \frac{dT}{dy}\right]^T \tag{2.19}$$

Because this gradient vector is normal to the local activation front, it is also an indication of the direction of propagation. The following relationships can then be applied to calculate the components of a differential vector $[dx,dy]^T$.

$$\frac{\mathrm{dy}}{\mathrm{dx}} = \frac{\frac{dT}{dy}}{\frac{dT}{dx}} \tag{2.20}$$

$$d\mathrm{T} = \frac{\partial T}{\partial x} dx + \frac{\partial T}{\partial y} dy \tag{2.21}$$

Finally, using Eq. 2.20 and Eq. 2.21, the velocity vector estimate $\mathbf{v_e}$ is obtained where $T_x = \partial T/\partial x$ and $T_y = \partial T/\partial y$.

$$\boldsymbol{v_e} = \begin{bmatrix} \frac{dx}{dT} \\ \frac{dy}{dT} \end{bmatrix} = \begin{bmatrix} \frac{T_x}{T_x^2 + T_y^2} \\ \frac{T_y}{T_x^2 + T_y^2} \end{bmatrix} \tag{2.22}$$

$$\frac{dx}{dT} = \frac{\partial x}{\partial T} + \frac{\partial x}{\partial y}\frac{dy}{dT} \tag{2.23}$$

$$\frac{dy}{dT} = \frac{\partial y}{\partial T} + \frac{\partial y}{\partial x}\frac{dx}{dT} \tag{2.24}$$

There are several advantages to using a fitted polynomial to estimate the velocity vector. First, it does not require all the points in the local vicinity to be activated to calculate a velocity vector, which makes this algorithm robust against missing or corrupt data. Moreover, this method does not require an evenly spaced array, but only knowledge of x and y coordinates of each sensing electrode. Second, by fitting the data to a polynomial, there is an intrinsic smoothing operation automatically performed on the data [85]. Finally, the quality of the velocity estimate can be quantitatively assessed by using a residual error of the fit.

### *2.5.3. Electrochemistry in Microelectrodes for Sensing and Pacing*

The interface between electrodes and the ionic solution bath is a highly complex region where electrochemical transduction from changes in ion concentration to an electrical voltage takes place for electrical recording. In this very narrow nanometer-scale region, a change in electrical potential from an action potential forms an electric field, which can be sensed by an electrode. In equilibrium, a space-charge double-layer of oriented water dipoles, solvated ions, and adsorbed molecules are able to form, and no current exists. This interface has been modeled extensively in the literature [4, 86-90], but a highly simplified representation of the electrode/electrolyte interface can be made up of non-linear passive resistive (transfer resistance) and capacitive elements (interfacial capacitance), as shown in Figure 2.8. A general interpretation of the electrode/electrolyte interface consists of an interfacial capacitive ($C_t$) element in parallel with an impedance element. The impedance may be dominated by the transfer resistance $R_t$, but the Warburg impedance $R_W$ and $C_W$ could become very significant when the charge transfer between the electrode and the electrolyte

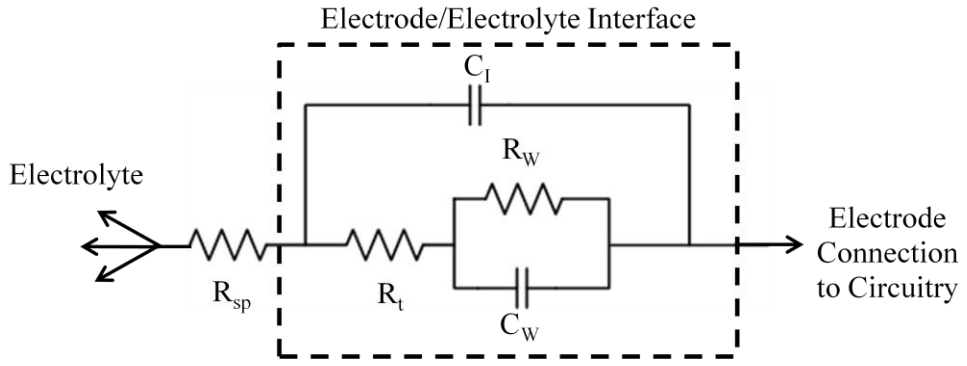


**Figure 2.8** A simplified electrical model of the electrode/electrolyte interface consists of passive resistive and capacitive elements for small signals. The interface itself contains Warburg impedance contributions from $R_W$ and $C_W$ in series with the transfer resistance $R_t$. These elements are in parallel with the interfacial capacitance $C_I$. The spreading resistance $R_{sp}$ is due to current flow in the electrolyte [4].

shift to a diffusion limited system. The spreading resistance $R_{sp}$ represents the resistance of the electrolyte, and is a function of the electrical conductivity $\rho$ (72 Ω·cm in physiological saline) and the radius of a circular planar electrode $r$ [91].

$$R_{sp} = \frac{\rho}{4r} \tag{2.25}$$

The simplified electrode/electrolyte interface depicted in Figure 2.8 would require many additional considerations if the electrodes are used for electrical stimulation because of possible toxic electrochemical effects. A very practical concern when using microelectrodes is the biocompatibility with living cells.

Based on the understanding of electrolytic cells, two primary mechanisms exist for charge transfer through the electrode/electrolyte interface. The first is a non-Faradaic reaction, where no electrons are transferred between the electrode and the electrolyte. Instead, such non-Faradaic reactions mainly redistribute charged chemical species in the electrolyte. The second mechanism of is a Faradaic reaction, where electrons are transferred between the electrode and electrolyte. If the application of an external potential is high enough to create Faradaic reactions, reduction and oxidation of chemical species in the electrolyte may occur at the cathode and anode, respectively. Operating within a Faradaic regime is characterized by the electrochemical reactions that take place, where the byproducts are toxic for cells. For commonly used platinum electrodes, largely irreversible reactions at the anode include the electrolysis of water (Eq. 2.26), oxidation of chloride ions (Eq. 2.27-2.28),

formation of corrosion by-products (Eq. 2.29), and the oxidation of organic molecules (Eq. 2.30). The primary cathodic reaction is the reduction of hydrogen ions to hydrogen gas (Eq. 2.31)

$$2H_2O \rightarrow O_2(g) + 4H^+ + 4e^- \quad (2.26)$$

$$Cl^- + 4H_2O \rightarrow ClO_4^- + 8H^+ + 8e^- \quad (2.27)$$

$$2Cl^- \rightarrow Cl_2(g) + 2e^- \quad (2.28)$$

$$Pt + 4Cl^- \rightarrow (PtCl_4)^{2-} + 4e^- \quad (2.29)$$

$$C_6H_{12}O_6 + 6H_2O \rightarrow 6CO_2 + 24H^+ + 24e^- \quad (2.30)$$

$$2H_2O + 2e^- \rightarrow H_2(g) + 2OH^- \quad (2.31)$$

Some Faradaic reactions are reversible depending on the type of potential applied across the electrodes and the electrode material. The goal of safe electrical stimulation is to prevent or minimize irreversible reactions. Often times, generated products may be recovered by reversing the direction of current applied across the electrodes to create a "charge-balanced" signal. However, generated products may not be recovered if the generated chemical products diffuse away from the electrode before the reversal of charge occur [92]. Reversible reactions are therefore constrained within a particular duration of an applied signal. If the total amount of charge delivered is small enough for no Faradaic reactions to take place, only charge redistribution occurs over the electrode surface and there is no transfer of electrons across the interface. Electrical pulsing within this regime will primarily charge and discharge the electrical double layer.

During stimulation, the electric field generated at the electrode must be high enough to shift the membrane potentials of surrounding cells enough to induce depolarization. The parameters of stimulation are therefore dependent on the type of cells in use, and will also vary from batch to batch. In order to minimize irreversible reactions that may take place during stimulation, potentials across electrodes should not exceed the voltages presented in Table 2.2 [2]. These values were determined using platinum electrodes, and should not be considered exact thresholds. Reaction rates also must be considered on a case by case basis.

**Table 2.2 Reversible potentials of selected electrochemical reactions with platinum [2]**

| Electrode Reaction | Reversible Potential, $E_o$ (V) Referenced to a reversible hydrogen electrode |
|---|---|
| Oxygen evolution | 1.228 |
| Hydrogen evolution | 0.00 |
| Saline oxidation/reduction | 1.389 |
| Chlorine evolution | 1.774 |
| Glucose oxidation | -0.015 |
| Platinum oxidation | 0.980 |
| Platinum hydride formation | N/A (Voltage-dependent) |

## 2.6. Summary

In this chapter, basic background was presented to understand the biological and engineering aspects involved in this study. Starting with an appreciation of how the heart functions as a whole, the ionic contributions to a single action potential were described to further demonstrate the complexity in each heart beat. The coordinated propagation of action potentials throughout the heart initiates mechanical contractions, but is easily disturbed by tissue damage. The delicate nature of cardiac tissue is primarily due to its limited regenerative abilities, which have made conditions such as heart failure debilitating. Nonetheless, this has motivated the use of various types of stem cells to repair and regenerate damaged tissue. Many questions about stem cell viability in the myocardium are still unanswered, especially regarding the arrhythmogenic risk involved. As a result, greater *in vitro* analysis must be performed, starting by probing the electrophysiology of stem cells as well as their interactions with host tissue. Microelectrode arrays are unique tools that are especially useful in this endeavor because they provide spatial and temporal information. In addition, microelectrodes can also be used to electrically pace cells, but consideration must be made to prevent irreversible chemical reactions at the electrode/electrolyte interface.

# 3 Conduction Analysis Using Microelectrode Arrays

## 3.1. Introduction

Stem cell transplantation in the heart remains a highly controversial procedure because the mechanisms behind the integration process remain unclear. Even the type of graft cells to transplant is under fierce debate. In addition to using cells from a cardiac linage, there is evidence that cells outside this lineage, such as mesenchymal stem cells [42] or skeletal myoblasts [23], may regenerate cardiac tissue as well. The arrhythmogenic risk associated with transplantation is highly dependent on the type of cell being used and how quickly they can differentiate into cardiomyocytes. The complexity of live models has made it difficult to truly understand how host tissue reacts electrically to transplanted cells. Therefore, further work using *in vitro* methods is necessary to probe how the electrical environment affects stem cell integration.

Although the ability of transplanted cells to eventually differentiate into cardiomyocytes is uncertain, the introduction of exogenous cells to the heart will undoubtedly risk the disruption of normal electrical activity and at worst, cause arrhythmias. Such pro-arrhythmic consequences were examined *in vitro* by Chang, et al., who studied the interaction between human mesenchymal stem cells and neonatal rat ventricular myocytes [30]. By examining two-dimensional electrical conduction by optical dyes in mixed co-cultures and screening the resulting patterns for reentry, mismatched cell types were shown to be a large risk for arrhythmia. While this study was insightful, the techniques for analysis were performed using dyes that are considered cytotoxic in long term cultures. More importantly, the demonstration of pro-arrhythmic potential was not quantitative.

Before further studies can be performed on the arrhythmogenic risk associated with stem cell transplantation, quantitative metrics should be created to assess the

propagation on an action potential. This chapter describes the development of various metrics to analyze information obtained from heterogeneous cell populations cultured over an array of microelectrodes.

Microelectrode arrays (MEAs) were used to study electrical conduction patterns in murine cardiomyocytes co-cultured with murine fibroblasts. By introducing a different cell type into otherwise normally beating cardiomyocytes, the system can be used to model the initial stages of stem cell therapy if a non-cardiomyocyte stem cell is introduced into a myocardial syncytium. Quantitative analysis of the resulting conduction patterns using a novel mathematical transform was used to identify minimum thresholds for uniform depolarization to take place, and highlighted the potential dangers of using non-cardiomyocyte stem cells for cardiac therapy.

## 3.2. Microelectrode Arrays

Microelectrode array technology has been used in numerous applications to study a wide range of electrically active tissue types. The MEAs used in this study were created by Whittington, et al. to monitor and electrically stimulate cardiac cultures. Thirty-six microelectrodes were arrayed in a 6x6 square on a glass substrate for electrical recording [68]. Each microelectrode was 22 μm in diameter and spaced 100 μm apart. Additional, larger auxiliary electrodes were also located on the outer perimeter of the MEA with varying surface geometries capable of electrically pacing cardiomyocytes (Figure 3.1). A bench-level system based on these MEAs had been shown to monitor the status of cell cultures in real time, and through closed-loop pacing control, allowed the determination of pacing thresholds necessary to activate a depolarization wave in murine cardiac cultures [28, 93]. Using this information, strength-duration curves could be derived directly from experimental data, and used to characterize cell cultures before and after the addition of various pharmacological agents.

Data from MEAs were acquired from 32 channels, with the four corner electrodes excluded. The signals were then processed using a custom recording system that consisted of a 32-channel amplifier with a two-stage gain of 60 dB, 7 Hz 1st-order

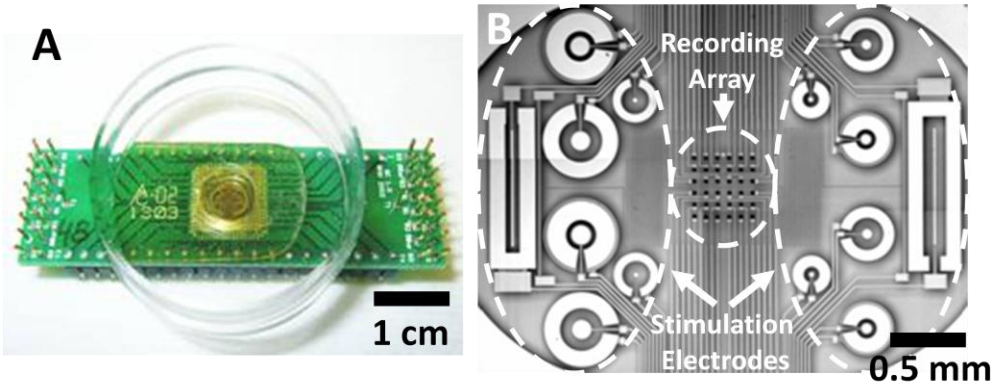


**Figure 3.1** The microelectrode array platform. (A) the array of microelectrodes was wire-bonded to a PCB board carrier. A 35mm Petri dish with an open center was adhered to the PCB board through bio-compatible epoxy (EP42HT, Master Bond; Hackensack, NJ), which was used to contain fluids for cell culture. (B) A 6x6 array of microelectrodes are fabricated on a glass substrate for electrical recording. Larger auxiliary electrodes located on the outer perimeter of the array may be used for electrically pacing cell cultures.

high-pass cutoff, and 3 kHz 8$^{th}$-order low-pass cutoff, as previously reported by Gilchrist, et al. [27]. Analog signals from the amplifier board were digitized with 16-bit resolution at 10 ksps and acquired by a custom-designed visualization and extraction tool, written in Matlab™ (The MathWorks; Natick, MA) [94].

### *3.2.1. Cardiac Cell Culture*

The MEA system could be used to non-invasively monitor electrical activity of cell types over the course of several days. The cardiomyocytes used in this study to model host cells were from the murine atrial tumorgenic cell line HL-1 derived by Claycomb, et al., in 1998 [95]. HL-1 cardiomyocytes underwent mitosis approximately every 18 hours, and more importantly, they were capable of beating spontaneously at a rate between 60-180 beats per minute when cultured to confluency. Using an MEA, electrical activity from the spontaneously beating HL-1 cardiomyocytes could be clearly observed consistently on all 32 channels, as shown in Figure 3.2, where each trace represents a single channel plotted over time. The extracellular voltage of the cells typically ranged within the order of 0.1 to 1 mV. In general, each action potential consisted of a positive upstroke followed by a rapid downstroke before returning to baseline values. The morphology of extracelluar action

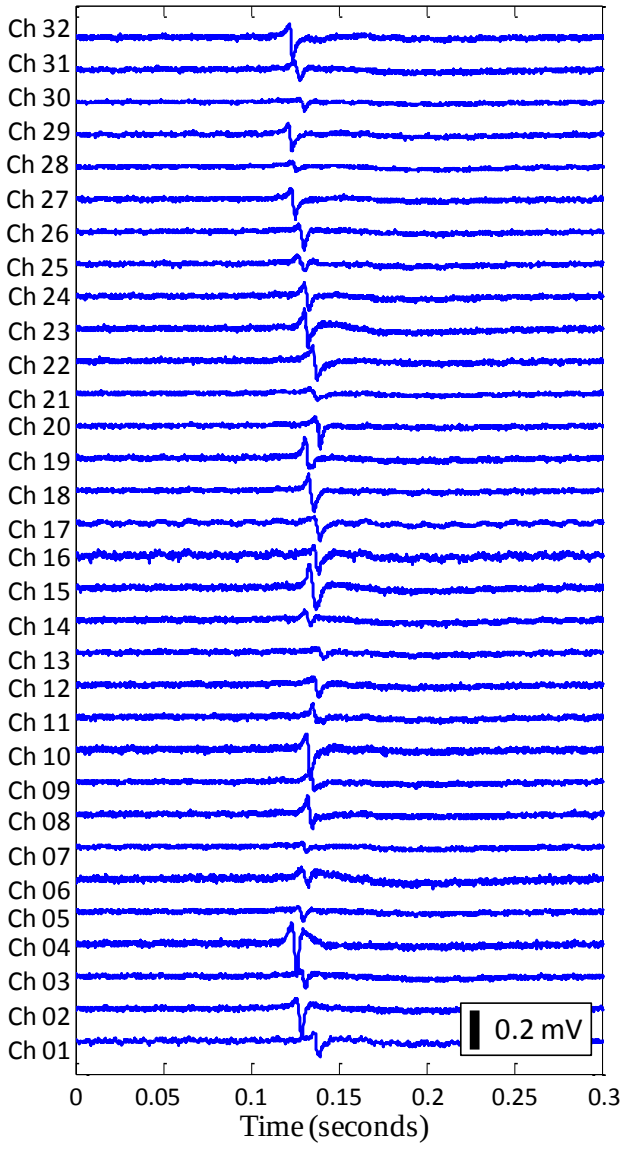


**Figure 3.2** Extracellular action potentials from murine HL-1 cardiomyocytes after one day of plating are observed in real time using the MEA on all 32 channels. Each trace represents a single channel over time.

potentials may vary based on the orientation of the cells over a microelectrode and the degree of physical coupling at the surface.

As previously described in Chapter 2, the morphology of the extracellular action potential may be considered a function of the second derivative of the intracellular potential. The amplitude of the extracellular signal is therefore heavily influenced by the rate of the upstroke in the intracellular action potential. Other parameters that can be extracted from an extracellular action potential include the duration of the up- and down-stroke, the maximum slope of the down-stroke, and the length of repolarization time. However, one of the major advantages of using an array of microelectrodes is the spatial resolution it provides in studying impulse propagation throughout a culture.

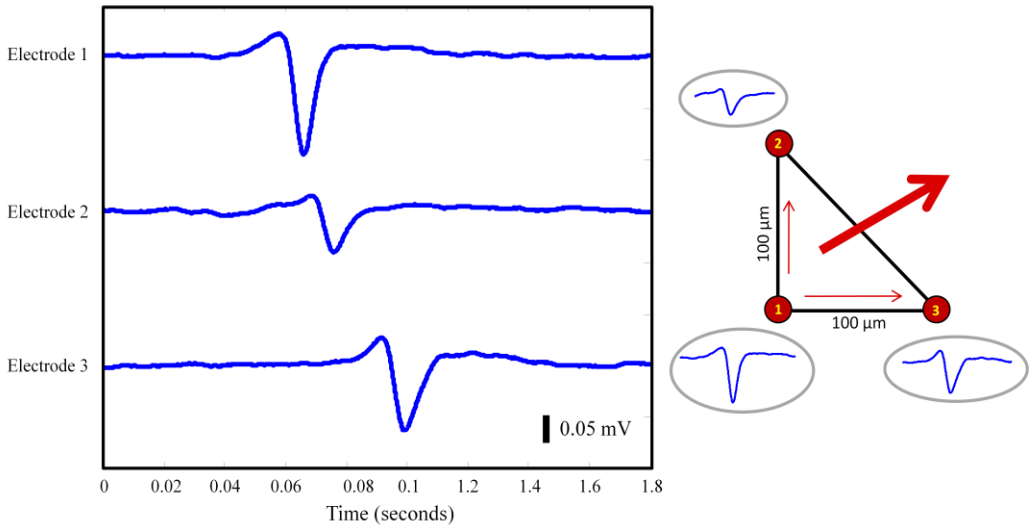


**Figure 3.3** Analysis of the conduction relied on finding the time delay between electrodes. The local activation time (LAT) was calculated by finding the time of the maximum negative slope. By correlating this timing with the spatial location of the electrodes, information on the direction and speed of propagation can be solved for.

### *3.2.2. Conduction Analysis*

Because each electrode in the MEA is located at a known spatial location, information on the conduction within a culture can be extracted by studying the time delay of an action potential between electrodes (Figure 3.3). By timing the action potential event at each electrode and correlating it to its spatial location, both the speed and direction of propagation can be estimated. The time that an action potential takes place is calculated by taking the first derivative of the signal and noting the time when the maximum negative slope occurs. This time is called the local activation time (LAT).

The propagation of electrical activity can be visually represented in two ways. The first is in a lateral isochrones map, which is formed from the LAT of each electrode in the array. A 6x6 array of LATs positioned according to its spatial location is normalized by subtracting the minimum time value from each position. Next, a cubic spline interpolation is performed between each LAT to generate a 41x41 pixel image of the conduction, termed a "phase plot." Values within phase plots are further fitted to a contour to create a lateral isochrones map that display the propagation pattern of the cells using different shades of color, as shown in Figure 3.4. The lateral

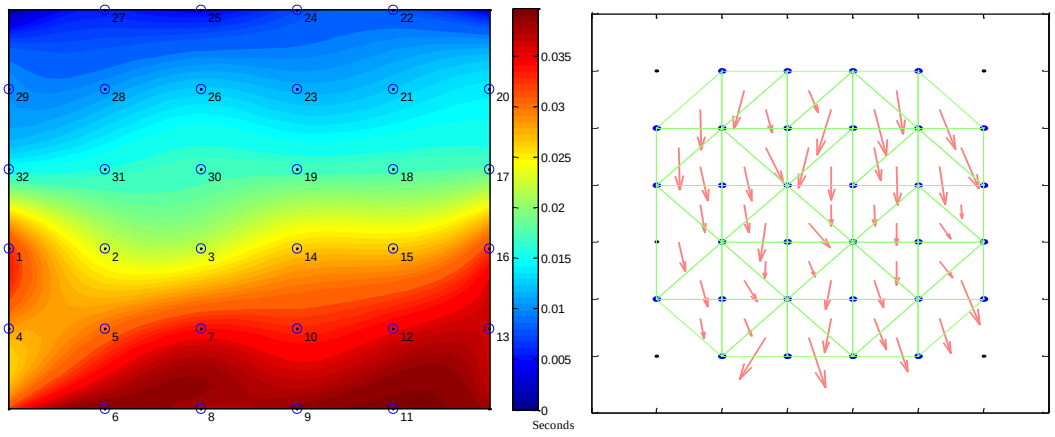


**Figure 3.4** The electrical propagation patterns over an MEA could be represented as a lateral isochrones map (left), or as a vector field (right). The lateral isochrones map is an interpolation of the time delay between electrodes, which is displayed by varying shades of color overlaid on a representation of the 6x6 MEA. The number next to each electrode corresponds to its assigned identification number. The depolarization wave is initiated in the blue region (time=0 seconds), and propagates towards the red region (time = 0.04 seconds). The vector field is calculated by grouping active electrodes by three, and solved for the direction and magnitude of the time delay. The average of each triplet vector could be used to calculate a global velocity value over the MEA.

isochrones map illustrates the initiation of a depolarization wave in the blue region, and propagates towards the red colored region.

A second way to represent conduction is in a field of velocity vectors. Electrodes that detect an action potential are grouped together by three, and for each "electrode triplet," the magnitude and direction of propagation are calculated as previously described by Bayly, et al.[84], and in Chapter 2 through equations 2.17 to 2.24. All velocity vectors in this field can be further averaged to generate a global velocity value of the entire culture over the MEA.

## 3.3. Heterogeneous Cell Cultures

Transplanted exogenous cells in the heart must be able to electrically integrate with myocardium or electrical pathways may be disrupted. Especially with graft stem cells that originate from a non-cardiomyocyte lineage, there is even greater concern because these cells may not immediately possess the necessary electrical characteristics to conduct an action potential. Even if transplanted cells were able to eventually form gap junctions and electrically conduct, a period of time is required for

proper integration. Until electrical integration takes place, transplanted cells may not play any functional role.

The presented MEA system and analysis techniques described in the previous section of this chapter provided a robust *in vitro* platform for studying the arrythmogenic potential following the introduction of stem cell grafts to myocardium. Co-cultures of murine HL-1 cardiomyocytes and the murine fibroblast cell line 3T3 were used to model the initial stages of stem cell transplantation when graft cells may not electrically conduct.

### *3.3.1. Cardiomyocyte-Fibroblast Co-Culture*

Electrical conduction in murine cardiomyocyte cultures was purposely disrupted by the addition of non-conducting murine fibroblasts. A series of co-cultures were created with varying proportions of HL-1 cardiomyocytes to 3T3 fibroblasts. A representative set of micrographs demonstrating the resulting cultures is shown in Figure 3.5, where cardiomyocytes and fibroblast can be distinguished by differences in cell morphology. In order to quantitatively confirm the differences between the ratio

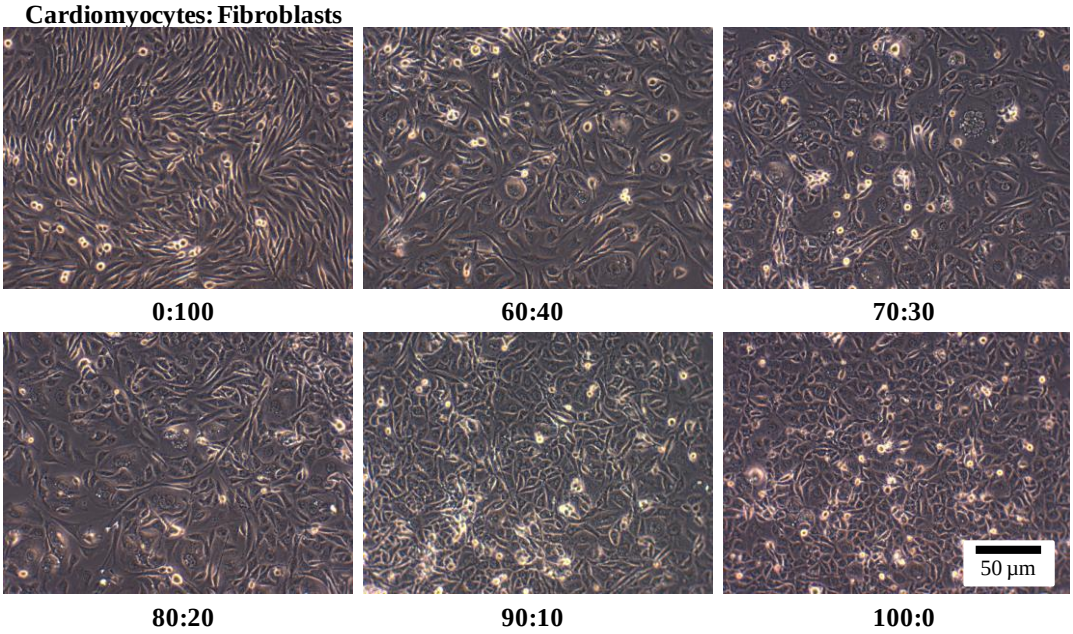


**Figure 3.5** Optical micrographs of co-cultures of murine HL-1 cardiomyocytes and murine 3T3 fibroblasts were created in varying proportions. The spindle shaped morphology of the fibroblasts was distinct from the more evenly proportioned cardiomyocytes.

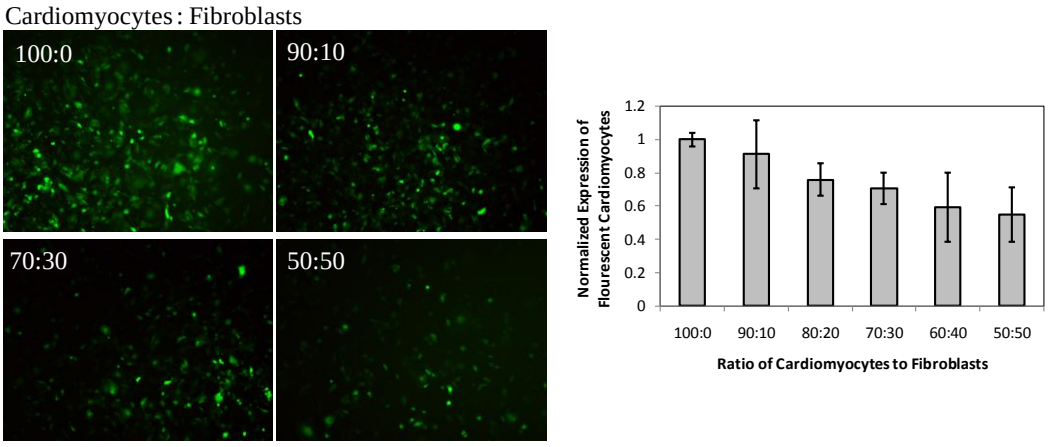


**Figure 3.6** The proportion of cardiomyocytes to fibroblasts were confirmed by imaging GFP expressing cardiomyocytes (Left). The relative expression of the emitted fluorescence was quantified, and demonstrated an appropriate increase in GFP expression as the proportion of cardiomyocytes increased (Right; N=3 per group).

of cardiomyocytes to fibroblasts and validate the co-culture method, HL-1 cardiomyocytes were transfected with a green fluorescent protein (GFP) marker through lentiviral vector LentiLox PLL3.7 [96]. Fluorescent imaging (450 nm excitation and 515 nm emission wavelengths) verified the relative differences between the successive proportions of cardiomyocytes as shown in Figure 3.6. Although the pure population of cardiomyocytes was confluent, GFP expression was not ubiquitous throughout the entire culture of transfected cells, and therefore fluorescent intensities were normalized to pure cardiomyocyte populations. Nonetheless, quantification of the overall expression of GFP through image processing revealed a trend of fluorescence appropriate to the proportion of GFP-expressing cardiomyocytes.

### *3.3.2. Thresholds for Electrical Conduction*

Heterogeneous cell populations were analyzed for the presence of electrical signals, with representative traces shown in Figure 3.7 (N=3 per group). Compared to a pure population of cardiomyocytes (100:0 ratio of cardiomyocytes to fibroblasts), a 50:50 ratio was observed as the threshold necessary to ensure any signal detection. In two out of three MEAs plated with this ratio, action potentials were sensed in only two channels, whereas the third MEA in the group did not display action potentials at all. It is likely that the population of fibroblasts inhibited electrical propagation through the

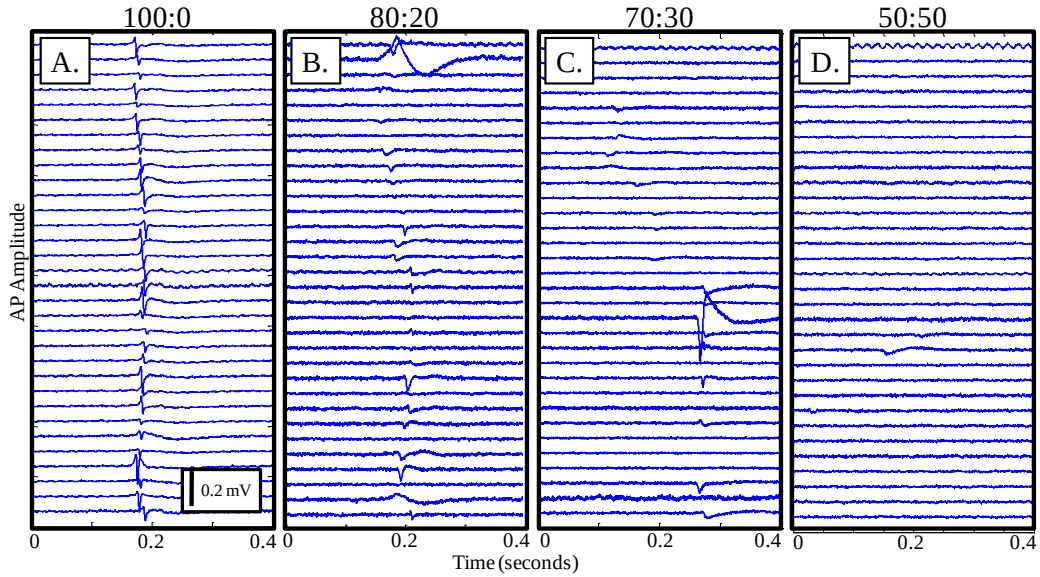


**Figure 3.7** Plot of all 32 traces on an MEA with different proportions of HL-1 cardiomyocytes to 3T3 fibroblasts. (A) Signals detected in 100:0 ratio control culture, (B) 80:20, (C) 70:30, and (D) 50:50 culture. Signals are only seen in specific channels in the 50:50 culture, with no sign of homogenous conduction, as seen in the 100:0 control group. The 80:20 and 70:30 cultures demonstrate intermediary behavior depicting groups of beating and non-beating cells.

HL-1 cardiomyocytes. Indeed, the observed rhythms were often asynchronous between channels, which demonstrated that the 50:50 ratio, while sufficient for islets of activity of about a square millimeter each, was not enough to support continuous conduction throughout the whole array.

Beginning from as little as a 30% proportion of fibroblasts in culture (70:30 ratio), samples delineated a similar asynchronous pattern of beating between 12±2 channels (N=3) and typically grouped into two beating patches of approximately six square millimeters each. An 80:20 ratio appropriately demonstrated a small depolarization wavefront throughout the heterogeneous population, with one large synchronous patch of beating that averaged 20±3 active electrodes (20 square millimeters). The number of electrodes that detected electrical activity is plotted as function of the cardiomyocyte to fibroblast ratio in Figure 3.8.

A lack of signal observed in ratios below 50:50 was likely due to insufficient cardiomyocyte connectivity to support conduction, or even electrical activity. Even an 80:20 ratio of cardiomyocytes to fibroblasts did not exhibit homogeneous conduction throughout the culture. Instead, patches of non-contractile tissue impeded the

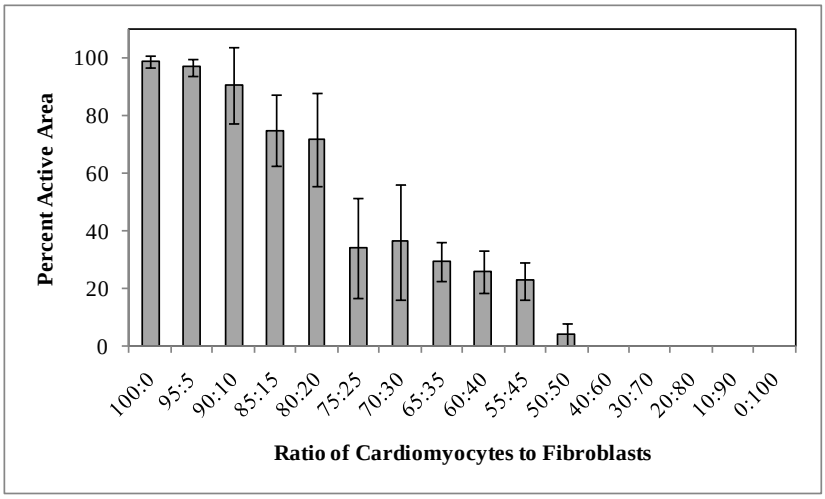


**Figure 3.8** Relationship between the proportion of cardiomyocytes to fibroblasts and the average number of electrodes detecting electrical activity (N=3 for each ratio, *P<0.05). Action potentials began to be consistently observed on multiple electrodes at a 70:30 ratio, although activity was not synchronous. With increasingly higher ratios of cardiomyocytes, larger regions of synchronous activity were observed. However, uniform propagation was only found in 95:5 ratio and pure populations of cardiomyocytes.

unidirectional propagation of the depolarization wavefront. By displaying the action potential propagation through vector fields (Figure 3.9), the pathway of conduction was unable to support a uniform depolarization wave across the culture.

Despite the value in analyzing conduction through vector fields as shown in Figure 3.9, it was difficult to quantitatively assess the uniformity of conduction. One direct method might be to measure the angle of individual vectors and calculate the standard deviation, which should increase as a culture becomes more heterogeneous. However, there are instances in pure cardiomyocyte populations where conduction patterns will fan outward depending on the proximity of the point source, leaving the angle of the initial set of vectors pointing in a very different direction compared to the terminal set of vectors. A more robust method of quantification must examine changes locally, and yet be able to yield results representative of the entire culture. In order to address this, a novel mapping technique using a "co-occurrence matrix" was developed as a quantitative metric of *in vitro* electrical conduction. Originally designed in 1962 by Julesz as a method for texture discrimination experiments [97], the co-occurrence matrix can be similarly adapted to studying the phase plots obtained from an MEA.

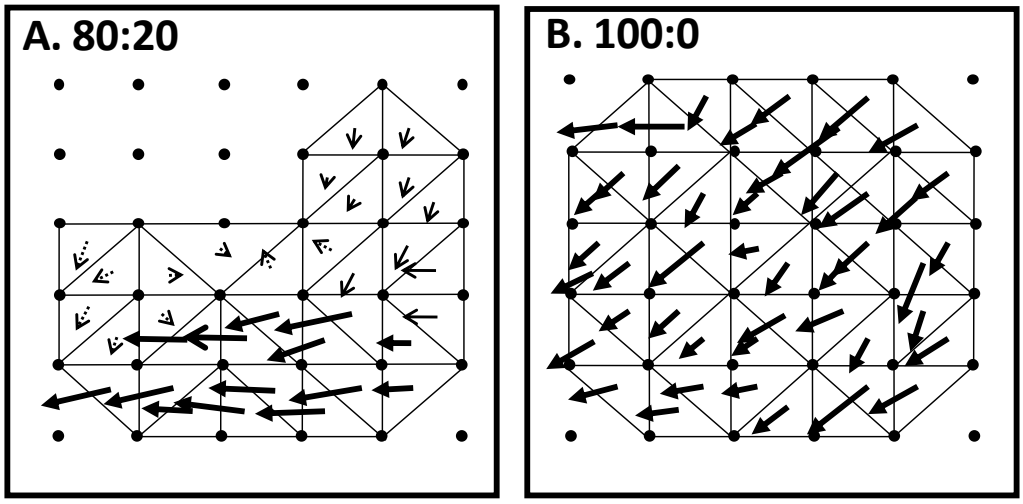


**Figure 3.9** Representation of conduction across a MEA using vector fields. (A) Propagation exhibited by a heterogeneous population of ratio 80:20 cardiomyocytes to fibroblasts where the conduction pattern is impeded by non-conductive fibroblasts. Smaller arrows depict inconsistent wavefront directions, and dotted arrows depict significantly slower velocities. Action potentials were not observed on all electrodes. Note the non-uniform propagation wavefront resulting from tissue heterogeneity. (B) 100:0 (pure) cultures of cardiomyocytes support continuous, almost unidirectional, propagation throughout the homogeneous population.

## 3.4. The Co-Occurrence Matrix

The co-occurrence matrix serves to map changes in the LAT into a form that would allow quantitative analysis of the consistency in a depolarization wave. The phase plot as described in Section 3.2.2 consists of a 41x41 array where each entry is an interpolation of LATs. Each entry in the phase plot is examined relative to neighboring entries at a specified distance and orientation from each other. The co-occurrence matrix *C(i,j)* is a collection of how often two neighboring coordinates "occur" on the array, one with LAT *i* and the other with LAT *j*. For example, if the co-occurrence matrix component *C(2,1)=8,* a LAT of 1 is next to a LAT of 2 a total of 8 times. Because the co-occurrence matrix is a transform based on LATs, its dimensions are dependent on the maximum LAT found within the phase plot.

**Table 3-1 Possible co-occurrence orientation vectors**

| x | y |
|---|---|
| 0 | 1 |
| 1 | 1 |
| 1 | 0 |
| 0 | -1 |
| -1 | -1 |
| -1 | 0 |
| -1 | 1 |
| 1 | -1 |

During the construction of the co-occurrence matrix, the distance between pairs of LATs can be set depending on the sensitivity required [98]; the more sensitive the analysis, the shorter the distance between pairs. For a fixed distance, LAT pairs are counted in eight directions, as shown in Table 3-1, where the direction is specified as a vector. Examining the occurrence of pairs in all eight directions effectively captures all possible pairs for any index location and its nearest neighbor. LAT pairs also do not take into account how the pair is ordered (2 to 1, versus 1 to 2 is irrelevant, for example), making the co-occurrence matrix symmetric

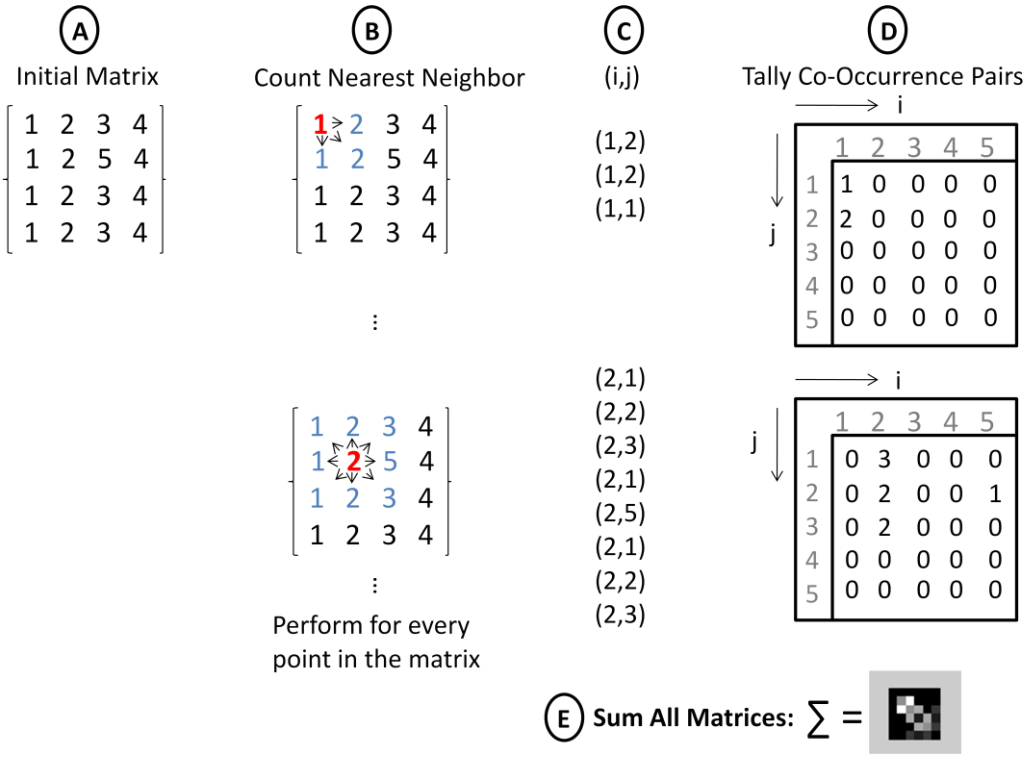


**Figure 3.10** Formation of the co-occurrence matrix is based on counting the number of times each LAT occurs in a phase plot. Within a given matrix of LATs (A), each entry is paired with its nearest neighbor (B), and noted (C). The values within each pair correspond to coordinates of the co-occurrence matrix, and number of occurrences are tallied (D). Steps B-D are repeated for each entry in the original matrix in (A), and final co-occurrence matrix is the sum of these matrices.

about its diagonal. In addition, because the matrix is a count of occurrences, the total number of co-occurrence pairs within phase plots of the same size is equivalent. This allows the matrix to be normalized by dividing each entry by the total occurrence pairs, making the co-occurrence matrix a collection of probability of occurrences. Analysis of phase plots was performed through Matlab (The Mathworks, Natick, MA), where the algorithm used to solve for the co-occurrence matrix is demonstrated in Figure 3.10.

Uniform conduction patterns would exhibit an array of LATs that change steadily as the depolarization wave propagates from one side to the other. This level of regularity creates a co-occurrence matrix with values heavily concentrated along the diagonal. On the other hand, non-uniform conduction patterns would exhibit inconsistent differences between pairs of LATs, yielding a co-occurrence matrix with values farther away from the diagonal. In addition, inconsistencies in phase plots may generate values clustered around various regions of the matrix. For example, if a depolarization wave was not evenly propagated through the surface, the co-occurrence matrix would indicate if a larger proportion of the activation times were either "early" or "late." A disproportionate amount of early activation times would result in a cluster of occurrences in the upper left corner while a disproportionate amount of late activation times would result in a cluster of occurrences in the lower right corner. The co-occurrence matrix is therefore a measure of uniformity.

The co-occurrence matrix can be summarized quantitatively by two separate metrics: energy and contrast. Both of these indicators represent key characteristics of the co-occurrence matrix, and are able to quickly portray the status of a depolarization wave. The energy of a co-occurrence matrix is the sum of the squares of each value, and is represented by Eq. 3.1 for a co-occurrence matrix *C* that is *n* by *m* large.

$$Energy = \sum_{i=1}^{n}\sum_{j=1}^{m} C^2(i,j) \tag{3.1}$$

The energy is a measure of the consistency of the co-occurrence matrix. While this is a useful value of whether there are many particular occurrences, it is not able to assess whether values are clustered along the diagonal or not.

On the other hand, the contrast of the co-occurrence matrix is focused primarily on determining whether a large proportion of the occurrence pairs are located along the diagonal. The contrast is calculated in a similar way as the energy, but values that are farther from the diagonal have greater influence.

$$Contrast = \sum_{i=1}^{n}\sum_{j=1}^{m}(i-j)^2 C(i,j) \tag{3.2}$$

As shown in Eq. 3.2, the contrast is a way to measure how far values in the co-occurrence matrix are from the diagonal by applying greater weight to the upper right and lower left regions. High contrast images would be representative of non-uniform conduction.

Examples of phase plots with their corresponding co-occurrence matrices are shown in Figure 3.11, and demonstrate how the energy and contrast are modulated based on the distribution of pixel intensities. A linear gradient of gray-tones resulted in a co-occurrence matrix heavily populated along the diagonal. With more complex images, the co-occurrence matrix contained values farther away from the diagonal. Asymmetric clustering in the corner or of the co-occurrence matrix was observed in

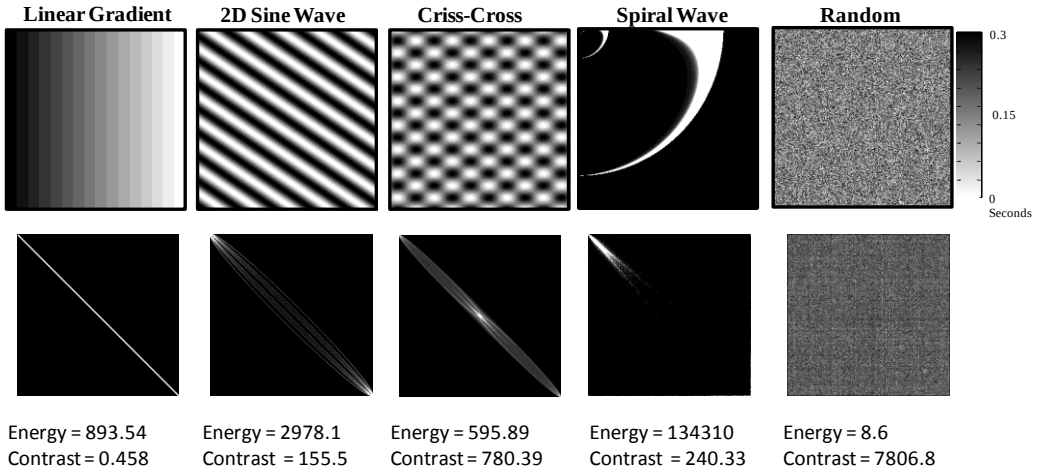


**Figure 3.11** The co-occurrence matrix demonstrated with a set of sample images. Each image consists of 300x300 pixels and exhibit grayscale intensities from 0 to 255 (top row). The corresponding co-occurrence matrices are displayed on the bottom row. Images that are uniform exhibit co-occurrence matrices that are clustered around the diagonal. The more an image is disordered, the farther away from the diagonal the co-occurrence matrix becomes. The energy and contrast values were all divided by $10^6$ for easier representation.

the spiral wave example, where the distribution of values in the image was heavily skewed towards early LATs, resulting in a large amount of co-occurring pairs in the upper left corner. It is important to note that the co-occurrence pattern is not necessarily representative of the geometric pattern (spiral wave), but only the local distribution of pixel pairs.

### *3.4.1. Analysis of Electrical Conduction*

A uniform conduction pattern observed from a MEA will exhibit LATs that consistently increase in the same general direction between electrodes, and produce a "smooth" phase plot. A co-occurrence matrix of such a phase plot will contain values distributed along the diagonal with relatively low energy and contrast. Co-occurrence analysis was applied to the work described in the previous section of this chapter to both quantify the uniformity of conduction within heterogeneous cultures, and validate this technique.

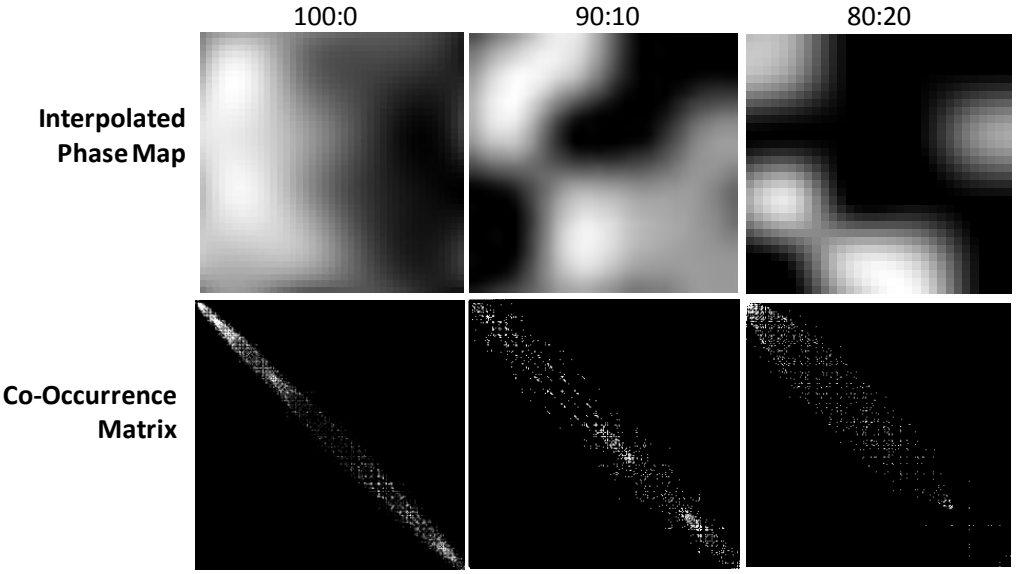


**Figure 3.12** Co-occurrence analysis was performed on heterogeneous co-cultures of murine HL-1 cardiomyocytes and murine 3T3 fibroblasts. Representative phase maps display the relative LAT from the MEA as a depolarization wave travels from the white region to the dark region. Three groups of cardiomyocyte:fibroblast ratios exhibited unique co-occurrence matrices, with values less distributed along the diagonal of the matrix as cultures contained a higher concentration of fibroblasts.

Phase plots were generated from each heterogeneous culture with electrical activity observed in at least half of the MEA, making a 20% concentration of fibroblasts the maximum threshold for electrical conduction. Analysis of samples with more than a 20% concentration of fibroblasts would be based more on the interpolated values than actual data, and were therefore not included in the co-occurrence analysis.

Visually, heterogeneous samples all exhibited co-occurrence matrices that were not evenly distributed along the diagonal (Figure 3.12). This suggested that there was an uneven distribution of time delays between the electrodes, with a greater proportion of cells being activated within a certain time than another. Even the 90:10 ratio of cardiomyocytes to fibroblasts, which was qualitatively the most similar to a pure culture of cardiomyocytes, displayed signs of this breakdown.

Co-occurrence matrices from each group (N=3 per group) were quantitatively assessed by calculating the energy and contrast in each one. Large changes in both of these metrics were observed as greater proportions of fibroblasts were increased (Figure 3.13). Variation within groups was small, as shown by the relatively small standard deviation between samples.

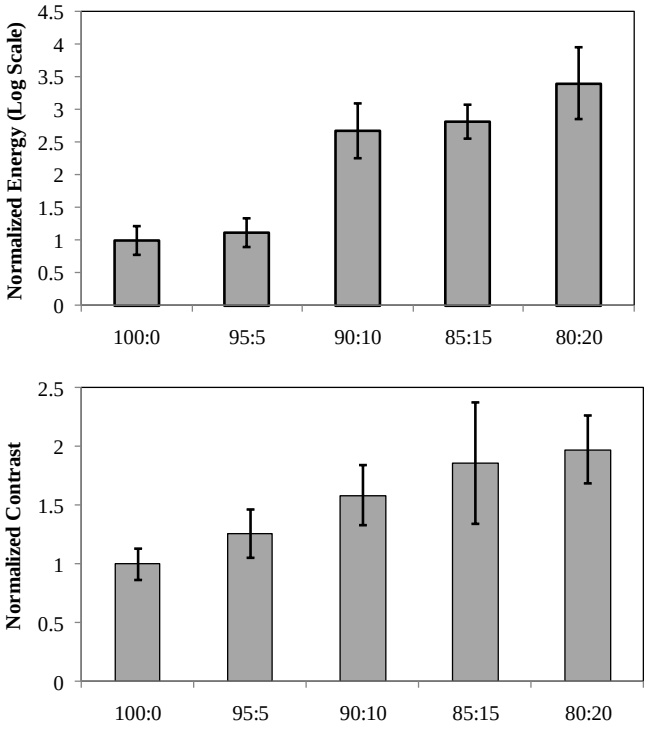


**Figure 3.13** Energy and contrast values were averaged for three co-culture groups, and normalized to the average value of the 100:0 group (N=3). Within both of these metrics, the 90:10 ratio was significantly greater than the 95:5 and 100:0 ratios, further confirming previous results that a 90:10 proportion of cardiomyocytes to fibroblasts severely disrupt electrical conduction.

Because the energy is the sum of squared values of the whole co-occurrence matrix, it will increase if

there is a large number of a particular pair of LATs. In this case, areas on the array that did not exhibit electrical activity would produce phase plots with regions that are all the same value. High energy therefore indicates inconsistency in a culture due to lack of conduction.

The contrast steadily increased as the concentration of fibroblasts increased in culture, but not as dramatically as the energy. As a metric that quantifies the deviation from the diagonal in a co-occurrence matrix, large contrast values will indicate increased disruption in conduction.

The significant changes observed in the energy and contrast supported the previous assumptions derived from Figure 3.9 that concentrations of fibroblasts greater than 10% of the total culture severely disrupted electrical conduction. It is fitting to infer from the data collected that a very high ratio (close to 100:0 cardiomyocytes: fibroblasts) is necessary to sustain a conduction that is homogeneous enough to prevent arrhythmic behavior. Thus, it can be concluded that though electrical activity was observed at relatively low ratios of contractile to non-contractile tissues, conduction was especially sensitive to any presence of fibroblast-like tissue. Following transplantation, the ratios of differentiated contractile tissue necessary for conduction must be better understood to avoid abnormal rhythms. While this model only considered a two dimensional environment, it can still be inferred that a nearly pure proportion of contractile cardiac tissue is necessary for proper conduction.

### *3.4.2. Finite Element Model and Analysis*

A finite element model was created to verify the co-occurrence analysis technique on heterogeneous cultures. Similar to the *in vitro* model using MEAs, this model consisted of a mixed culture of simulated cardiomyocytes and fibroblasts represented in a two-dimensional mesh containing a 41 by 41 grid of nodal points spaced 20 μm apart. Cardiomyocytes were represented as elements, and were constructed using parameters previous described by Goktepe and Kuhl in 2000 [99]. Fibroblasts in the model consisted of non-conducting nodes. A series of co-cultures were created consisting of varying proportions of cardiomyocyte to fibroblasts. A total

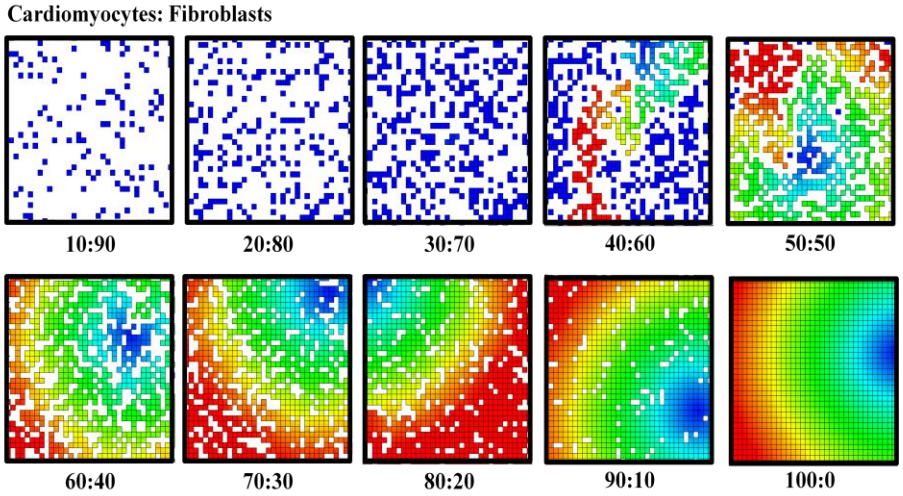


**Figure 3.14** Finite element models were created of mixed co-cultures of cardiomyocytes and fibroblasts in successive proportions. Within each group, a cardiomyocyte was chosen at random to initiate an electrical impulse. Similar to the lateral isochrones map in Figure 3.4, early stage depolarization is shown in blue (time = 0), while late stage is shown in red. A path for electrical conduction was not present until the culture contained at least 40% cardiomyocytes.

of twenty ratios were created from 5% cardiomyocytes to 100% in 5% increments. Each element was then given a corresponding probability to exhibit either cardiomyocyte or fibroblast properties. Depending on a generated random number, the element was then assigned the appropriate cell type. Within each mesh, a cardiomyocyte was picked at random to initiate an electrical impulse. Each stimulated culture was then assessed using a co-occurrence matrix based on its ability to propagate the depolarization wave. Each ratio was computed five different times, and representative conduction plots are presented in Figure 3.14. Excitation of the depolarization wave began in the blue region and propagated into the red region, similar to the lateral isochrones maps shown in Figure 3.4. Cells in the 10:90 to 30:70 groups all remained at the first time step and did not propagate due to a lack of conductive elements (cardiomyocytes), hence all elements were colored blue.

In order to quantitatively assess the resulting conduction patterns, a co-occurrence matrix was formed for each finite element model (Figure 3.15), and the energy and contrast values were calculated (Figure 3.16). By increasing the proportion of fibroblasts in culture, fewer co-occurrence pairs were situated along the diagonal, as observed by the growing increase in contrast. The energy, as plotted in Figure 3.16 on a log scale, had minimal change until the fibroblasts made up more than about 45% of

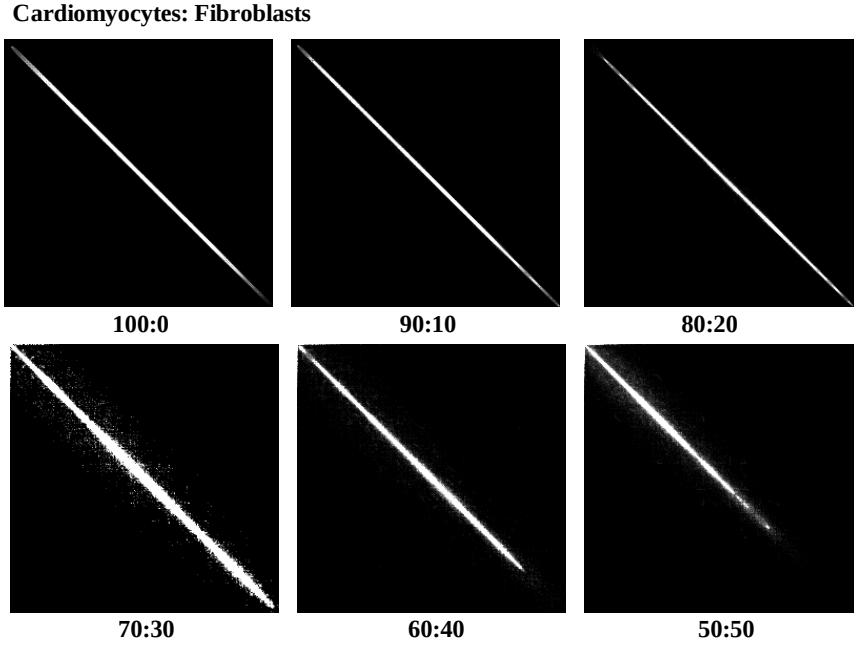


**Figure 3.15** Representative samples of co-occurrence matrices from finite element models of heterogenous cultures. As the proportion of fibroblasts increased, co-occurrence pairs were no longer as aligned along the diagonal, but began spreading outward.

the culture. As the proportion of fibroblasts increased, the energy began to increase due to large patches of non-conducting regions which led to large quantities of the same co-occurrence pairs. With more of the same co-occurrence pairs, fewer variations were observed, which led to the decrease in the contrast when fibroblasts consisted of more than 60% of the culture.

The analysis performed using a co-occurrence matrix on finite element models helped validate experimental results using MEAs, and demonstrated the co-occurrence matrix as a method sensitive enough to detect changes in conduction. The observed trends in the finite element model correlated well with experimental results on MEAs, but the threshold for conduction was much higher than expected. Compared to the 80:20 ratio of cardiomyocyte to fibroblast threshold from *in vitro* conduction measurements, conduction was observed in the finite elements model well past the 50:50 ratio. This could be due to a number of factors in the *in vitro* experiment, including the mismatch of cell shape, which is vastly different between spindle shaped 3T3 fibroblasts and round HL-1 cardiomyocytes. In addition, because HL-1 cardiomyocytes are a cell line, the portion of the culture undergoing mitosis may be

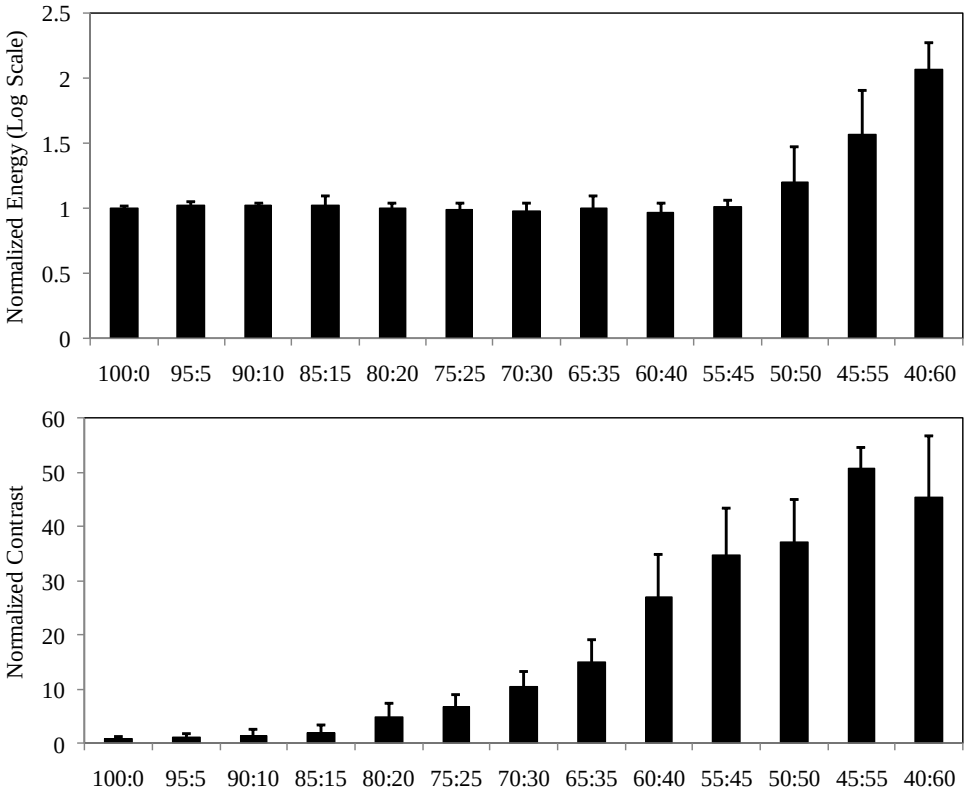


**Figure 3.16** Co-occurrence analysis on finite element models revealed trends as the proportion of fibroblasts increased. Disruption of conduction did not significantly change the energy value, but did heavily influence the contrast value. However, as the proportion of non-conducting fibroblasts made up the majority of the culture, larger regions did not exhibit any electrical activity leading to a sudden increase in energy. N=5 per group.

unable to conduct an action potential. This may significantly decrease the assumed concentration of active cardiomyocytes in culture.

## 3.5. Conclusions

An MEA platform was applied as a tool to study the risk of arrhythmia following stem cell transplantation of non-conductive cells. Examination of conduction block was first performed by noting the proportion of active electrodes in heterogeneous co-cultures of murine cardiomyocytes and murine fibroblast. However, standard methods of analysis cannot be used to quantitatively assess the degree of disrupted conduction patterns within electrically active areas. In order to address this,

a mathematical transform known as a co-occurrence matrix was developed to quantitatively assess the uniformity of conduction in phase plots. The method was applied to data from heterogeneous co-cultures, and could distinguish differences between uniform (100:0 and 95:5 cardiomyocyte to fibroblast ratios) and disrupted (more than 5% fibroblast concentration) conduction plots. The co-occurrence matrix was very robust in quantitatively analyzing the uniformity of conduction, revealing a very high sensitivity of cardiomyocytes to conduction block from non-conducting cells.

The modeled graft cells used in co-culture are representative of undifferentiated stem cells (capable of cardiac differentiation or not) that may not be able to electrically conduct. Many studies have claimed that stem cells from different regions of the body have the ability to transdifferentiate into cardiomyocytes, but such plasticity remains controversial and may be accounted for by alternative explanations [58]. The mechanisms of any process leading to cardiomyocyte differentiation involve many factors, not the least of which is electrical signaling from host tissue. The coupling of electrically active cardiomyocytes to modeled graft cells described in this chapter successfully blocked conduction, but it has also raised questions about whether the coupling of cells may have influenced differentiation had the graft cells been a type of stem cell. The described method of co-culture did not allow different cell types to be distinguished for their roles in the integration process, which calls for a more advanced technique for studying stem cell integration. The next chapter will introduce a novel device to spatially separate and merge two cells types over a MEA to allow a more realistic model of host-graft interactions.

# 4 *In Vitro* Host-Graft Integration Model

## 4.1. Introduction

After demonstrating the dramatic inhibition of electrical signals from cardiomyocytes using non-conducting fibroblasts, further study of the mismatch in cell properties between host and graft tissue required additional tools. While many methods are available to study individual cellular properties, probing the interactions between multiple cell types remains challenging because of the difficulty in maintaining a proper microenvironment while examining parameters of interest.

Many cellular interactions have been studied with various cell types cultured together in numerous experimental systems. Utilizing microfabrication and more recently, micropatterning, investigators have achieved defined co-cultures by patterning biologically-reactive molecules on the culture surface prior to cell plating. These techniques have allowed the creation of stripes [31, 100], islands [33, 101] and other patterns of tissue for the investigation of cell-cell interactions or geometrical dependencies. The limitation of these methods was that patterning was often irreversible for the duration of an experiment. These methods of co-culture also involved a modified surface that resulted in changes to the cell-substrate interaction which may alter cell motility and function.

A new technique to study electrical interactions is presented in this chapter for the reversible separation of two populations of cells on the same surface (Figure 4.1). A divided surface was created using a laser-etched mold in the form of a small biocompatible ring bisected by a dividing wall. The dividing wall was only 50-100 μm thick in the culture area, achieving a narrow separation between the two cell culture chambers. The contact surface was planarized to allow isolation of two cell populations without the addition of a sealant or grease. Either of these substances may

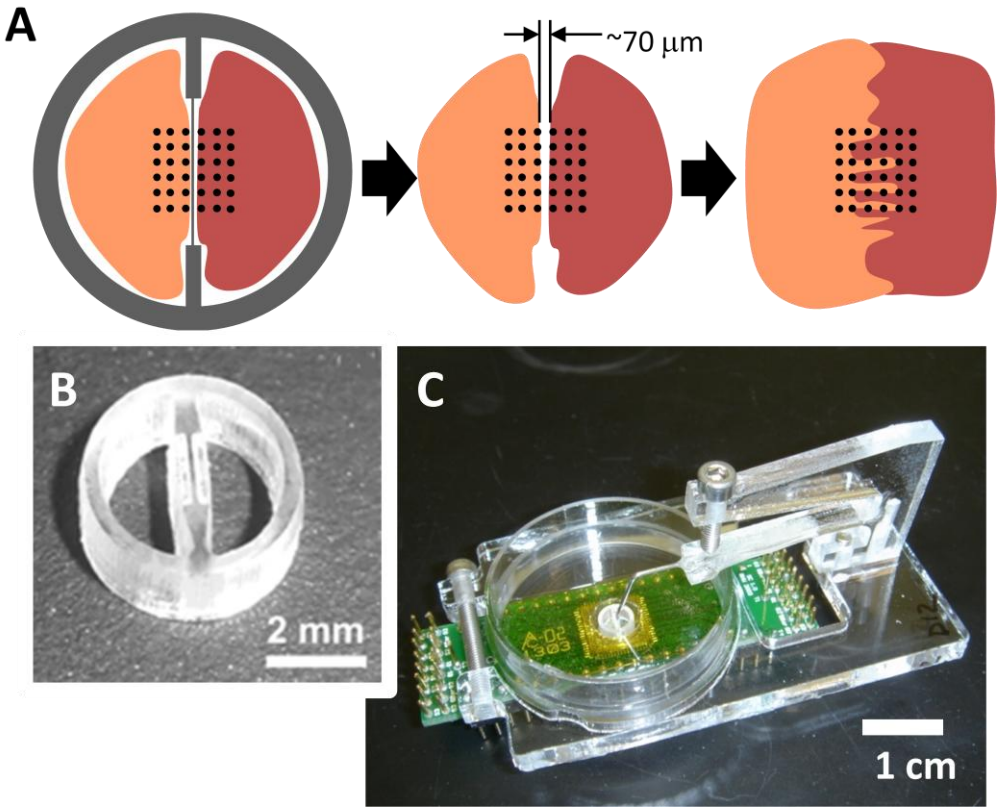


**Figure 4.1** Co-culture apparatus. (A) A co-culture wall divides the center recording array into 6 x 3 sub-arrays and allows analysis of the boundary between cultures. (B) The reusable acrylic barrier bisects the ring and defines two chambers. (C) The ring is held face-down in place with an accompanying support structure, consisting of a base clamped around the petri dish, and an overhanging arm contacting the ring through a 20-gauge needle.

leave residue on the substrate and impede cell migration, or worse, impair cell function. Using acrylic as a material for this device offered the additional advantage of being relatively low cost, yet durable enough to be reused following common sterilization techniques.

The co-culture ring defined two small, isolated chambers that could be seeded with cells individually. After the cells have adhered to the surface, the co-culture ring could be removed without disturbing the specific pattern of cultures. Without the barrier, the two cell populations could interact either indirectly through diffusible factors, or directly by establishing cell-cell contacts over time to form a connected, heterogeneous culture.

Traditional *in vitro* methods such as voltage- or calcium-sensitive dyes and optical contraction assays can be applied in concert with the co-culture ring.

Nonetheless, combining this co-culture technique with microelectrode array (MEA) technology [28] was done to provide real-time, non-invasive, and long term electrical monitoring of two distinct populations. With the barrier in place over a MEA, it was possible to culture two distinct cell populations on the same device, and following removal of the barrier, measure differential responses. Validation of separation was performed by demonstrating differential responses in the beat rate and action potential amplitude between co-cultured wild-type and genetically modified murine cardiomyocytes.

In order to demonstrate this co-culture device as a method to model host-graft interactions, murine cardiomyocytes were cultured on one side of the MEA as a model host population, and skeletal myoblasts were cultured on the opposite side of the array to model a graft population. Skeletal myoblasts have been proposed as a possible candidate for cardiac cell therapy due to their autologous origin, exclusive differentiation into muscle-fiber cells, and high resistance to ischemia [15]. Although transdifferentiation into cardiomyocytes does not take place [57], skeletal myoblasts have been shown to properly integrate [102], electromechanically couple [103], and even fuse [104] with cardiac tissue. Specifically, C2C12 cells have been implanted into host myocardium in several animals studies [102, 104], which made them an ideal candidate to demonstrate the co-culture device as a model for cell transplantation. Studies have already provided evidence that cell transplantation may lead to pro-arrhythmic consequences *in vitro* [30] and *in vivo* when autologous myoblasts were transplanted in humans [23]. Electrical monitoring during the merging process between cardiomyocytes and skeletal myoblasts in co-culture provided real-time analysis of propagation patterns between them. In particular, it highlighted the mismatch in conduction velocity between the two cell types. Illustrating this change *in vitro* may provide a useful understanding of a possible pro-arrhythmic potential associated with cells that are not included in the cardiomyocyte lineage.

In contrast, murine cardiomyocytes were co-cultured with a cell type that includes the cardiomyocyte lineage: differentiating murine embryonic stem cells (ESC). Following several days of culture, electrical signals were observed on the graft

region, and the conduction velocity was not significantly different from that found in host.

## 4.2. Co-culture Device Development

The co-culture device was designed with AutoCAD software (Autodesk, San Rafael, CA), and machined by etching and cutting a 2.8 mm thick cast acrylic sheet (Chemcast GP; Plastiglas de Mexico, Bosques delas Lomas, Mexico) with a $CO_2$ laser ablation system (V-460 Laser Platform; Universal Laser Systems, Scottsdale, AZ). The device consisted of three parts: the ring (which is bisected by the barrier), the base, and the contact arm (Figure 4.1C). Following batch cutting, the rings were planarized with 1500-grit sandpaper, ultrasonically cleaned in 5% detergent, and rinsed in deionized water before use. The thickness of the wall separating cell cultures averaged 70±30 μm, measured from micrographs acquired following planarization.

The contact arm was attached to the base of the device through screw holes on the underside of the arm. A 20-gauge needle bent at a 45° angle was attached to the end of the arm with epoxy and contacted the ring to apply pressure, maintain a seal, and prevent movement. The flexible arm and needle were lowered into the co-culture ring by applying pressure from the top using a finely-threaded screw (0.5 mm pitch). Once the ring was in place, the needle from the over-hanging arm was attached to the co-culture ring using a room temperature vulcanizing (RTV) sealant (3140 RTV Coating; Dow Corning, Midland, MI). To remove the ring, the top screw was removed, relieving pressure from the arm, and returning it to its original position while lifting the attached co-culture ring without lateral motion.

### *4.2.1. Controlled Merging of Two Cell Populations*

To validate the ability of the device to separate cultures and demonstrate integration, HL-1 cardiomyocytes were cultured on both sides of the co-culture divider at a density of $2x10^4$ cells per chamber (Figure 4.2). Following the removal of the barrier, a defined separation was observed between cultures, with two asynchronous sets of action potentials (AP) detected over an MEA. Over the course of 24 hours,

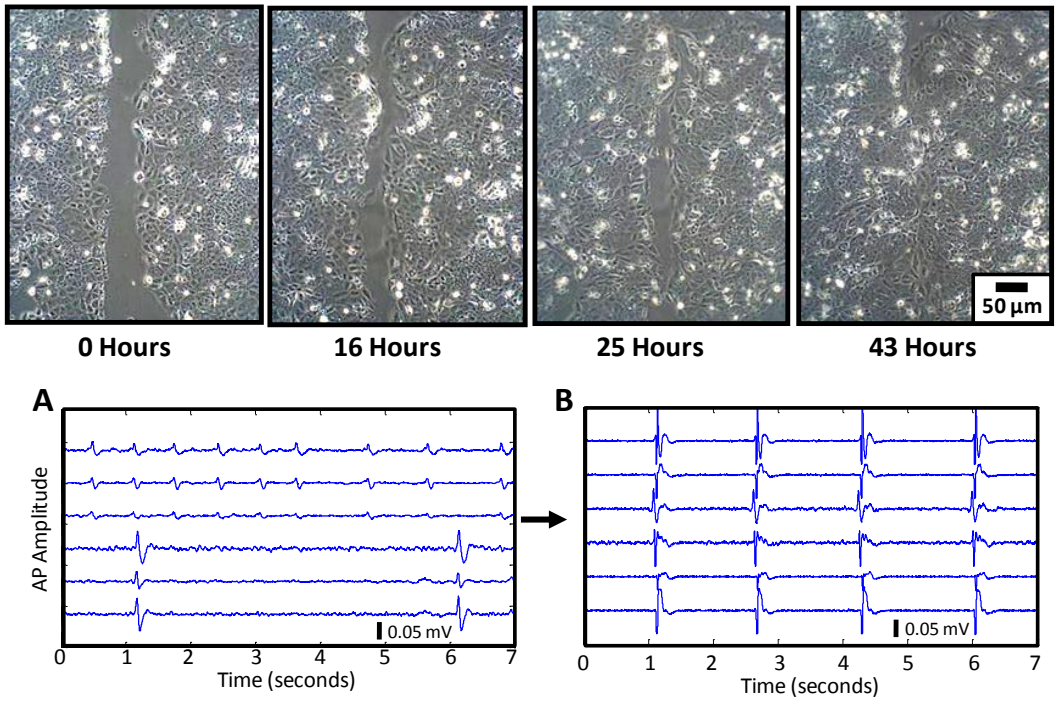


**Figure 4.2** (A) HL-1 cardiomyocytes were seeded on both sides of the barrier in a standard 35 mm Petri dish and allowed to merge. Initial cell contact was observed at 25 hours. (B) The same experiment was performed on a MEA, where two asynchronous sets of electrical signal were initially observed, but synchronized after merging also 25 hours after removing the barrier.

HL-1 cardiomyocytes merged and formed a confluent culture with synchronous electrical activity (N=5).

### *4.2.2. Analysis of Differential Signals*

The co-culture device was further used to examine differential responses between wild-type and genetically modified cardiomyocytes in order to verify the spatial separation between two cell types. This experiment was initiated by Whittington in 2007, but finished by Chen, et al. [29].

Neonatal cardiomyocytes from wild-type (WT) and $\beta_{1,2}$-adrenergic receptor knockout (DKO) mice were co-cultured at a density of $2x10^4$ cells per chamber and stimulated with the β-adrenergic receptor (β-AR) agonist isoproterenol (ISO). *In vivo*, β-ARs initiate cellular responses to sympathetic stimulation that lead to increases in the rate and strength of contraction. Cardioyocytes from DKO mice are not expected to respond to treatment with ISO while cardiomyocytes from WT mice should show

an increase in both action potential frequency and amplitude [105]. Different characteristic responses were observed in DKO-WT cardiomyocyte co-cultures depending on whether they were in a separated or merged state, illustrating the relationship between role of secondary messenger signaling and cell coupling.

Separation of the cell populations was verified by microscopy and the presence of asynchronous action potentials from the two cell types on the MEA (Figure 4.3B). DKO cells exhibited a higher beat rate and lower action potential amplitude than WT cells, but were still within the range of normal activity. Shortly after the barrier was removed and the two populations were still separated, the co-cultures were exposed to 10 µM ISO. The WT cells responded to ISO with an initial increase in beat rate and action potential amplitude, followed by a bursting rhythm of contractions (N=7,

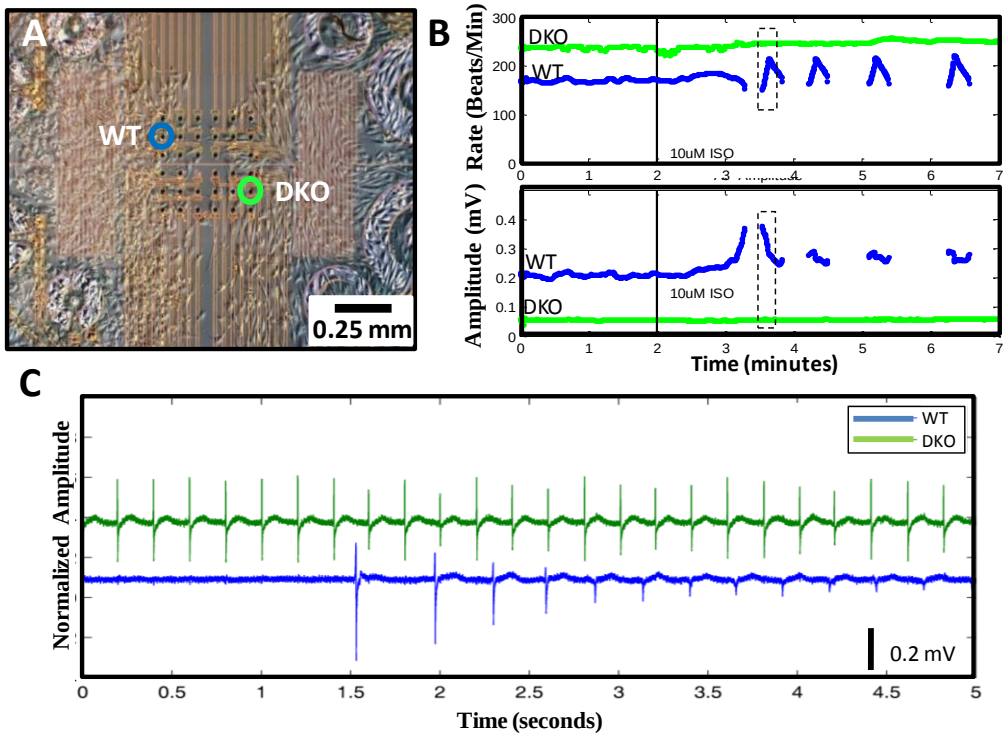


**Figure 4.3** (A) Following removal of the co-culture device, cells were divided over the surface of the MEA and exposed to 10 µM ISO. (B) A differential response between WT and DKO cultures was observed in action potential rate and amplitude as shown from two representative electrodes. WT activity displayed a bursting rhythm of contractions while DKO cells did not respond due to a lack of appropriate receptors. The spaces in between WT data points indicate no activity. (C) Extracellular action potential traces during the time indicated by the dashed boxes in (B) are shown during ISO exposure, revealing the change in action potential amplitude in the WT cells as a result of the bursting contraction behavior.

Figure 4.3C). This response was consistently seen optically in WT cultures in the presence or absence of co-cultured DKO cells. The action potentials measured on the side of the MEA containing DKO cells were not modulated.

After removal of the barrier, the two cell populations began to migrate across the resultant space and form electromechanical connections. The co-culture behaved as a syncitium with a single synchronous beat rate that increased in response to ISO treatment. Addition of 10 µM ISO caused the AP amplitudes for WT cardiomyocytes to increase, while the AP amplitudes for DKO cardiomyocytes increased only marginally, as shown in Figure 4.4A. In this particular example, the consistency among electrodes on each side of the MEA was demonstrated by analyzing each individual electrode, excluding the two columns of electrodes where the two cell populations had merged (only three representative traces from each side are shown in Figure 4.4 for simplicity). Amplitudes on the WT electrodes increased 2.43±0.26 fold over baseline ($P<0.05$), and were significantly greater ($P<0.05$) than the increase of

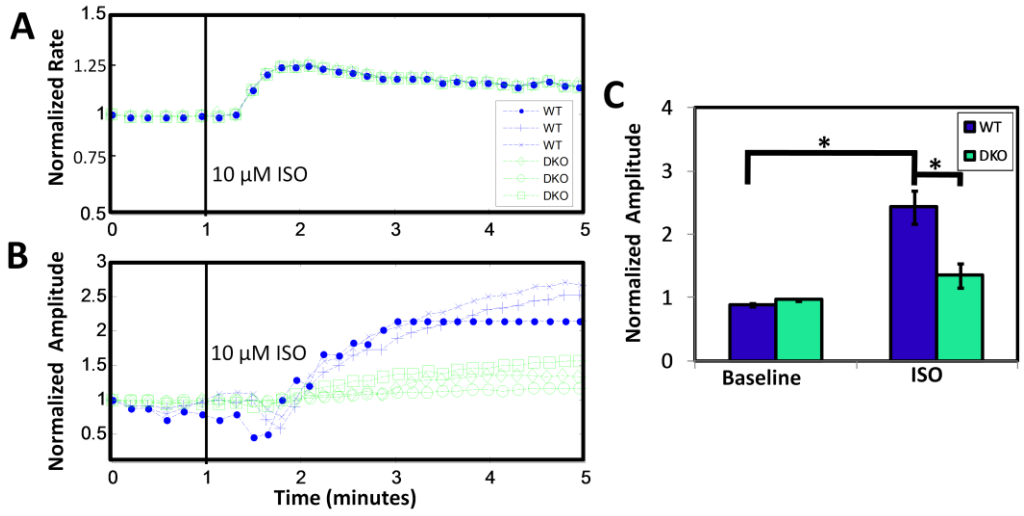


**Figure 4.4** The beat rate response of WT and DKO co-cultures in a heterogeneous population behaved as a single syncitium with synchronous rates of contraction across six representative electrodes. (B) WT cells responded with an increase in signal amplitude to 10 µM ISO, while DKO cells revealed a much smaller response that was likely due to the change of beat rate in both populations. (C) Analysis across electrodes within each region were consistent, and revealed a significant (*$P<0.05$, represented as a bar between significant groups) increase in WT culture signal amplitudes due to ISO exposure. Repeated trials (N=4) displayed similar significant increases in WT culture signal amplitudes without any bursting behavior as seen in Figure 4.3.

1.35±0.19 fold over baseline from DKO electrodes (Figure 4.4C). Similar results were observed in repeated trials (N=4) where on average WT cells increased in amplitude 2.40±0.67 fold, while the DKO cells increased 1.14±0.15 fold.

The observed differences demonstrated the ability of the device to separate two cell types, allow controlled merging over an MEA, and measure extracellular APs over the course of several days without any adverse affects on cultures.

## 4.3. Host-Graft Interactions

Following verification of the co-culture device to separate and merge two cell cultures over a single MEA, the co-culture device was applied as a model for studying host-graft interactions. Graft cells with properties inconsistent with those of the host may pose the risk of arrhythmia. If graft cells do not include a cardiomyocyte lineage, integration may still take place with host myocardium and graft cells may pass an electrical signal, but the resulting conduction patterns may not be consistent across the host-graft boundary. Non-cardiomyocyte cells may present differences in cell morphology, gap junction density, or ion channel distribution, which may all severely influence electrical propagation.

### *4.3.1. Merging Cardiomyocytes with Skeletal Muscle Progenitor Cells*

A host-graft model was first explored by co-culturing murine cardiomyocytes with murine skeletal myoblasts and studying their conduction velocity on opposing sides of the MEA. HL-1 cardiomyocytes (host) and C2C12 skeletal myoblasts were seeded into opposing sides of the co-culture chamber at a density of $2x10^4$ cells per chamber. Following one day of culture, the barrier was removed. Within 24 hours of removing the barrier, the two cell populations had physically merged on the MEA, as observed by microscopy. At this point, all channels displaying electrical activity were assumed to be originating from the host, which was validated by noting that the active electrodes were located on the appropriate side of the MEA. In longer term culture conditions (four days), electrical activity was also observed on the side of the graft

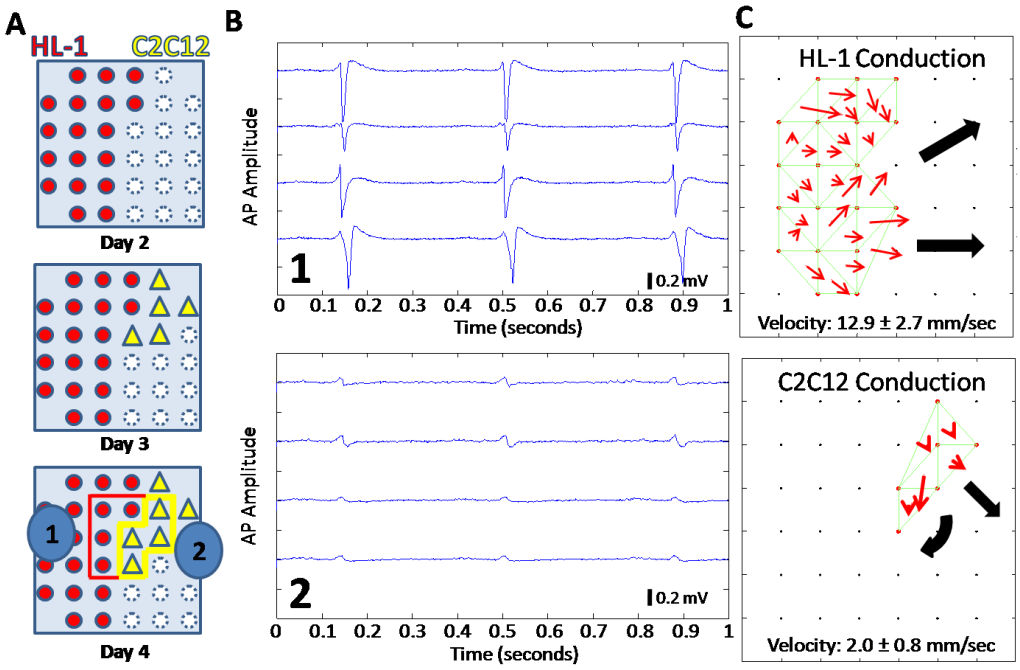


**Figure 4.5** HL-1 cardiomyocytes (host) were co-cultured with C2C12 skeletal myoblasts (graft). (A) A representation of the MEA displays electrodes after cultures have merged on Day 2. Electrodes displaying electrical activity on Day 2 were assumed to originate from the host, and are represented by solid circles. Additional electrodes on the graft side that previously did not display activity began exhibiting action potentials in subsequent days and are represented by triangles. (B) Activity from the highlighted electrodes are displayed for Day 4, showing a difference in amplitude between cultures, but still synchronous behavior (N=5). (C) Conduction analysis on both sides on Day 4 indicated that electrical activity originated from the host, and experienced a significant ($P<0.05$) decrease in conduction velocity on the graft side, as averaged across five beats.

cells, but primarily in the vicinity of cells bordering the cardiomyocytes (N=5; Figure 4.5A).

The action potentials originating from the graft side of the MEA, while synchronous, had lower amplitudes than simultaneous host action potentials (Figure 4.5B). Analysis of conduction patterns within the sample shown in Figure 4.5C also demonstrated a significant decrease ($P<0.05$) in the velocity of action potential propagation from 12.9±2.7 mm/sec on the host side, to 2.0±0.8 mm/sec on the graft side. Over all cultures (N=5), conduction velocity through the graft decreased to only 37±26% of the velocity through host tissue.

For all samples, conduction analysis indicated that action potentials originated from the host side and propagated into the graft side. This was confirmed by the addition of 10 µM ISO which should only stimulate cardiomyocytes [103] because

skeletal myoblasts lack the necessary β-ARs to appropriately respond. After ISO addition, all samples (N=5) remained synchronous and beat rates increased within a range of 12% to 130%. The amplitudes of the APs on the host side increased as expected within a range from 3% to 30%, while the amplitudes of the graft APs did not change more than 3%.

Analysis of the conduction using co-occurrence matrices was performed to quantify the degree of uniformity within the cultures. Phase plots were first generated from local activation times of the entire MEA, and cropped according to the region of analysis. Because HL-1 cardiomyocytes were electrically active over half of the MEA, the respective half of the phase plot was used to calculate the co-occurrence matrix. On the other hand, the only portion of MEA that detected electrical activity in the C2C12 region was limited to the boundary, so the phase plot was cropped around the respective region. Co-occurrence matrices calculated from different sized phase plots can be compared with each other because they can be normalized by the maximum number of co-occurrence pairs within the phase plot. Normalizing in this way makes the co-occurrence matrix

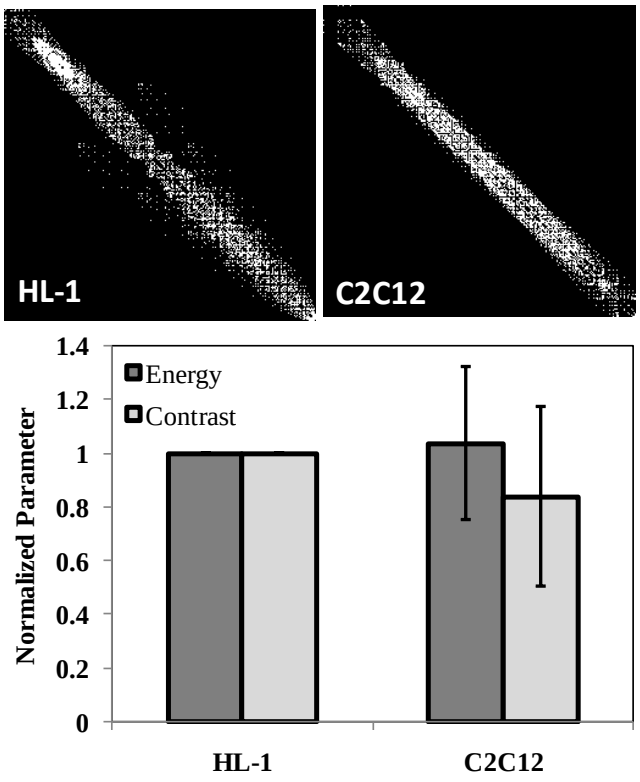


**Figure 4.6** Co-occurrence analysis was performed on the conduction of the HL-1-C2C12 co-culture. An example of co-occurrence matrices from a single co-culture is shown on top. Normalized energy and contrast metrics (bottom) did not exhibit significant differences, suggesting that conduction was fairly uniform in the cultures (N=6).

a distribution of the probability of co-occurrence rather than a tally of co-occurring pairs.

Despite the significant differences observed in the conduction velocity, no such changes were observed in either the energy or contrast values (Figure, 4.6). Instead, the energy slightly increased, and the contrast decreased, but not significantly since the standard deviation of both these values where quite high. Still, the lack of any clear differences between host and graft cell populations suggested that skeletal myoblasts are able to conduct relatively uniform depolarization waves, which is reasonable given the fact that they are a muscle cell line.

In order to rule out the possibility of that only passive conduction occurred within the C2C12 skeletal myoblasts and not the propagation of an action potential, a control study was performed using murine 3T3 fibroblasts as the model graft cell population. HL-1 cardiomyocytes and 3T3 fibroblasts were co-cultured for seven days, and while normal electrical activity was observed from HL-1 cardiomyocytes, no electrical activity was exhibited from the 3T3 fibroblasts (N=6).

Overall, the use of MEA technology allowed the examination of the electrical interface between host and graft cells, in which the limited ability of graft cells to conduct an electrical signal beyond the host graft boundary was observed. In the case of using C2C12 skeletal myoblasts, only the graft cells at the host boundary displayed action potentials, which typically did not extend past one or two electrode spacing lengths (100-200 μm). It has been shown that the early stage C2C12 skeletal myoblasts used in this study develop proteins for electrical connections (connexin43) and mechanical coupling (N-cadherin) within days of plating, but down-regulate these proteins as the skeletal myoblasts differentiate unless they are coupled with cardiomyocytes [103]. The absence of downregulated connexin43 likely explains why electrical activity was found only in graft cells close to the boundary and not further into the graft region.

Conduction is influenced by a number of factors, including cell size, orientation, gap junction density, or ion channel configuration [41], which makes a depolarization wave propagate differently through skeletal myoblasts as it would

through cardiomyocytes. The observed slowing of conduction velocity from skeletal myoblast populations demonstrated the unique ability of this model to examine electrical connectivity at, and propagation through, heterogeneous tissue boundaries.

### *4.3.2. Merging Cardiomyocytes with Murine Embryonic Stem Cells*

Despite evidence that non-cardiomyocyte stem cells such as skeletal myoblasts may integrate into myocardium *in vivo*, the resulting *in vitro* experimental data suggested that electrical conduction patterns are nonetheless affected. Graft cells may not conduct in a similar manner as host cells for the simple reason that they are not cardiomyocytes. To address whether stem cells grafts which include the cardiomyocyte lineage could appropriately match the conduction properties of host tissue, murine embryonic stem cells (ESCs) were co-cultured with murine cardiomyocytes.

The murine embryonic stem cell line ES-D3 (CRL-1934) was obtained from the American Type Culture Collection (ATCC; Manassas, VA), and were cultured in medium as previously described by Boheler, et al. [63]. ESCs were developed into embryoid bodies using the "hanging drop" method [106] to allow spontaneous differentiation to take place. Leukemia inhibitory factor (LIF), which is used to maintain an embryonic state, was withdrawn from the medium, and a cultivation of about 400 cells was suspended in 18 μL hanging drops to form an aggregate of cells termed embryoid bodies (EB). At this point, the differentiation stage of the EB was noted as Day 0. After two days, each EB was transferred into its own well in an ultra-low attachment 96-well plate (Costar 96-Well Microplate; Corning Life Sciences, Lowell, MA) for two days, after which they were further seeded onto 48-well plates. By Day 7, whole EBs were dissociated with collagenase B (Worthington, Lakewood, NJ) and cells were plated into the one side of the co-culture chamber at a density of $4x10^4$ cells per chamber. HL-1 cardiomyocytes were seeded on the opposing side of the co-culture chamber at a density of $2x10^4$ cells per chamber. The seeding density was determined based on the observed proliferation rates of both cell types to minimize the overcrowding of cells over time.

Following removal of the barrier, the two cell cultures merged within one day. After two days of merging (Day 3), synchronous electrical activity was observed on the side of the ESCs, implying cardiac differentiation. By this time, murine ESCs should have reached a differentiation stage that includes electrically active cardiomyocytes [63, 107]. At Day 3, impulse propagation originated from the host region, and only extended 100-200 μm into the graft region. Similar to the case with co-cultured C2C12 skeletal myoblasts, coupling of hESCs with cardiomyocytes may encourage cardiac differentiation.

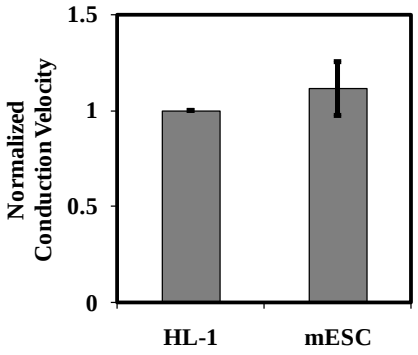


**Figure 4.7** Murine ESCs were co-cultured with HL-1 cardiomyocytes. After two days of co-culture, electrical signals were observed on the graft region of the MEA. Analysis of the conduction velocity did not display any notable changes between the two cultures

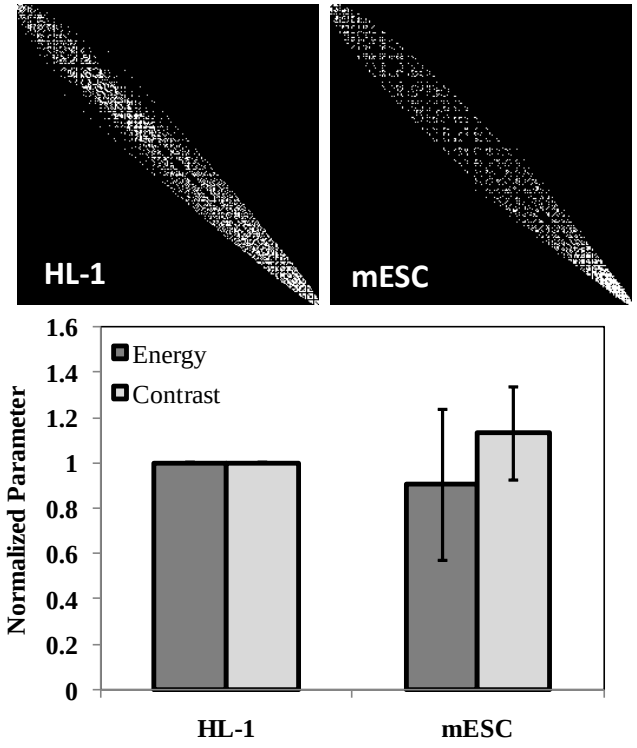


**Figure 4.8** Co-occurrence analysis was performed on the conduction of the HL-1-mESC co-culture. An example of co-occurrence matrices from a single co-culture is shown on top. Normalized energy and contrast metrics (bottom) did not exhibit significant differences, suggesting that conduction was fairly uniform in the cultures (N=9).

Analysis of the resulting conduction velocity showed no significant variation from that of host cultures (Figure 4.7; N=9). Instead, the observed depolarization wave appeared to propagate

unimpeded through the heterogeneous culture. Unfortunately, electrical activity decreased dramatically after three days, and is likely due to overcrowding of the MEA.

In spite of similar conduction velocities between the HL-1 cardiomyocytes and differentiating hESCs, it is possible that graft cells contained a portion of cells that could propagate a depolarization wave especially fast, but was impeded by non-conducting cells to bring the averaged conduction velocity lower. In order to address this, co-occurrence analysis was performed to examine the relative uniformity of conduction between the host and graft cell populations. Indeed, no significant differences in the energy or contrast were observed (Figure 4.8), implying that a relatively pure population of cardiomyocytes was differentiated within the graft region, and possessed conduction properties well matched with that of the host cell population.

## 4.4. Conclusions

A method was demonstrated for the reversible separation of two cell populations on an MEA through a physical barrier, which upon removal allowed cell growth and migration. Planar MEAs were well matched with the co-culture barrier technique because of the ability to record electrical activity in multiple regions of the culture simultaneously. The capabilities of this co-culture device were demonstrated using murine HL-1 cardiomyocyte cultures, murine neonatal cardiomyocytes with different genetic compositions (WT and $\beta_{1,2}$-AR DKO), murine C2C12 skeletal myoblasts, and finally murine ESCs.

The simplicity of the device lends itself to modifications to fit other experimental platforms, culture dishes, or microscope stages, and is further supported by its low fabrication costs and its ability to be reused. Because the barrier technique does not require surface coating of either the ring or the substrate, the separation of cells was reversible and not limited to specific cell types.

With a robust method of studying the electrical interaction of modeled host and graft cell populations, the next step is to apply this technique to more clinically relevant graft candidates. In particular, differentiating human embryonic stem cells

will be used as an *in vitro* model graft cell population in the next chapter to explore how coupling graft cells to a host cardiomyocyte cell population affects cardiac differentiation.

# 5 Trans-Species Host-Graft Integration Model

## 5.1. Introduction

Ever since human embryonic stem cells (hESCs) were first isolated by Thomson, et al. in 1998 [7], they have been under intense scrutiny as an ideal source of material for tissue regeneration. The ability to indefinitely proliferate and also differentiate into almost any cell type may enable hESCs to be used in a wide range of clinical applications. More importantly for cardiac tissue regeneration, hESC derived cardiomyocytes capable of electromechanical function [108, 109] have been shown to be able to integrate into the myocardium of various animal models [110-112]. However, as demonstrated in Chapter 4, integrating graft cells into myocardium may result in the disruption of conduction patterns due to mismatched electrical properties between host and graft tissues. Understanding how graft cells electrically interact with host cells is a critical step toward finding viable regenerative therapies.

Currently, all *in vivo* studies examining hESC engraftment are performed in animals and not humans. While trans-species models are appropriate given the unknown side-effects of hESCs in human, it is nonetheless of interest to explore the validity of these models. Undoubtedly, crucial insight into hESC behavior within a host have been obtained using animal models [111, 113, 114], but unless the issue of a conduction mismatch between an animal host and a human graft is resolved, it is difficult to translate such results into clinically relevant data.

In this work, trans-species stem cell transplantation was studied by focusing on electrical integration between murine cardiomyocytes and human stem cell grafts. The device developed for the reversible separation of two cell populations was used by culturing murine cardiomyocytes with two human graft candidates. The first graft was

modeled using spontaneously differentiating hESCs, whereas the second was modeled using late stage hESCs purified for cardiomyocytes.

In an effort to examine whether electrical pacing may mitigate the conduction mismatch between host and graft cell populations, co-cultures of murine cardiomyocytes and spontaneously differentiating hESCs were also subjected to continuous electrical stimulation at physiologically relevant levels. Many differences were observed in the graft's conduction characteristics between paced and non-paced cultures, which would suggest a significant role of the electrical environment during the differentiation process.

## 5.2. Culture of Human Embryonic Stem Cells

The hESCs used for both graft models were from the H9 lineage (WiCell Research Institute, Madison, WI) and underwent differentiation by embryoid body (EB) formation as previously described by Kehat, et al. [78]. After seven days of culture, floating EBs were gathered and seeded 0.1% gelatin-coated Petri dishes or microelectrode arrays (MEAs) to monitor the development of electrical activity and to determine the appropriate differentiation stage for subsequent co-culture experiments.

Spontaneous action potentials were initially observed beginning as early as seven days following EB formation, but no later than Day 14 (N=12 for optically observed EBs in Petri dishes). Beating was typically found to continue for over several

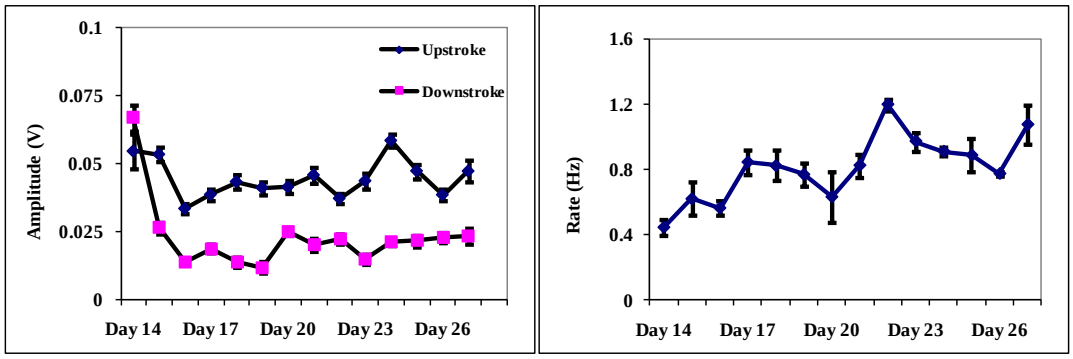


**Figure 5.1** An example of EB activity on a MEA over several weeks is shown. Action potentials collected from two minutes of recording each day were used to calculate the beat rate and action potential amplitudes. Over the course of two weeks, signals remained robust without any noticeable loss of activity.

weeks without showing any signs of degradation (Figure 5.1). Only one EB was recorded over a MEA due to the difficultly of seeding them directly over the recording array.

Whole EBs are not directly transplanted *in vivo*, they must first be dissociated into single cells prior to injecting them into a heart. Because EBs were found to typically start exhibiting electrical activity before Day 14, it was desirable to use a dissociated monolayer of electrically active hESCs shortly before Day 14. As a result, EBs cultured to Day 12 were dissociated using collagenase IV (Sigma-Aldrich, St. Louis, MO) and seeded onto MEAs. Beating was often observed within several focal points throughout the array within days after plating. Over time, cells around the focal beating points showed signs of differentiation, eventually leading to synchronized contractions (N=4; Figure 5.2).

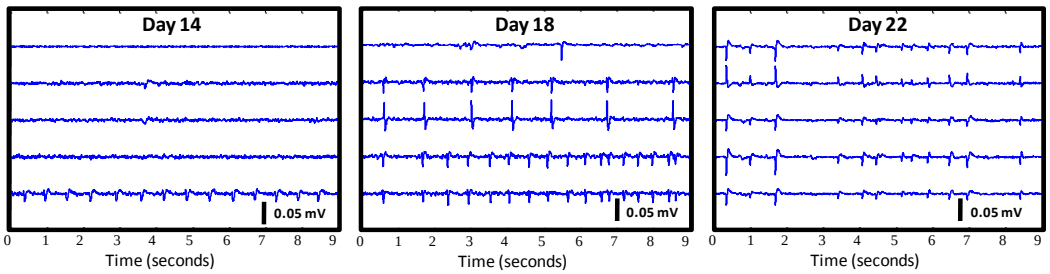


**Figure 5.2** Over the course of 22 days, different electrical patterns developed in human embryonic stem cells (hESC). Each trace in the above figure represents the raw signal from individual electrodes. Eventually, synchronized beating was sometimes achieved, as evidenced by similar electrical activity over all the active electrodes. These results were used to characterize the development of electrical activity and determined the appropriate differentiation stage of hESC to be used in co-culture experiments (N=4).

## 5.3. Co-Culture Validation

Before conduction was studied between modeled host and graft cell cultures, the co-culture device described in Chapter 4 was further tested to verify that cells on either side of the MEA do not cross the boundary after merging. Because previous co-culture experiments demonstrated beating only at the boundary, a major concern was that the HL-1 cardiomyocytes migrated towards the other side of the boundary over time.

In order to track the potential movement of cells, HL-1 cardiomyocytes were fluorescently labeled using a lentiviral vector LentiLox PLL3.7 to express green fluorescent protein (GFP) [96]. The separation of cultures using the co-culture devices was performed over 35mm Petri dishes to aid in visualizing fluorescent intensities. Non-fluorescent EBs were dissociated at Day 12, and seeded into one chamber of the co-culture device at a density of $4\times10^4$ cells per chamber along with HL-1 cardiomyocytes seeded in the opposite chamber at a density of $2\times10^4$ cells per chamber. The seeding density was determined based on the observed proliferation rates of both cell types to minimize the overcrowding of cells over time. After both cell populations had merged, cultures were optically tracked for six days to address any concern that cardiomyocytes may migrate into the graft region and mask any electrical signal from hESCs (Figure 5.3).

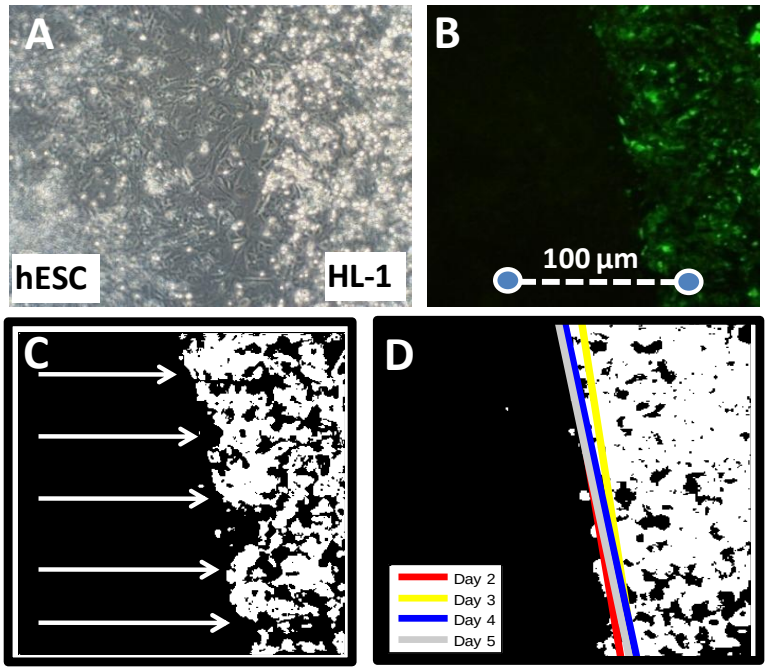


**Figure 5.3** A verification study was performed to ensure that any electrical activity observed by the MEA was not due to migrating cardiomyocytes. (A) Micrograph of hESC-HL-1 cardiomyocyte co-cultures after 6 days. (B) HL-1 cardiomyocytes were GFP labeled for optical analysis of the boundary. The scale bar indicates the distance between electrodes on the MEA in a fluorescent image (all images are at the same scale). (C) Fluorescent images were converted into a binary matrix, and the boundary was mapped. (D) A linear fit was then calculated using the point at the boundary, and the resulting line from each day was overlaid. Over the course of six days, the boundary moved only 5.7 ± 2.0 µm (N=5).

Fluorescent images (Figure 5.3B) were analyzed in Matlab™ (The MathWorks; Natick, MA) as a binary image where a white pixel indicated green color from GFP fluorescence (Figure 5.3C). A pixel was considered fluorescent if the green component of the color was greater than one quarter of the maximum (measured from 0 to 255). By choosing such a threshold, noise was not observed to be an issue in the identification of fluorescent cells.

The definition of the boundary was characterized by scanning each row of the image from the non-fluorescent hESC region towards the GFP-labeled HL-1 region, and noting the location that fluorescence was first observed. A linear fit of the boundary was then created for each image, which was used to characterize the boundary. The boundary lines from each day of co-culture were overlaid (referenced to a point made by a permanent marker on the culture dish), and the largest lateral movement was calculated for each sample (Figure 5.3D).

The average movement of the boundary was calculated to be 5.7 ± 2.0 μm (N=5), which is indicative of a very stable interface. Indeed, the spacing between electrodes (100 μm) is two orders of magnitude larger than the recorded movement of the boundary. It is therefore highly unlikely for HL-1 cardiomyocytes to migrate across the boundary and disrupt signals from the graft population.

## 5.4. Trans-Species Integration Model

The co-culture device was used in conjunction with MEAs to electrically map the conduction between host and graft cell populations. In Chapter 4, HL-1 murine cardiomyocytes were co-cultured with species-matched murine ESCs. Over time, electrical activity was observed on the side of the graft with a similar conduction velocity exhibited by the host culture. In this case, the use of human cells highlighted specific conduction issues with trans-species animal models. In particular, the co-culture method was used to examine whether the plasticity of spontaneously differentiating hESCs could allow them to differentiate into cells that match the conduction properties of the host murine cardiomyocytes. Analysis of the resulting

conduction was carried out by examining the conduction velocity and the uniformity of conduction of hESCs compared to host cardiomyocytes.

### *5.4.1. Cardiomyocyte Recruitment at the Co-Culture Boundary*

HL-1 cardiomyocytes (host) co-cultured with hESCs (graft) demonstrated conduction mismatches across both sides of the MEA over time. Following the removal of the barrier (Day 1 of co-culture), both populations of cells merged together within 24 hours. Electrical signals were confirmed as originating from the host side by correlating the microelectrode channels exhibiting activity to its spatial location. Between Day 3 to Day 4, additional action potentials were observed on the graft side (N=11) beating synchronously with the host.

By Day 5, the propagation velocity significantly increased to 2.6±0.8 times the conduction velocity from the host region (N=11; Figure 5.4). The conduction velocity within HL-1 cardiomyocytes, consistent with homogeneous HL-1 cultures, averaged 8.9±3.1 cm/sec, while the conduction velocity of the differentiating hESCs averaged

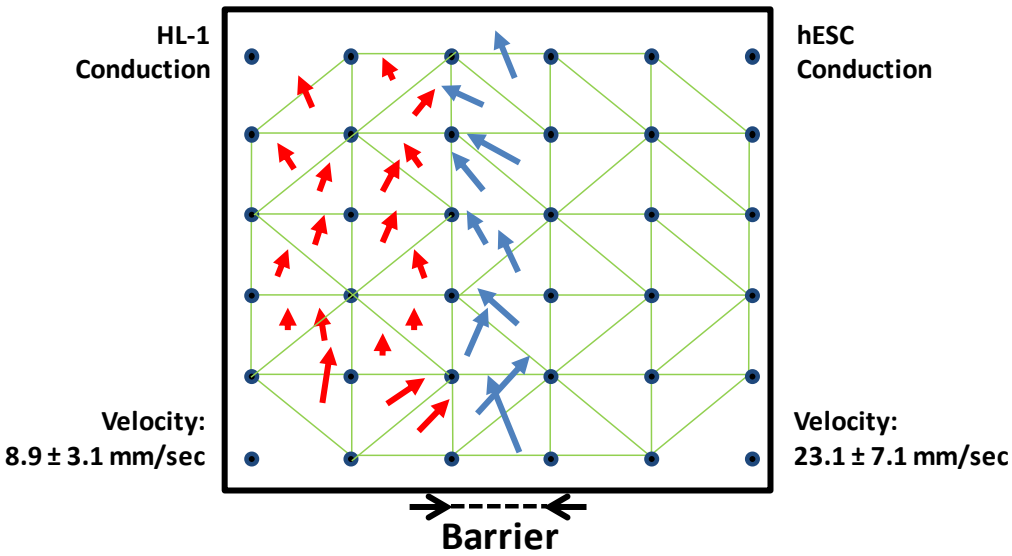


**Figure 5.4** Representative conduction map of host-graft model with differentiating hESCs. HL-1 cardiomyocytes (host, left) were co-cultured with differentiating hESCs (graft, right). By Day 5 of co-culture, additional electrodes on the graft region exhibited synchronous action potentials, with a conduction velocity significantly greater than host tissue. Over multiple samples, conduction velocity was 2.6±0.8 times higher than host region (N=11, $P<0.05$).

23.1±7.1 cm/sec. At this observed conduction velocity, it is likely that the graft cells have differentiated into atrial cardiomyocytes, which are reported to possess a conduction velocity in the range of 28 to 33 cm/second by Gelband, et al. [115].

The differences in conduction velocity between the host and graft cell populations may be attributed to inherent characteristics between human and murine cardiomyocytes. Studies performed by Walton, et al., on cardiomyocyte electrophysiology demonstrated that the conduction velocity is proportional to the square root of the maximum upstroke velocity in the transmembrane action potential, or $dV_m/dt_{max}$ [116]. The upstroke velocity is heavily dependent on the sodium current $I_{Na}$, and is therefore a unique property to each cell type. Atrial-like cardiomyocytes derived from human embryonic stem cells possess a $dV_m/dt_{max}$ that is 5.5 times higher than HL-1 cardiomyocyte [108, 117]. If the square root of the proportion of $dV_m/dt_{max}$ of atrial-like cardiomyocytes over HL-1 cardiomyocyte is taken, hESCs should have a conduction velocity 2.3 times greater than HL-1 cardiomyocytes (2.6 times observed), if all else was equal (cell volume, intracellular resistance, membrane capacitance, and peak membrane voltage). While this simple calculation cannot comprehensively explain the observed velocity mismatch, it does lend further evidence that trans-species animal models

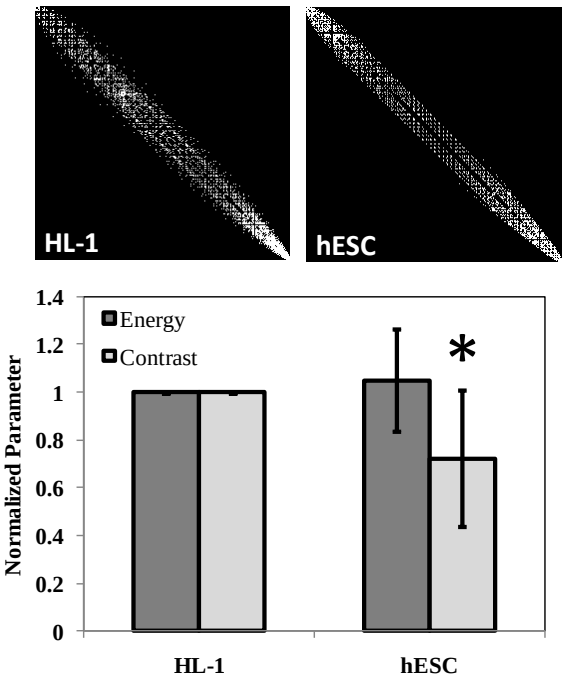


**Figure 5.5** Co-occurrence matrix analysis on co-cultures between HL-1 cardiomyocytes and normally differentiating hESCs (labeled "hESC") at Day 14. An example of co-occurrence matrices from a HL-1- hESC co-culture is displayed on top. Energy and contrast values are depicted in the chart below. Conduction exhibited by hESCs resulted in a slight increase in energy and a decrease in contrast (N=11; *P<0.05). Conduction within the graft region appeared even more uniform than in the host region.

may not be able to functionally integrate certain graft cells in myocardium due to their inherent electrophysiologic properties.

It is possible, however, that the depolarization wave observed within the hESC graft region was not uniform, which would cast doubt on the validity of an averaged velocity measurement. The uniformity of conduction within differentiating hESCs was quantified using a co-occurrence matrix. Phase plots of co-cultures were generated and divided into two parts appropriate to the region where electrical activity was observed. Each portion was then analyzed for its resulting energy and contrast values as described in Chapter 3. As shown in Figure 5.5, the co-occurrence matrices in the graft region exhibited steady energy values, and significantly lower contrast values than that of host cardiomyocytes. Such a decrease in contrast is especially indicative of a highly uniform depolarization wave relative to the pure population of host cardiomyocytes.

Negative control studies were performed using the non-conducting human fibroblast cell line IMR90 co-cultured with murine HL-1 cardiomyocytes. Normal signals were observed from cardiomyocytes, while no signals were detected from fibroblasts for up to 7 days (N=6).

### *5.4.2. Verification of Cardiac Differentiation.*

The presence of electrical activity in the graft regions of co-cultures implied cardiac differentiation, and was verified though immunofluorescent staining. GFP-labeled hESC cultures were co-cultured with non-GFP-labeled HL-1 cardiomyocytes for seven days, fixed, and stained for nuclei (DAPI) and either troponin-T (N=4) or gap junction protein Cx43 (N=4).

The results of fluorescent imaging indicated that cardiac differentiation does indeed occur at the boundary (Figure 5.6). GFP-labeled hESCs expressed both troponin-T and Cx43 at the boundary, but were not expressed in appreciable amounts more than ~200 μm away. Simultaneous observations of HL-1 cardiomyocytes were verified to express both troponin-T and Cx43, but not GFP in all cases. The immunofluorescent images were consistent with observations on MEAs, where electrical activity was observed primarily at the boundary of mature cardiomyocytes.

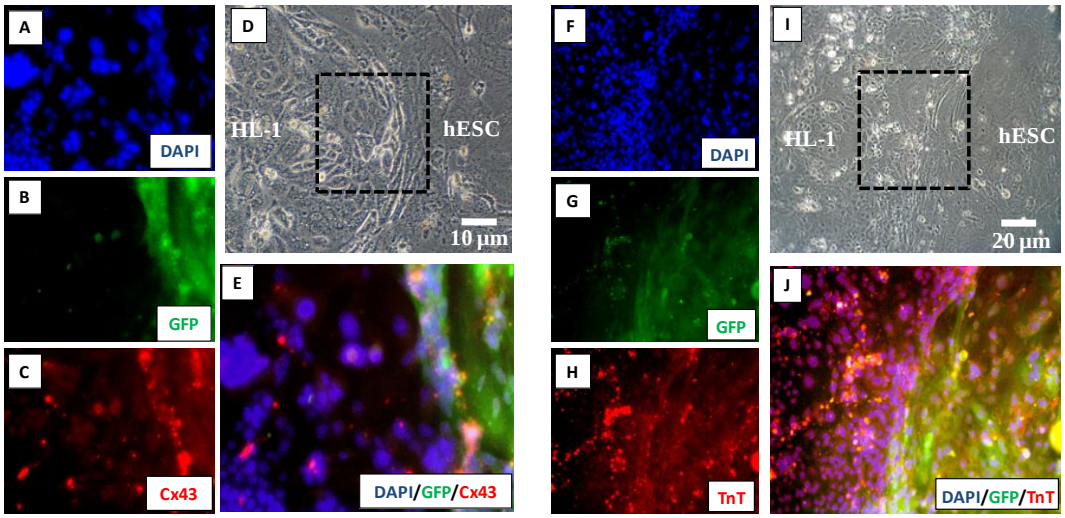


**Figure 5.6** Immunoflourescent analysis of the co-culture boundary in two samples. HL-1 cardiomyocytes and GFP expressing hESCs were co-cultures for seven days and fixed (D, I). Immunofluorecent imaging was performed in the region outlined in the dotted box for nuclei (A, F; DAPI), GFP (B, G), gap junctions (C; Cx43), and troponin-T (H). Images were also overlaid (E,J). Cardiac markers were observed at the boundary, but did not extend further than approximately 200 µm from the boundary. Similar results were found for cardiac troponin-T (N=4 with Cx43, N=4 with troponin-T). All images for Cx43 and TnT share the scale bar in images D and I, respectively.

## 5.5. Cardiomyocyte Purified Graft Model

The relatively low level of cardiac differentiation often observed with spontaneously differentiating hESCs is certainly not ideal for *in vivo* use. Not only may non-cardiac cells impede or disrupt conduction, but the prolific nature of hESCs may also lead to teratoma formation, as reported when transplanted into mice [118]. Despite efforts to condition hESCs for cardiomyocyte differentiation, the actual yield of cardiomyocytes tends to vary significantly, and almost never reaches a pure population. One common method for sorting cells from a heterogeneous population is fluorescence-activated flow cytometry (FACS). Unfortunately, FACS sorting is based on fluorescently tagging a surface marker that is specific to the cell of interest, and currently, there are no known surface markers specific to human cardiomyocytes. Instead, a purification method is often used based on the relatively large density of cardiomyocytes. In what is known as a Percoll gradient, heterogeneous cell populations are suspended in a gel-like solution that separates the cells by density. Using calibration standards, portions of the Percoll gradient containing cells that

possess the same density as cardiomyocytes can be extracted and prepared for further culture or *in vivo* transplantation [118].

To increase the proportion of hESC-derived cardiomyocytes in co-culture experiments, Percoll purification was performed as previously described by Cao, et al. [118] using late stage differentiating EBs (Day 25) in order to maximize the amount of mature cardiomyocytes. Day 25 EBs were dissociated using Liberase Blendzyme IV (Roche, Indianapolis, IN), and the resulting cell suspension was separated by Percoll density centrifugation. In order to assess the success of purification, a portion of the purified cells were fluorescently labeled for troponin-T and analyzed using flow cytometry. In this experiment, the proportion of cells expressing troponin-T reached up to 70%, as opposed to spontaneously differentiating EBs, which consisted of about 5-10% cardiomyocytes.

The higher proportion of hESC derived cardiomyocytes (labeled "PP hESCs") was expected to support a depolarization wave that could extend much farther into the graft region than before and provide a more complete map of electrical conduction

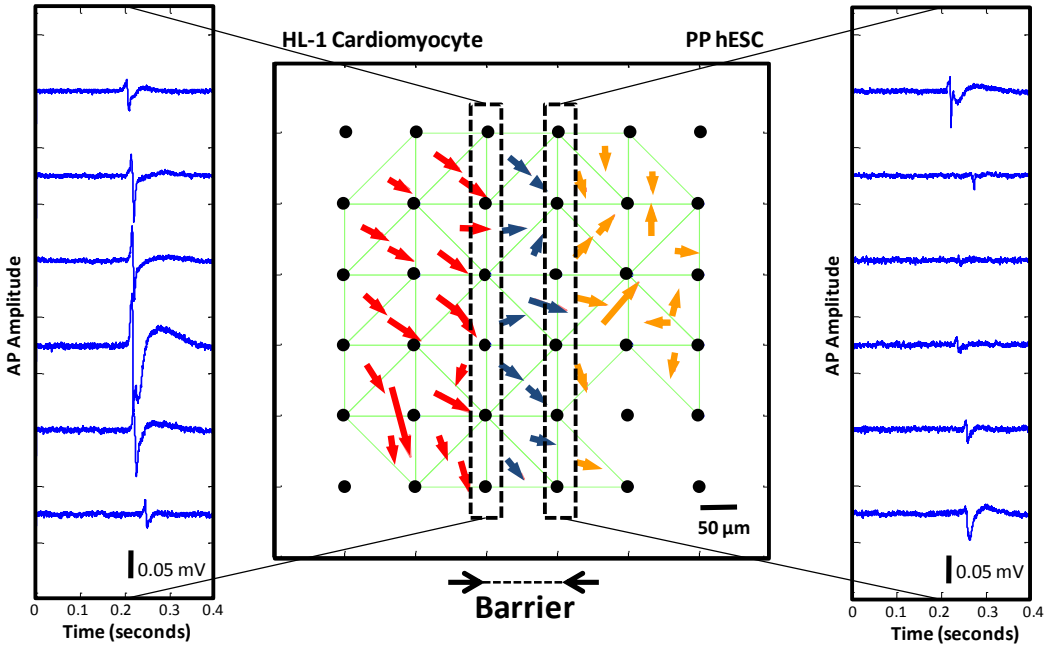


**Figure 5.7** EBs (Day 25) were purified using a Percoll gradient and co-cultured with HL-1 cardiomyocytes. A plot of the conduction over the MEA revealed that a depolarization wave can be passed from "host" to "graft," but the uniformity of the signal degrades past the boundary region. Action potentials observed on the "graft" region also exhibited smaller amplitudes.

pathways. After merging with host HL-1 cardiomyocytes, conduction on the graft region was observed almost immediately following the merging of cultures (approximately one day following the removal of the co-culture barrier).

Individual action potentials observed in the region of the graft were, in general, small in amplitude compared to those of the host cardiomyocyte signals. The difference in signal strength may be due to relatively immature cardiomyocytes, or imperfect coupling to the recording electrodes due to interference from non-conducting cells present in culture.

A representative map of the conduction displayed as a vector field is shown in Figure 5.7. A depolarization wave in the host region appeared unidirectional and uniform as expected, with an average velocity typical of HL-1 cardiomocytes at 10.5±6.7 cm/second. However, the direction of propagation began to diverge as the depolarization wave entered the boundary region, and the velocity significantly decreased to 46±21% from the velocity of the incoming depolarization wave (N=6; $P<0.05$). However, this decrease in velocity was clearly due to non-uniformities in the graft region, where it is assumed that non-conducting cells blocked conduction pathways.

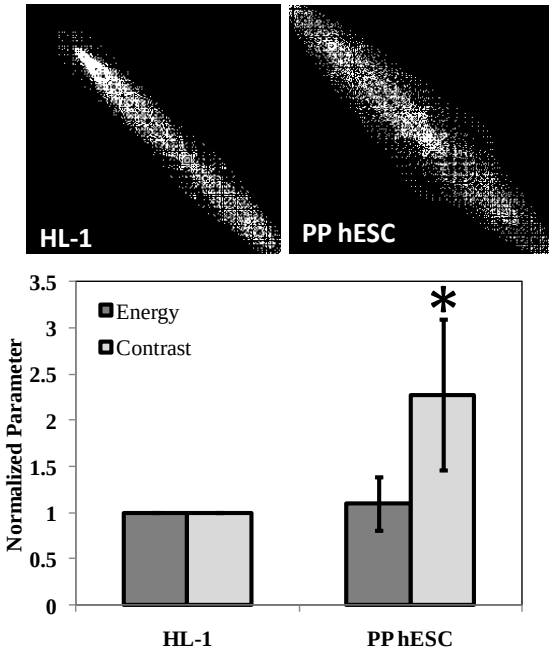


**Figure 5.8** Co-occurrence matrix analysis on co-cultures between HL-1 cardiomyocytes and Percoll-purified hESC at Day 25 (labeled "PP hESC"). An example of co-occurrence matrices from a HL-1- PP hESC co-culture is shown on top. Energy and contrast values are depicted in the chart below. PP hESC were highly non-uniform, with a significant increase in the contrast value (N=6, *$P<0.05$).

PP hESCs exhibited co-occurrence matrices that were not tightly clustered around the diagonal compared to the conduction in the host region. The energy did not significantly vary, indicating that in general,

electrical activity was observed throughout the region of analysis. Importantly, the contrast was notably greater in the graft region than in the host region by about 2.3 times. This significant increase in contrast would thus classify the conduction as non-uniform (Figure 5.8).

Co-cultures were observed for seven days in anticipation of improved conduction uniformity within the graft region. Instead, the conduction patterns did not change, but maintained similar conduction velocities, energies and contrasts as that on the first day of merging. Because PP hESCs were purified from later stage EBs, stem cells may have already reached a committed lineage.

By maintaining non-uniform conduction, it is clear that even a Percoll purification was insufficient to enable hESCs as an appropriate stem cell graft. In addition to having a mismatch of conduction properties between host and graft, the graft itself may have differentiated into unnecessary cell types that block conduction pathways and contribute to possible arrhythmia.

## 5.6. Electrical Stimulation of Heterogeneous Cultures

The observed differences between the co-cultured murine cardiomyocytes and hESC have prompted efforts to examine methods to either improve the yield of differentiation in the graft, or ideally, mitigate the mismatch between conduction properties of the two cell populations. As a preliminary effort towards this goal, the stimulation electrodes located on the outer region of the MEA were used to electrically pace the co-cultures during and after the integration process. Stem cells undergoing electrical stimulation have been shown to not only improve the yield of cardiac differentiation [67], but also to improve the ultra structural organization in three-dimensional tissue constructs [119]. It is hypothesized that at the very least, conduction uniformity should improve within a graft region following electrical stimulation.

HL-1 cardiomyocytes and spontaneously differentiating hESCs were co-cultured as described in Section 5.4.1. Once the barrier was removed, a biphasic, anodic-first square wave at 30 μA amplitude (24.9 $\mu A/mm^2$ current amplitude) was

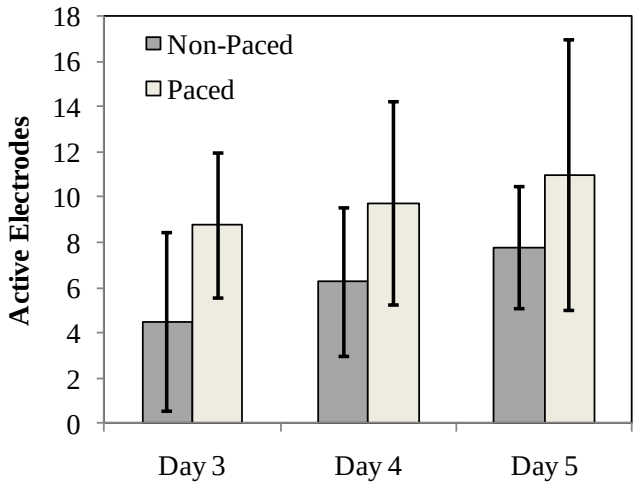


**Figure 5.9** Co-cultures of HL-1 cardiomyocytes (host) and differentiating hESCs (graft) were paced throughout the integration process, and the number of electrodes that displayed electrical activity within the graft region was counted. Paced samples displayed a consistently higher number of active electrodes, although the differences were not statistically significant (N=4 per group).

applied to all the stimulation electrodes in parallel at 1 Hz for the duration of the experiment. The maximum voltage swing was 0.5V, and within the window of hydrolysis [120]. The amplitude of 30 µA was chosen based on levels used to stimulate cardiac cultures [28]. The supporting hardware used to enable electrical pacing has been described previously by Chen, et al. [121] and is described in further detail in Chapter 6.

In both paced and non-paced samples (N=4 per group), action potentials were observed by Day 3 of co-culture until Day 5. After Day 5, most samples began exhibiting a sharp drop-off in the level of electrical activity, which was assumed to be from proliferative cells overcrowding within the MEA. The degree of cardiac differentiation was initially quantified by counting the number of active electrodes within the graft region of the MEA (Figure 5.9). In general, a consistently higher number of active electrodes were found in paced samples compared to non-paced samples, but was not statistically significant. The observed differences are nonetheless evidence of increased differentiation. Electrodes within the MEA are spaced 100 µm apart, so it is possible that this resolution was insufficient to properly quantify the degree of cardiac differentiation.

The average conduction velocity in the graft regions was greater in paced sampled than non-paced (Figure 5.10). By Day 5, the conduction velocity in paced sampled were 2.9±0.02 times that of the host velocity (26.0±0.2 cm/second). In non-paced cultures, the conduction velocity in the graft regions was 2.3±1.1 times that of

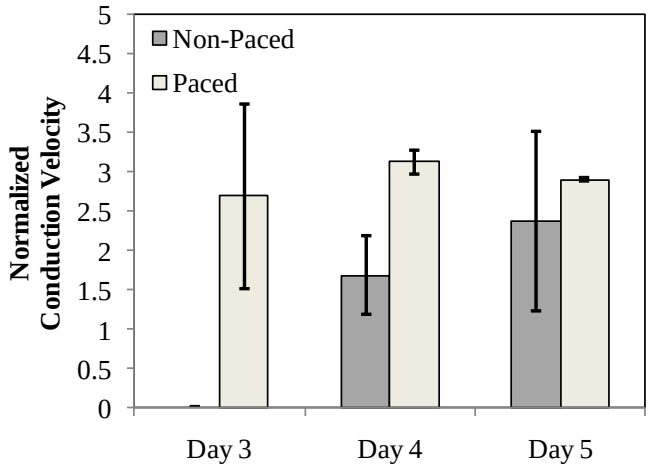


**Figure 5.10** Co-cultures of HL-1 cardiomyocytes (host) and differentiating hESCs (graft) were paced throughout the integration process, and the conduction velocity within each region was calculated and normalized to the velocity in the host region. No detectable conduction was observed on Day 3 in non-paced samples (N=4 per group).

the host velocity by Day 5 (17.4±3.5 cm/second). Strangely, the maximum conduction velocity in paced samples was observed on Day 4 at 28.0±1.4 cm/second, but was not dramatically different than the velocity observed on Day 5. It is possible, however, that pacing may have slightly increased the proliferation rate of cells in the hESC region, which may lead to non-conducting cell that impede the depolarization wave and lead to non-uniformities.

The uniformity of the depolarization wave can be measured using co-occurrence matrices. (Figure 5.11). Energy levels in the graft region normalized to the

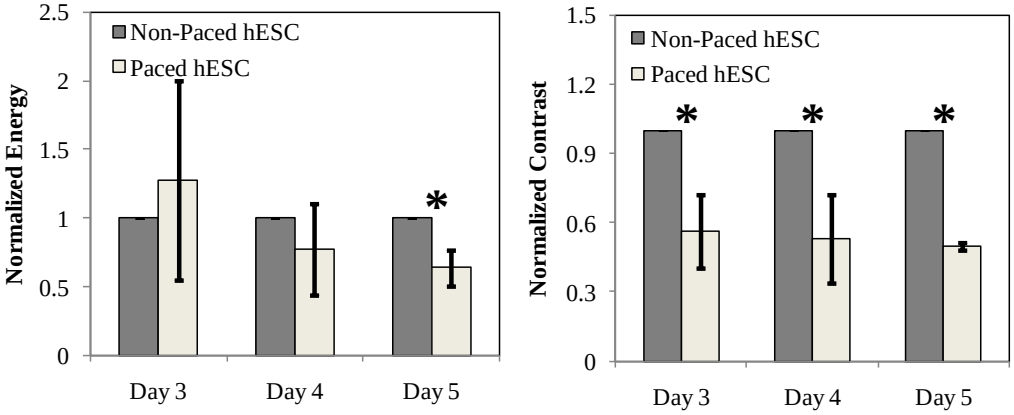


**Figure 5.11** Co-occurrence analysis of paced co-cultures of HL-1 cardiomyocytes (host) and differentiating hESCs (graft) demonstrated widespread differences between paced and non-paced samples. Energy levels remained relatively similar during Day 3 and 4, but dropped significantly by Day 5. A decrease in energy suggests a more distributed co-occurrence matrix. Contrast levels in paced cultures were significantly lower than non-paced cultures beginning on Day 3 (N=4 per group; *P<0.05).

energy in the host regions did not significantly change during Days 3 and 4, but decreased significantly by Day 5. As discussed in Chapter 3, a decrease in energy would suggest a co-occurrence matrix with evenly distributed values. Furthermore, a decrease in energy accompanied by a similar decrease in the contrast is an inference to a highly uniform distribution along the diagonal of the co-occurrence matrix.

The significant decrease in contrast within paced cultures was observed as soon as electrical activity was observed within the graft region of the co-culture. Throughout Day 4 and 5, the contrast levels of paced samples remained around 50% of the non-paced controls. The dramatic increase in conduction uniformity is a strong argument that there is a greater degree of differentiation among the graft cell populations due to electrical pacing.

The differences between paced and non-paced graft regions observed in the area of electrical activity, conduction velocity, and the uniformity of conduction is evidence that pacing is beneficial during the differentiation process. The stimulus amplitude used to pace the co-cultures was also not an optimized value. It is very likely that the differences between paced and non-paced cultures could be much more apparent if dose-response curves were created. Nonetheless it is of interest to note that the standard deviation of the conduction velocity, energy, and contrast all decreased over time, which is indicative of the level of control electrical pacing had on this type of co-culture environment. Without pacing, the only source of electrical stimulation would originate from spontaneously beating host cardiomyocytes located at the host-graft boundary. Moreover, the electrical activity from host cardiomyocytes is fairly irregular, ranging from 60-180 beats per minute. With electrical pacing, graft cells received a consistent level of stimulation from electrodes. In addition, if the same electrical pacing on the host region could consistently pace the host cardiomyocytes, stimulation at the boundary would be equally regular.

## 5.7. Conclusions

The observed changes in conduction between modeled host and graft cell populations validated the co-culture system as a method to address the effects of

electrical connectivity at, and propagation through, heterogeneous tissue boundaries. Indeed, the implication that cell transplantation may adversely affect the host system is a reminder that successful myoplasty must not only include functional integration but also the restoration of proper electrical conduction and intracardiac propagation.

The conduction model between host and grafts cells is also a powerful tool to examine and screen potential graft candidates. The boundary between incompatible, trans-species, cell types was clearly mapped by the presence of mismatched conduction properties between two cell cultures, exhibited by the differences in propagation velocity and in the uniformity of conduction.

Moreover, by electrically pacing co-cultures, a technique was initially explored for modulating the differentiation process. Pacing was able to improve the uniformity of conduction, and also enabled a level of consistency to the electrical environment. However, while the presence of improved electrical activity due to pacing may imply cardiac differentiation, it is not an undisputed claim. In the following chapter, the system used for electrical stimulation is further characterized to examine how long term pacing affects the gene expression in graft cell populations.

# 6 Electrical Stimulation of Embryonic Stem Cells

## 6.1. Introduction

The risk of arrhythmia following stem cell transplantation may be largely influenced by non-conducting, and often undifferentiated, graft cells. As demonstrated in Chapter 3, even a very small proportion of non-conducting cells may significantly alter electrical pathways in heterogeneous cells cultures. However, as graft cells remain coupled to myocardium over time, the interactions between the graft and host may play a role in their eventual differentiation into cardiac tissue. Within the heart, chemical signaling, mechanical stress, and electrical stimulation will all have a major impact on graft stem cells. While most of these processes are relatively well studied, the influence of electrical activity of the surrounding host tissue on graft differentiation and integration is poorly understood.

It is well known that during fetal development, electrical signals are present and may help guide stem cells towards a cardiomyocyte cell fate [67]. Similarly, it is reasonable to hypothesize that comparable stimuli may play a role in the differentiation and integration of stem cells introduced into host cardiac tissue. A system for *in vitro* electrical stimulation may provide further insight into the role of endogenous electric signals from native tissue, and also offer a novel way to control the differentiation and integration of implanted cells.

A study by Radisic, et al. demonstrated that electrical field stimulation over an eight day period increased the amplitude of synchronous contractions in a tissue construct of rat neonatal ventricular cardiomyocytes [119]. Stimulation also led to improved physiological structure and function, as confirmed by the presence of striations, gap junctions, and cell coupling. With murine embryonic stem cells (ESCs), the application of a DC electric field for 90 seconds over an embryoid body (EB) had

in certain cases doubled the yield of beating EBs [67]. However, cells in the myocardium are depolarized by local currents, propagating in a wave-like pattern, and not by synchronous field stimulation. Therefore, such techniques may not adequately mimic the electrical micro-environment that stem cells may be subjected to in a graft.

In order to study electrical signaling under controlled conditions, an *in vitro* stimulation system was developed to deliver current-controlled pulses through microelectrodes simulating the local activation resulting from contact with surrounding electroactive tissue. In the previous chapter, it was demonstrated that electrically paced human embryonic stem cells (hESCs) co-cultured with murine cardiomyocytes exhibited improved conduction uniformity. From the resulting data, it was implied that improved conduction was a result of increased cardiac differentiation. However, before further experiments could be carried out with electrically paced host-graft co-cultures, characterization of the system was required to verify that stimulation could significantly alter stem cell differentiation. Murine embryonic stem cells (ESCs) were initially used as the model graft cell because of their relatively fast differentiation rates.

Cells stimulated for up to four days were analyzed for cardiac and gene expression using real-time PCR, immunofluorescent imaging, and genome microarray analysis. Results varied among ESCs from three progressive differentiation stages and three stimulation amplitudes (nine combination), indicating a high sensitivity to electrical pacing. Overall, a robust system capable of long term stimulation of murine ESCs is demonstrated in this chapter, with specific conditions outlined to most encourage cardiomyocyte differentiation.

## 6.2. A System for Electrical Stimulation

Electrical stimulation was performed with a local “point-source” stimulation approach using controlled current. By using a current source, stimulation thresholds will remain relatively constant despite potentially drifting electrode impedance [122]. In addition, a voltage drop across a load (i.e., cells) can be readily measured to ensure that voltages stay within a safe margin, thus preventing electrode corrosion and water

electrolysis [123]. The waveform of the input current can be configured such that the first phase of a stimulus is theoretically recovered during a second phase with an opposite polarity, and hence "charge balanced." It is understood that charge balanced waveforms have been adequate for minimizing electrochemical reactions [123]. As a result, the design of the current source is critical because non-linearities can lead to an imbalance in the waveform. Over time, a non-balanced waveform can lead to built up charges at the electrode-electrolyte interface, eventually causing the voltage at the electrode to be outside the safe region of operation and initiate irreversible Faradaic reactions. Irreversible Faradaic reactions should be minimized to prevent the generation of cytotoxic byproducts that would destroy cell cultures, and to prevent corrosion that would compromise the experimental setup. However, with the amount of delivered charge sufficiently small, chemical reactions should be reversible and allow for safe operation if the stimulation signal is charge balanced [92].

A stimulation circuit was designed to generate a voltage waveform that is input through a voltage-controlled current source, and finally delivered to stimulation electrodes. Planar microelectrode arrays (MEA) with integrated recording and stimulation electrodes [28] were used, as described in Chapter 3. Electrical stimulation over a limited area helped to determine the importance of graft cells being physically coupled to an electrically active substrate in the differentiation process. In addition, the configuration of the electrodes mimicked the boundary conditions of the graft, where only the peripheral cells in contact with parts of the healthy myocardium would be subjected to local currents and their resulting fields.

### *6.2.1. Pulse Generation and Stimulation Circuitry*

The MEAs used for this study contained stimulation electrodes symmetrically arranged across the surface with varying surface geometries (Figure 6.1). All of the outer stimulation electrodes were connected in parallel to each other and then used to stimulate the cells from a signal source. A platinum wire was placed in the medium bath to serve as a return path for the applied current. An MSP430 microcontroller (EZ430-T2012; Texas Instruments, Dallas, TX) was used to control a 16-bit bipolar

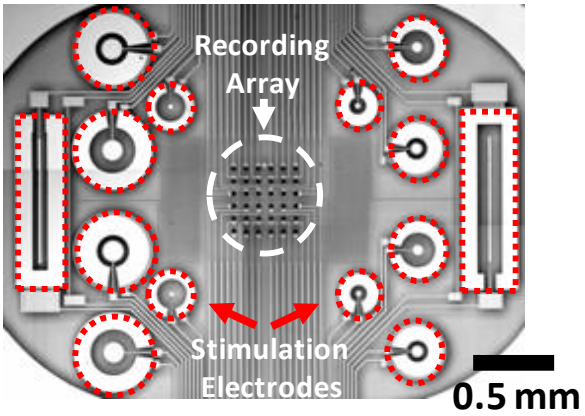


**Figure 6.1** ESCs were stimulated using the larger auxiliary electrodes located (highlighted in red) on the microelectrode array.

digital-to-analog converter (DAC), which drove a modified Howland voltage-controlled current source (Figure 6.2). The two operational amplifier configuration used for the voltage-controller current source allows a user-defined voltage to be fixed across a resistor in series with the load, ensuring precise and accurate current control. The configuration of amplifiers as well as choice of components resulted in a slew rate of 3

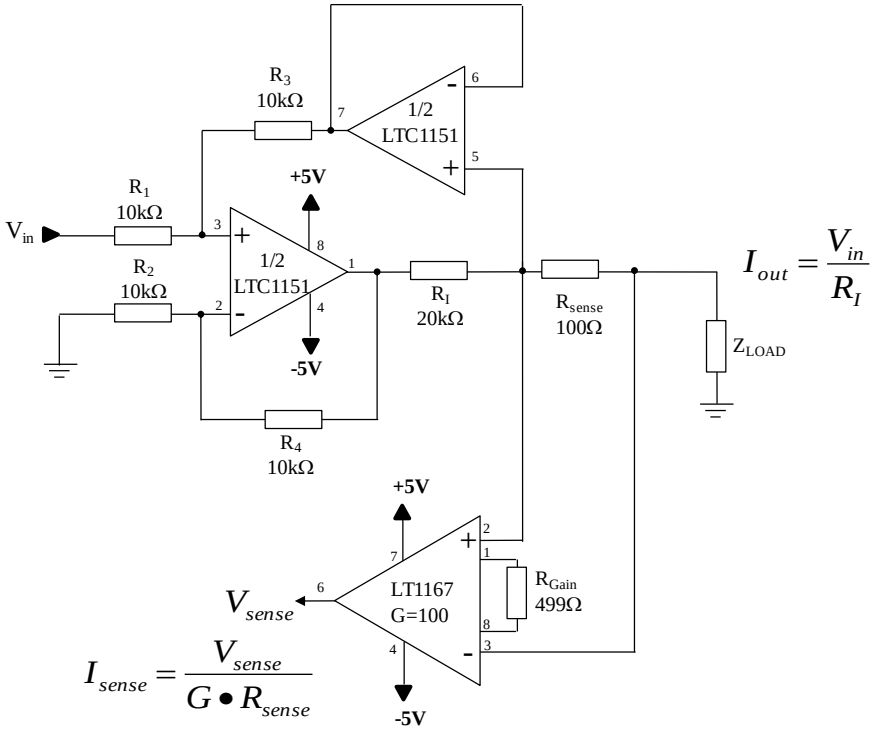


**Figure 6.2** Two LTC1151 operational amplifiers were configured as a voltage-controlled current source to deliver a precise current pulse. A high-side current sense circuit (shown on the lower right) was applied using a LT1167 instrumentation amplifier to monitor the current delivered to the load (ie. electrodes and cell culture).

μA/μs, and a signal-to-noise ratio of 59 dB with a 60 μA sine wave output into a 100 kΩ resistive load.

An anodic-first biphasic waveform with 10 msec duration was applied once per second. In between pulses, the electrodes were actively grounded by the microcontroller to clear away residual charges [124]. The amplitude of the applied current was varied depending on the experiment with 10, 30, and 60 μA (8.3, 24.9, and 49.8 μA/mm$^2$, respectively). These values were chosen to be of a similar order of magnitude to that of estimated transmembrane currents through a cell during a physiological action potential [125]. In addition, 100 Ω series resistance was placed before the load, and an instrumentation amplifier was used to verify the current waveform and amplitude.

After four days of continuous pacing, stimulation electrodes did not display signs of corrosion or other structural damage upon visual inspection with a microscope. The electrode impedance and phase angle over a range of frequencies (100 Hz to 100 KHz) for a single MEA also did not notably change (Figure 6.3).

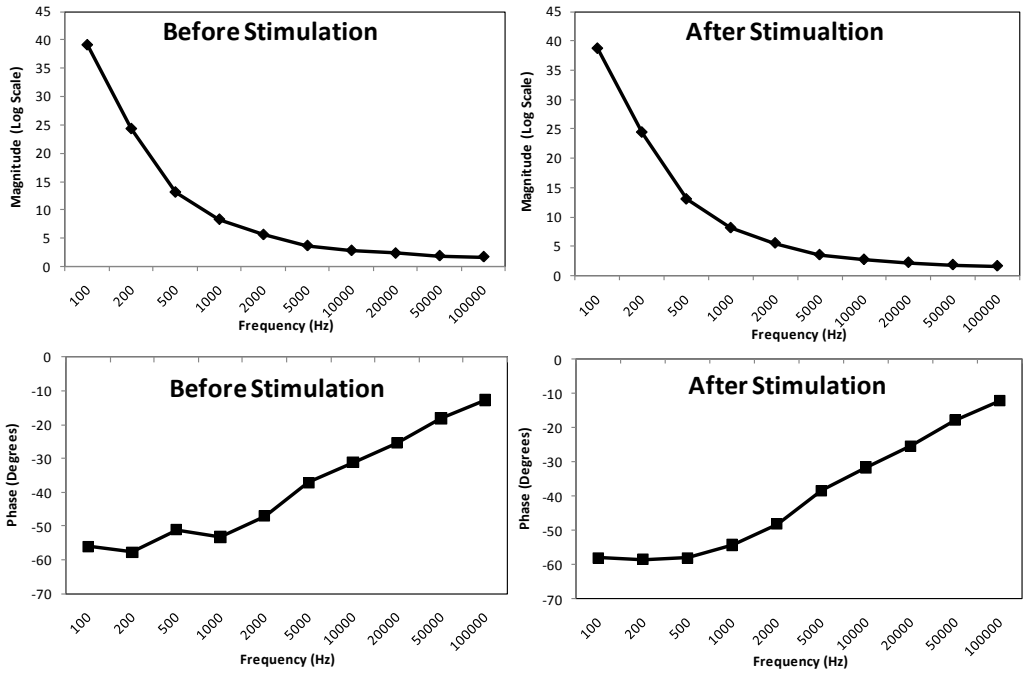


**Figure 6.3** The magnitude and phase angle of the impedance of the stimulation electrodes in a single MEA chip was measured before and after stimulation experiments. No notable changes were observed, which would suggest that the stimulation system did not adverse impact the electrodes.

Analysis of the individual electrode impedance values before and after four days of pacing indicated that the current density through each electrode did not vary more than 2.6 $\mu A/mm^2$.

The voltage across the load was checked frequently in all experiments to verify a consistent amplitude under the 0.9V threshold described for hydrolysis [120]. A voltage of 0.9 V across the load corresponded to a stimulus amplitude of 65 μA.

### *6.2.2. Experimental Stimulation Methods*

The murine embryonic stem cell line ES-D3 (CRL-1934) was obtained from the American Type Culture Collection (ATCC; Manassas, VA). The ESCs were cultured in an undifferentiated, pluripotent state using 1000 IU leukemia inhibitory factor (LIF; Millipore, Billerica, MA), and grown over a layer of murine embryonic fibroblast feeder cells [63]. The culture medium for the ES cells was changed daily, and cultures were passaged every one to two days. Differentiation of ESCs was initiated by developing them into form an aggregate of cells termed embryoid bodies (EB) using the "hanging drop" method [106]. On the first day of EB formation (designated Day 0), LIF was withdrawn from the medium, and a cultivation of about 400 cells was suspended in 18 μL hanging drops to. After two days, each EB was transferred into its own well in an ultra-low-attachment 96-well plate (Corning Life Sciences, Lowell, MA) for another two days, after which they were further seeded onto 48-well plates. At the desired differentiation stage, whole EBs were dissociated with collagenase B (Worthington, Lakewood, NJ) and the cells were plated onto the MEA surface at a density of 32,000 cells/$cm^2$ (80K total cells).

EBs were dissociated prior to plating for two reasons. First, it ensured that an evenly distributed layer of cells was attached to the electrode surface, which was especially helpful in controlling variability between samples. Second, the process of dissociating EBs was done to mimic the approach used in *in vivo* transplantation, as described by Cao, et al. [62]. At least two hours prior to plating, the MEA surface was coated with hESC-qualified matrix Matrigel™ (BD, Franklin Lakes, NJ). The cells

were allowed to settle and attach to the surface for 20 to 30 hours before electrical simulation was applied for four days. The medium was replaced on the second day.

Stimulation was applied at three different current amplitudes, 10, 30, and 60 μA. At each amplitude, cells were stimulated continuously for four days in order that the end of the stimulation period corresponded to three differentiation stages, described as Early (Day 3-9), Intermediate (Day 9-17), and Terminal (Day 17 and on). During the Early Stage, undifferentiated ESCs are destabilized and begin differentiating. Cells at the Intermediate Stage have further diverged towards a particular cell fate. By the Terminal Stage, cells have differentiated to a mature state [63, 107].

Following stimulation of cells for four days, cells were harvested and counted using a hemocytometer. No significant differences were observed between stimulated and non-stimulated cells, which implied that stimulation did not result in any increased cell death. In all samples, the number of cells increased by about a factor of five, and appeared healthy under a microscope.

## 6.3. Gene Expression Analysis

The stimulation system was used to evaluate the effect of localized electrical current on the differentiation of embryonic stem cells at three differentiation stages. The original aim in using a MEA for stimulation was to record resulting electrical activity in the cultures. However, observed beating in ESC cultures was not consistent across experiments, and was not a reliable metric. Alternatively, the effects of electrical stimulation on the gene expression were quantified using real-time PCR.

Gene expression analysis was performed at the end of the stimulation period for cardiac and embryonic stem cell markers. After four days of continuous stimulation, cells were harvested from the MEA using trypsin-EDTA (Invitrogen, Carlsbad, CA). The RNA was then extracted and purified for reverse-transcriptase (RT) PCR using an RNeasy kit (Qiagen, Valencia, CA, USA) followed by quantification of the cRNA by spectroscopy using an ND-1000 spectrophotometer (NanoDrop Technologies, Wilmington, DE, USA). Gene expression of the murine

ESCs were quantitatively measured using real-time PCR (7900 HT; Applied Biosystems, Foster City, CA) following the protocols outline for Applied Biosystems Taqman Gene Expression Assays. The four probes of interest were the cardiac cell markers *β-MHC* and *troponin-T* [63], the ESC maker *nanog* [126], and *gapdh*, a housekeeping gene for control (Applied Biosystems, Foster City, CA.). *β-MHC*, a ventricular specific protein, is typically regarded as an early stage marker while *Troponin-T* is essential for cardiac contraction and is regarded as a late stage marker [63]. Gene expression is normalized with *gapdh* expression, and then further normalized to the expression in control samples.

### *6.3.1. Real-Time PCR Analysis*

Stimulation of ESCs was performed at three differentiation stages (Early, Intermediate, Terminal) across three different stimulation amplitudes (10, 30, 60 μA), where the results are summarized in Figure 6.4. ESCs stimulated at the Early Stage at each of the three stimulation amplitudes (N=6-8 per group) did not result in significant changes in any of the three genes of study at a lower amplitude stimulus of 10 or 30 μA. However, stimulating at the highest amplitude of 60 μA yielded a statistically significant increase in the *β-MHC* levels. Otherwise, no statistically significant changes were observed with troponin-T or nanog.

Intermediate Stage (N=6-8 per group) stimulation exhibited a similar increase in *β-MHC* from the Early Stage but was observed at 30 μA instead of 60 μA. At the same amplitude, a six-fold increase was observed in *troponin-T* relative to non-stimulated samples. However, high amplitude stimulation at 60 μA may have had a detrimental effect on cardiac marker expression, with lower values of these cardiac markers. Interestingly, the ES cell marker *nanog* decreased significantly at 30 μA, but increased significantly at 60 μA.

In general, Terminal Stage stimulation (N=6-8) increased cardiac expression as the stimulus amplitude increased, yielding up to a significant six-fold increase in *troponin-t* levels when stimulated at 60 μA. Again, expression of the embryonic stem

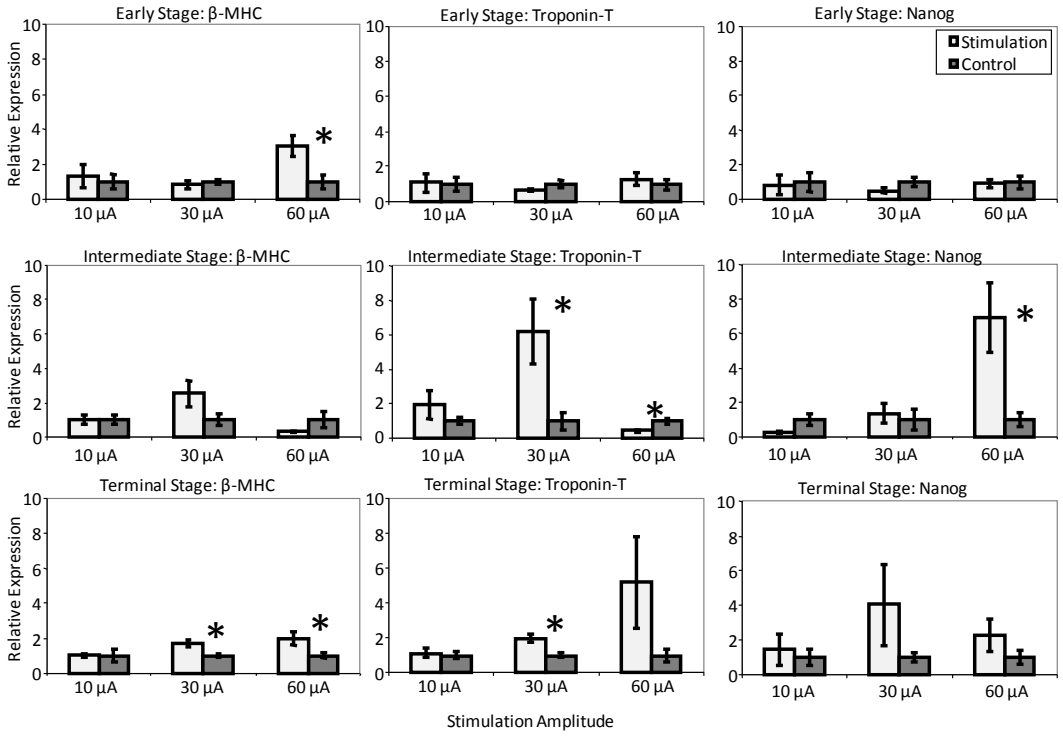


**Figure 6.4** Dose-response charts of electrically stimulated ESCs. ESCs at three different differentiation stages were locally stimulated using the MEAs over three stimulation amplitudes. Early Stage ES cells were relatively unchanged following low and mid-level amplitude electrical stimulation, but *β-MHC* was significantly upregulated at the highest level of stimulation. Intermediate Stage ESCs exhibited a greater increase in cardiac markers, especially at a stimulation amplitude of 30 µA. However, higher levels of stimulation may have the opposite effect, as seen by the decrease in *β-MHC* and *troponin-T*, and the increase in *nanog*. Stimulation at the Terminal Stage, on the other hand, exhibited an increase in both cardiomyocyte and stem cell markers. N=6-8 per differentiation stage; * $P<0.05$.

cell marker showed an increase at the highest stimulation amplitude, although not statistically significant.

Overall, later differentiation stages tended to correlate with larger changes in both cardiac and embryonic gene expression. At the Terminal Stage, stem cells exhibiting higher cardiac gene expression showed a positive correlation to the stimulation amplitude. However, higher amplitude stimulation was not always correlated with increased expression, as demonstrated in stimulating at the Intermediate Stage, where *β-MHC* and *troponin-t* were downregulated and *nanog* increased significantly. The increase in *nanog* levels was not expected, and it is possible that at this stimulation amplitude the ESCs remained in an embryonic state while control samples were differentiating. Such inflections of trends when high

amplitude stimulation is used were also observed in field stimulation studies with neuronal and muscular lineages [107].

In any case, these results demonstrate the sensitivity of ESCs at various differentiation stages to their local electrical environment, and in particular to a stimulation pattern mimicking endogenous physiological pacing [125] to yield statistically significant differences. Of particular interest is the fact that pacing Intermediate Stage cells at 30 μA can possibly increase the *troponin-t* expression by up to six-fold. Unlike field stimulation studies that uniformly depolarize large volumes of medium, simulating the physiological micro-environment by stimulating from a point-source highlights the importance of cell coupling (both electrical and chemical) in the differentiation process. Although quantitatively observing increases in the cardiac gene expression of electrically stimulated cells does not necessarily imply cardiac differentiation, it does give insight into how ESCs first respond to their new environment.

### *6.3.2. Effects of Stimulation Duration*

To determine if continuous pacing was necessary to induce the same upregulation of cardiac genes observed when Intermediate Stage ESCs were stimulated at 30 μA, a partial stimulation experiment was performed (Figure 6.5). Intermediate Stage ESCs were cultured and stimulated for two days only at 30 μA (N=7 per group), and then left without stimulation for an additional two days. In this case, the *β-MHC* levels increased significantly to the same level as observed for continuous four-day stimulation, while the *troponin-t* appeared unchanged. The stem cell marker *nanog*, however, was slightly increased, although without statistical significance compared to non-stimulated control samples.

The experiment was then reversed where Intermediate Stage ES cells were plated and the two day stimulation at 30 μA was delayed for two days (N=8 per group). In this situation, neither *β-MHC* nor *troponin-t* levels in the stimulated group were notably different from control samples. At the same time, the *nanog* levels exhibited an increase of almost four times, but not statistically significant.

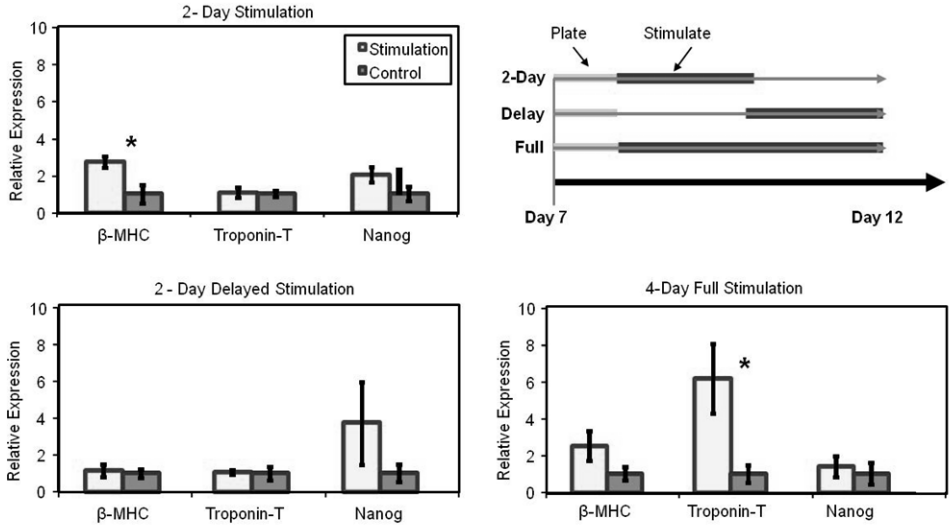


**Figure 6.5** Partial stimulation of ES cells. To investigate the role of continuous stimulation, ESCs at the Intermediate Stage were stimulated for only half the typical 4-day period at 30 μA. ESCs that were stimulated for the first two days and then incubated for another two days exhibited the same amount of β-MHC as continuous 4-day stimulation. However, troponin levels were relatively unchanged, and the stem cell marker nanog levels were slightly higher. In the reverse situation where ESCs were not stimulated until the second half of the experiment, both cardiomyocyte cell markers did not show significant changes, while nanog levels were increased, although not significantly. N=6-8 for each experimental condition; * $P<0.05$.

In addition to understanding the sensitivity of stimulated cells, the temporal patterns of stimulation appeared vital. A progression was found that started with an upregulation of *nanog* followed by *β-MHC*, and then *troponin-t* due to pacing.

## 6.4. Protein Expression Analysis

It was unclear whether the observed cardiac differentiation was due to direct effects of the electrical source, or to secondary messengers that were upregulated to elicit the differentiation through paracrine effects. Because current was applied at localized areas and did not stimulate the entire culture simultaneously, the direct effect of physical coupling to an electrically active substrate could be measured by examining where cardiac differentiation was taking place relative to the electrodes.

Intermediate Stage ESCs were stimulated at 30 μA for four days continuously, and then fixed with 4% paraformaldehyde and permeabilized by 0.1% Triton X-100 (Sigma-Aldrich Inc, Milwaukee, WI) for immunostaining analysis of cardiac *troponin-*

*t*. The primary antibodies selected were goat anti-troponin-T. Secondary antibodies were FITC conjugated rabbit anti-goat IgG (Santa Cruz Biotechnology, Santa Cruz, CA). Nuclei were stained by propidium iodide or DAPI (Sigma-Aldrich Inc.).

The resulting fluorescent images demonstrated that cardiac expression was not entirely isolated to the region around the stimulation electrodes (Figure 6.6). Immunofluorescence was analyzed by quantifying individual fluorescent pixels in Matlab (The Mathworks, Natick, MA), and normalizing it to the fluorescence from a nuclei stain. On average, stimulated samples contained 3.5±0.8 times the fluorescent area compared to non-stimulated samples (N=4). In further analysis of the fluorescent images, cells cultured directly over stimulation electrodes contained about a 25% higher concentration of *troponin-t* positive cells than the average concentration over the total area. Although this is not qualitatively this is not a large difference, the consistent increase in concentration levels did indicate an effect, however small, on

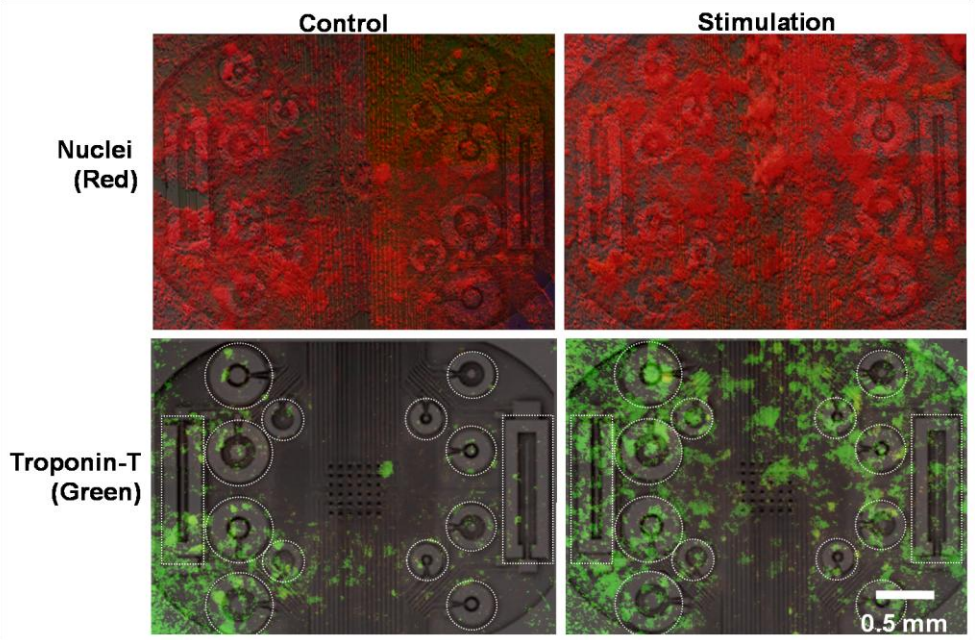


**Figure 6.6** Immunostaining of electrically stimulated cells. Following four days of continuous stimulation of Intermediate Stage ES cells at 30μA, samples were fixed for fluorescent analysis. In both stimulated and control cases, cells appeared confluent, and were confirmed with nuclei staining (top two panels). In addition, cells were stained for troponin-T (lower two panels). Qualitatively, stimulated samples displayed higher amounts of troponin-T and is repeatedly observed in other samples (N=4). The increase in tropnin-T due to stimulation was not limited to the areas around the electrodes (highlighted in the dotted regions), but nonetheless stayed within the general vicinity.

the spatial location of the electrodes and differentiation.

A separate set of stimulated ES cells were replated onto glass chamber slides and similarly stained for cardiac markers (Figure 6.7). Phenotypically, cell cultures did not display significant differences in the number of spontaneously beating foci by the end of the stimulation period between stimulated and control samples, as recorded by electrodes and visual observation.

Electrical pacing significantly increased the degree of cardiac differentiation in culture, but because the majority of the differentiation did not occur within the vicinity of the stimulation electrodes, it was likely that the mechanism of differentiation was through a joint paracrine signaling pathway. Electrical stimulation may locally trigger

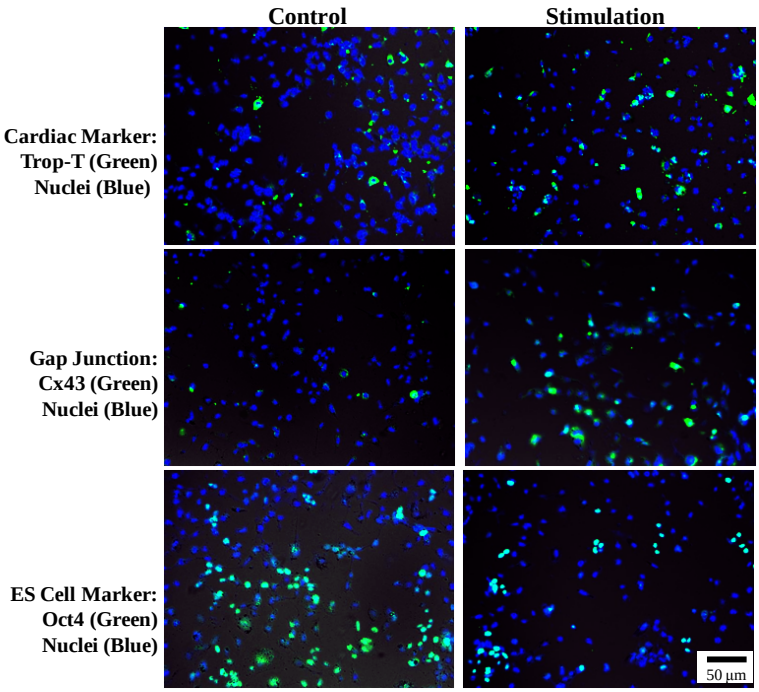


**Figure 6.7** Immunostaining of stimulated cells. Intermediate Stage ES cells stimulated at 30 µA for four days were trypsinized, lightly re-plated onto glass chamber slides, and imaged on a fluorescent microscope. Cardiomyocyte marker troponin-T, gap junction Cx43, and ES marker Oct4 were stained in green while nuclei were stained in blue.

the release of markers which may then promote cardiac differentiation throughout the culture. Although the stimulation conditions were different, this hypothesis aligns well with experiments done by Sauer, et al. [67], who proposed the idea that reactive oxygen species (ROS) act as secondary messengers as a mechanism to promote cardiac differentiation with application of a brief DC voltage field across the entire

culture. With a four day duration used in stimulation experiments, diffusion of molecular factors could certainly have influenced entire cultures.

## 6.5. Genome Microarray Analysis

While PCR analysis of a limited number of gene transcripts in electrically-stimulated ESCs is valuable, important genome-wide mRNA changes ("the transcriptome") that define the specific regulatory networks of genes and pathways responsive to electrical stimulation will be missed. Global gene expression profiling of embryonic stem cells thus enables a systems-based analysis of the biological processes, networks, and genes that drive cell fate decisions. To understand these transcriptome changes, a genome microarray analysis of electrically-stimulated Intermediate Stage ES cells at 30 μA versus non-stimulated controls was performed.

Using Low RNA Input Fluorescent Linear Amplification Kits (Agilent Technologies, Santa Clara, CA, USA), cDNA was reverse transcribed from each RNA sample (N=8 per group), and cRNA was then transcribed and fluorescently labeled from each cDNA sample. cRNA samples derived from four biological replicates of a pooled collection of electrically stimulated ESCs, as well as a pooled reference of RNA taken from control (non-stimulated) ESCs, were labeled with Cy5 and Cy3, respectively. The resulting cRNA was purified using an RNeasy kit (Qiagen, Valencia, CA, USA) followed by quantification of the cRNA by spectroscopy using an ND-1000 spectrophotometer (NanoDrop Technologies, Wilmington, DE, USA). A mixture of 825 ng of Cy3- and Cy5- labeled and amplified cRNA was fragmented according to the Agilent technology protocol. cRNA was hybridized to 4x44K whole mouse genome microarray slides from Agilent Technologies (Santa Clara, CA). The hybridization was carried out in a rotating hybridization chamber in the dark at 65°C for 17 hours. The resulting fluorescence was acquired using an Agilent G2505B DNA microarray scanner. The image files were extracted using Agilent Feature Extraction software version 9.5.1 applying LOWESS background subtraction and dye normalization.

Microarray data analysis was performed using GeneSpring GX 7.3.1 (Agilent Technologies, Santa Clara, CA). A gene was considered significant if the expression from a stimulated sample was greater or less than 1.4 times the expression in a non-stimulated sample and had a *P*-value of less than 0.05. The value of 1.4 times difference was arbitrarily chosen based on the observed data. Because of the small changes in overall transcription between the two groups, multiple testing corrections to remove false positives in the resulting data were not possible. Further analysis was performed using GeneSpring's Gene Ontology browser and Ingenuity Pathway Analysis (Ingenuity Systems, Redwood City, CA).

Using a 1.4-fold change cutoff and $P<0.05$, analysis revealed 495 upregulated genes and 729 downregulated genes in ESCs that had been electrically stimulated. Overall, the fold change in expression level of these genes was less than 3.5 compared to controls, so electrical stimulation did not dramatically alter the transcriptome. However, a number of interesting developmental-related genes exhibited altered expression. Simultaneous to the mild upregulation of mature gene programs that suggest differentiation, such as *Ncam1, Isl1, Foxc1* and *Foxc2,* was the apparent downregulation of important self-renewal and pluripotency genes, including *Oct4* and *Foxd3*.

### *6.5.1. Stimulation Effects on Stem Cell Pluipotency*

Genes associated with pluripotency were downregulated with electrical stimulation. ES cell self-renewal is dependent on a core set of transcription factors involved in the development of the embryo: *Oct4*, *nanog*, *Sox2,* and *Foxd3* [127, 128] These embryonic transcriptional factors are essential for the formation and maintenance of the inner cell mass during mouse preimplantation development and for self-renewal of pluripotent ES cells. Interestingly, two of these factors, *Oct4* (*Pou5f1*) and *Foxd3,* were both downregulated 1.4-fold after electrical stimulation, indicating that important changes were occurring in the cellular pluripotency programs. A 1.7-fold downregulation of *Lin28* was also observed, an important embryonic gene in

mice and humans [129] that was recently used by Thomson, et al. to reprogram fibroblasts into pluripotent stem cells [51].

### *6.5.2. Stimulation Effects on Mesoderm and Cardiac Development*

Mesoderm and cardiac development markers were upregulated with electrical stimulation. Mesoderm gives rise to cardiac, skeletal, and smooth muscle, as well as hematopoietic and endothelial cells. A number of early mesodermal genes were observed that were upregulated with electrical stimulation. Significantly, the mesodermal *Foxc1* and *Foxc2* genes were upregulated 1.6 and 1.5-fold respectively after electrical stimulation. These two genes are particularly important for heart development and morphogenesis. Another interesting finding was the upregulation of the transcription factor *Islet1* (*Isl1*, up 1.5-fold), which had been reported to be a marker of cardiac progenitor cells [130, 131]. Though there is not yet total agreement in the field, it is generally accepted that *Isl1*, which is expressed in the secondary heart field, directly regulates cardiac precursor cells. Further, *Isl1* had been shown to be expressed by progenitors of the outflow tract, right ventricle, and a majority of atrial progenitors [131]. It should be noted that Isl1 is not cardiac-specific since it is also expressed in motor neurons and the pancreas during embryogenesis, as well as in normal adult islet cells [132] so its initial activation and its actions on downstream targets likely require combinatorial mechanisms and influences [133].

A number of studies have shown that stage-specific inhibition of canonical Wnt signaling is required for cardiac development, so the upregulation of the Wnt signaling pathway antagonist Dickkopf homolog 1 (*Dkk1*, up 2.0-fold) was of particular interest. *Dkk1* is well known to specify cardiac mesoderm when expressed at the appropriate stage of development, and application of this factor has recently been shown to encourage *in vitro* differentiation of human ES cells into cardiac progenitors [134]. Other cardiac-related genes that were upregulated after electrical stimulation include the ATPase, $Ca^{2+}$ transporting, cardiac muscle, fast twitch 1 (*Atp2a1*, upregulated 1.4-fold), and *Sema6D* (upregulated 1.7-fold), which regulates endocardial cell migration in the developing heart [135] and spinal cord [136].

### *6.5.3. Stimulation Effects on Neuronal Development*

Genes and pathways involved in nervous system development were also observed to be upregulated after electrical stimulation. Perhaps the most striking example was the upregulation of neural cell adhesion molecule 1 (*Ncam1*, upregulated 1.5-fold), a common marker of primitive neuroectoderm. Another gene, Delta/Notch-like EGF-related receptor (*DNER*, upregulated 1.7-fold), is a neuron-specific transmembrane protein that functions as a ligand of Notch during cellular morphogenesis of glia in the mouse cerebellum [137].

Of particular interest is the fact that while cardiac differentiation may be triggered by electrical stimulation, this stimulation promoted differentiation into other tissues. The upregulation of non-cardiac tissues may help explain why statistical significance was not always observed in the real-time PCR analysis. In some field stimulation techniques on ESCs, major cardiac differentiation was not always elicited [107], but greater activation of neural pathways were observed instead.

### *6.5.4. Stimulation Effects on Gene Based Processes*

The alteration in developmental gene programs of electrically stimulated mESCs was clearly seen with Gene Ontology (GO) overrepresentation analysis, which categorized genes based on their annotations into functional groups. The overrepresented GO terms in stimulated ESCs revealed a number of processes related to embryonic development, pattern specification, and tissue and organ development and morphogenesis. In contrast, dowregulated GO processes included cell organization and biogenesis, RNA and DNA metabolism, cell cycle and cytoskeletal organization, and microtubule biogenesis. Ingenuity Pathway Analysis (Ingenuity Systems Inc, Redwood City, CA) also demonstrated significant changes in developmental processes after electrical stimulation (Figure 6.8). Based on Ingenuity's database of gene networks, the functional categories that were most significantly changed by electrical stimulation include gene expression, organismal and organ development, cellular development, cell cycle, and specific physiological systems

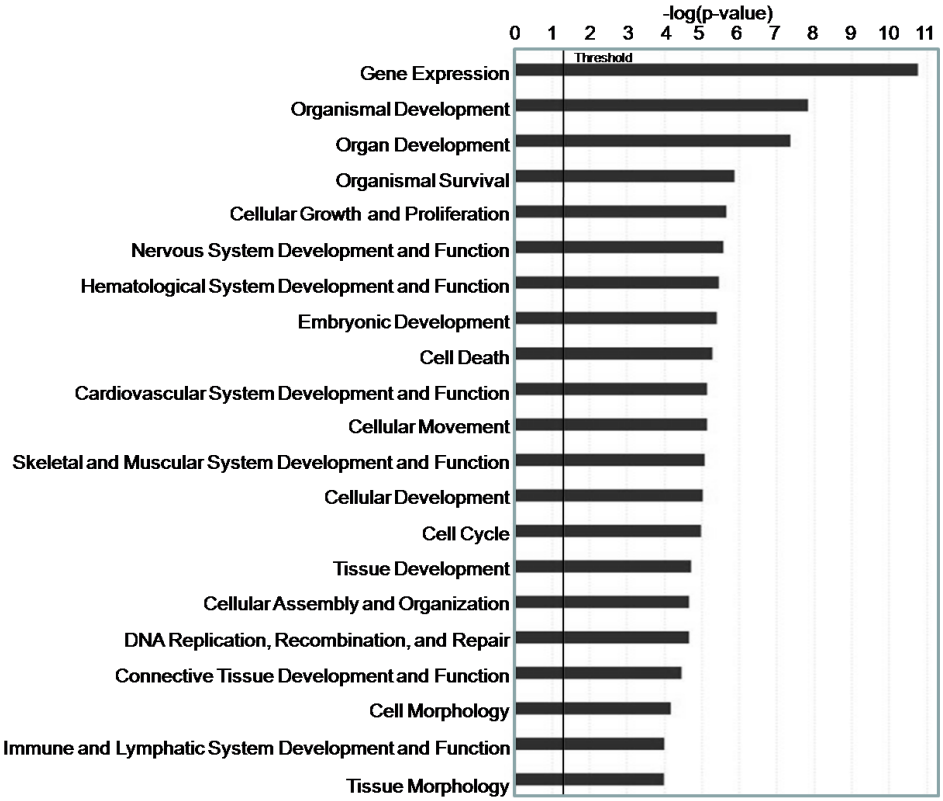


**Figure 6.8** Categories of altered gene expression following electrical stimulation. Ingenuity Pathway Analysis displays the function categories that exhibited the highest level of statistically significant changes following electrical stimulation. Among many changes in development, many specific physiological systems such as the nervous, hematological, musculoskeletal, and cardiovascular development were noted.

such as cardiovascular, neurological, hematological, and musculoskeletal development. Notably, the cardiovascular, neurological, and musculoskeletal systems are all electrically excitably tissues. Strangely, neither *troponin-t* nor *β-MHC* appeared on the microarray gene list, but that may only be because they did not reach statistical significance in this particular experiment. Microarray analysis is not as sensitive a method as real time PCR for evaluating gene expression, so previous results are not negated. Instead, this only means that specific conclusions about these genes cannot be drawn from microarray analysis.

## 6.6. Conclusion and Future Work

A novel system used to electrically stimulate ESCs safely over long periods of time was developed, and was capable of demonstrating subsequent changes in differentiation. Although some of the results were not statistically significant, it may be due to the small surface area that the stimulation electrodes cover relative to the total culture area. Originally conceived as a feature to probe the spatial effects of stimulation, the particular size and configuration of the stimulation electrodes may not be optimal for differentiation. Another similar limitation of the system is the configuration of the recording electrodes in the center of the culture. The area that the recording arrays covers (~4%) was unable to properly map any differences in the electrical activity between stimulated and non-stimulated samples. Differences were nonetheless quantified through real time PCR, immunofluorescence, and whole genome microarray analysis.

With the completion of a robust system for electrical stimulation of stem cells, attention was turned towards studying the effects of stimulation on a human model. Differentiating human embryonic stem cells (hESC) at Day 7 were seeded onto MEA surfaces have been paced with 30 μA biphasic pulses at 1 Hz for a period of seven days. By the end of the pacing period, cultures appeared healthy, and there was no significant difference between the number of cells in stimulated and non-stimulated control samples. The resulting gene expression will be the subject of future investigations. It is not likely that the stimulation protocols used to stimulate murine cells will be the same for human cells, so new dose-response charts will be constructed to find the optimum parameters for cardiac differentiation.

While understanding the gene expression and subsequent differentiation is a first and necessary step toward functional repair, understanding integration with host tissue (participation to electrical conduction and mechanical contraction) is also important. Future work using the presented system will use the full potential of MEAs to monitor the development of action potentials and propagation patterns in co-cultures (including conduction mismatches responsible for increased risks of arrhythmias), and study the impact of electrical stimulation on these parameters.

Especially given the transient effects observed in these pacing experiments, continuous pacing may be necessary and one might even suggest the coordinated effort of stem cell implantation and cardiac pacing in the region of interest.

# 7 Summary and Conclusions

## 7.1. Summary

Heart failure is one of the major causes of mortality in the western world [1]. While there are many options available for treatment such as pharmaceutical agents, implantable devices, or whole organ transplantation, their individual limitations prevent any of them from being a complete solution. Stem cell therapy, on the other hand, is a technique aimed at regenerating damaged tissue to fully restore cardiac function. However, before transplanting cells into myocardium, a number of challenges must be overcome. Among the many topics that require further research are the types of cell to transplant and the optimal method of cell delivery. Improper integration of graft cells may actually leave a patient worse off, with adverse consequences with include the risk of arrhythmia following the introduction of exogenous cells to the heart.

A set of *in vitro* tools was created to study the risk of arrhythmia after stem cells are transplanted into a damaged heart. This study focused on electrophysiologic characteristics of stem cells that could prevent proper integration: a lack of cardiac differentiation or a mismatch of conduction properties between the host and graft. Studying stem cell transplantation *in vitro* required innovative approaches which were addressed with three primary contributions. First, a mathematical transform known as a co-occurrence matrix was developed to quantify the uniformity of conduction in heterogeneous cultures [2]. Second, a device was created to observe the electrical interactions between two cell types over time [3,4]. Third, a system was built to explore the role of electrical stimulation on stem cell differentiation and integration [5,6].

### *7.1.1. Conduction Analysis*

The propagation of a depolarization wave in cardiac cultures grown on microelectrode arrays (MEAs) can be visually represented in many ways, such as through lateral isochrones maps or velocity vector fields. However, of these two methods of representing conduction, the only quantitative metric is the average conduction velocity. Even then, the average conduction velocity is an aggregate measure of the entire culture, and is unrelated to the uniformity of conduction.

In order to quantitatively measure conduction uniformity, new metrics based on a co-occurrence matrix transform were developed. Local activation times derived from raw MEA data were compiled to form a temporal-spatial image called a phase map. The co-occurrence matrix is essentially the result of mapping the values within a phase plot into a form that can describe spatial uniformity of conduction succinctly.

In order to characterize the co-occurrence matrix as a method to evaluate the uniformity of conduction, the electrical pathways of spontaneously beating murine cardiomyocytes were disrupted by adding increasing amounts of non-conducting murine fibroblasts. This method of creating heterogeneous cultures also modeled the initial stages of transplantation when graft cells may not have been fully differentiated. One limitation of this model was the planar configuration of the tissue and its lack of tissue structure. Conduction in a three-dimensional, fibrous structure similar to cardiac tissue may exhibit different characteristics in the presence of non-conducting cells because there are more pathways for a depolarization wave to travel. Nonetheless, the conclusion remains that conduction is easily disrupted by non-conducting cells

### *7.1.2. Host-Graft Interactions*

The second primary aim of this project was to create a device that could model the functional integration of stem cells in a host tissue *in vitro*, and in particular demonstrate the differences in conduction properties between host and graft tissue (a source of arrhythmogenicity). A co-culture system coupled to MEAs was developed to allow controlled experiments for the study of such conduction mismatch. Spatially separated cultures representing the host and the graft were grown and then allowed to

merge above a MEA, which enabled measurements of conduction during the integration process. Spontaneously beating murine cardiomyocytes were used as a host model and co-cultured with various graft candidates. By comparing conduction velocities and co-occurrence matrices, the conduction of a depolarization wave initiated from host cells to the graft was evaluated. The mismatch of conduction was especially apparent when graft stem cells that did not include the cardiomyocyte lineage where used. On the other hand, graft cells that included the cardiomyocyte lineage exhibited a well-matched tissue interface.

Due to the lack of human cardiac models, most clinical studies using human embryonic stem cells (hESCs) are carried out using animal models. Although such research is high informative, animal models may not be appropriate in evaluating whether stem cell candidates can conduct an electrical signal in the heart. A trans-species co-culture between murine cardiomyocytes and hESCs was performed, and differences in conduction were observed despite evidence that the hESCs had differentiated into cardiomyocytes. Such inherent differences in cellular properties between species may make functional integration highly unlikely. Nonetheless, while animal models are the best option short of *in vivo* human studies, they do not allow proper characterization of the electrical mismatch between host and graft cell populations.

### *7.1.3. Electrical Stimulation*

In most co-culture experiments, electrical activity was rarely observed over the entire graft region. Instead, only Percoll purified hESCs exhibited conduction well beyond the host-graft boundary region. The increased range of electrical activity was attributed primarily to their relatively high concentration of differentiated cardiomyocytes. In an effort to improve the rate of cardiac differentiation and to evaluate the impact of localized electrical currents on the integration of stem cells into host cardiomyocytes, a point-source stimulation system was created. Co-cultures of hESCs and murine cardiomyocytes were electrically paced, and while similar

differences between host and graft cultures were still observed, the uniformity of conduction within the graft region of the co-culture significantly improved.

Electrical pacing provided a major advantage towards controlling the electrical environment of *in vitro* cultures. With the assumption that the host cardiomyocyte population were be effectively paced, stem cells coupled to the host-graft boundary would be subjected to a very regular beat rate. If cardiac differentiation could be improved with the application of pacing *in vivo*, new possibilities involving coordinated therapies of pacemakers and stem cell transplantation deserve greater attention.

To further explore the role of electrical pacing, the gene expression of paced embryonic stem cells at different stages of differentiation was investigated using different stimulus amplitudes. A murine model was initially used in order to facilitate development of the stimulation protocols, and was particularly advantageous due to their relatively fast rate of development. Indeed, genetic changes were observed that tended to favor the development of electrically active cells, which included the upregulation of neuron and skeletal muscle genes in additional to key cardiomyocyte genes.

## 7.2. Future Work

The overarching goal of developing *in vitro* tools for studying stem cell transplantation was to better understand the mechanisms of integration between graft and host tissues. The results from this work have enabled two major undertakings that are still ongoing. The first is the use of the co-culture device as a screening platform for novel candidate graft cells. The second is further exploration of the role of the electrical environment on human embryonic stem cells.

### *7.2.1. Screening of Candidate Graft Cells*

While it is generally accepted that spontaneously differentiating embryonic stem cells would not be an appropriate graft cell to regenerate cardiac tissue, one

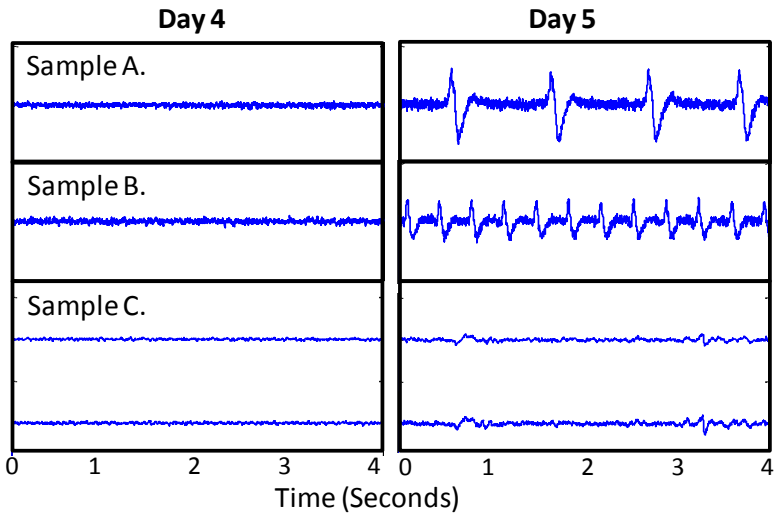


**Figure 7.1** Examples of developing action potentials in differentiating hESC cultures co-cultured with HL-1 cardiomyocytes. Only three out of six samples exhibited electrical activity on the graft regions. Traces are displayed one day prior to the observation of electrical activity in the graft region (left). One day later on Day 5 (right), the same traces displayed electrical activity, which was initiated by an action potential generated within the host population.

theoretical alternative is to use isolated cardiac progenitor stem cells from differentiating hESCs. If an appropriate population of progenitor cells can be isolated, the challenge would be in verifying that cardiomyocytes can be differentiated in a pure enough population to properly integrate into myocardium.

The co-culture device used for the reversible separation of cell cultures has provided a valuable tool to test the ability of novel candidate graft cells to conduct an electrical signal from a population of pure cardiomyocytes. In collaboration with the laboratory of Professor Irving Weissman, populations of candidate graft cells have been isolated using various techniques, and are subsequently co-cultured with HL-1 cardiomyocytes.

The ability to monitor the development of electrical activity in graft cells over time using MEAs is vital when searching for the appropriate cell type for transplantation. During initial experiments, one candidate population co-cultured with HL-1 cardiomyocytes began exhibiting electrical activity after three days in three out of six MEAs (Figure 7.1). Action potentials were in complete synchrony with the cardiomyocytes in the host population. However, electrical signals were only observed on one or two channels, and there was not enough data for conduction analysis. In

addition, no further electrical activity developed over time. While not entirely successful, these first experiments have provided a crucial first step in demonstrating the co-culture device as a method of screening.

### *7.2.2. Electrical Stimulation of Human Embryonic Stem Cells*

The stimulation system described in Chapter 6 was used to pace murine ESCs, which resulted in an upregulation of many important cardiac genes. The next step is to examine if hESCs can be modulated in a similar way. Stem cells will be paced with various stimulus amplitudes, rates, and durations to find conditions that will optimize cardiac differentiation. In addition, the role of cell coupling to host cardiomyocytes will also be explored by co-culturing cardiomyocytes with GFP-labeled hESCs. Following several days of merged co-culture, hESCs will be extracted and sorted using a flow cytometer for gene expression analysis.

One of the original aims for the stimulation system was to mimic the localized pacing that stem cells would encounter *in vivo* when physically coupled to an electrical substrate (i.e. myocardium). However, only a fraction of the stem cell culture was in physical contact with stimulation electrodes. In order to stimulate a larger proportion of cells simultaneously, an inter-digitated array was designed and fabricated (Figure 7.2). As opposed to "field-stimulation" methods where a large

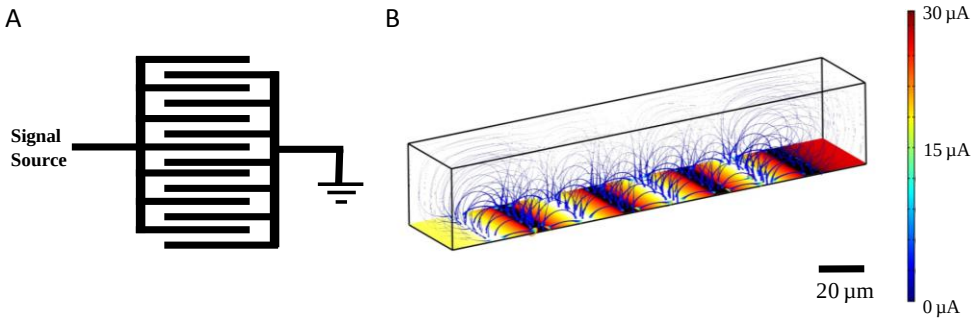


**Figure 7.2** A electrode design using an inter-digitated configuration. (A) One electrode is used for a signal input, while the opposing electrode is grounded. (B) A 3D finite element model of the resulting electric field from 30 µA biphasic square wave pulses was created using Comsol Multiphysics (Comsol, Stockhom, Sweden). Cross-sections of the stimulating electrodes are displayed as the black bars, and the ground electrodes are displayed as white bars. The color gradient on the surface displays the electrical gradient from stimulating electrode to the ground electrode. The maximum current density was found at the edges of the electrodes, and dissipated outward. The paths of current are represented by the blue traces.

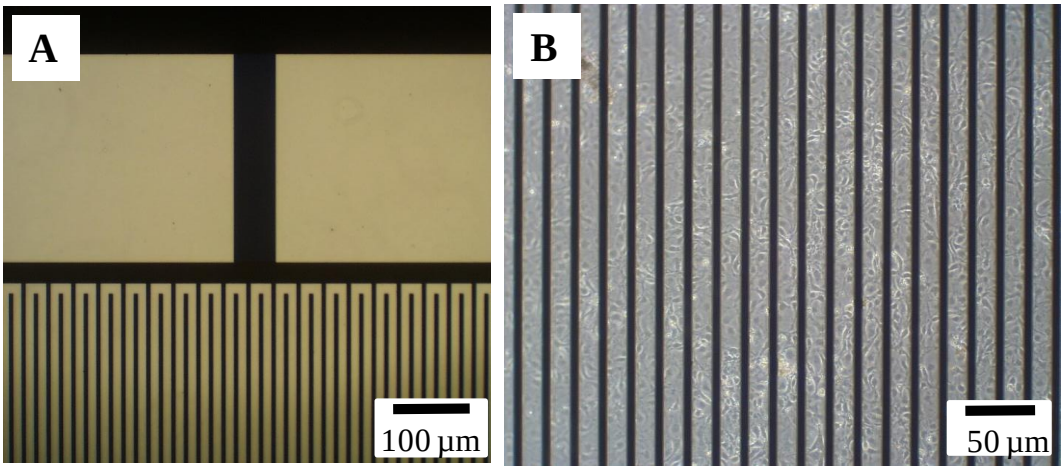


**Figure 7.3** Inter-digitated electrodes were fabricated and tested. (A) Two sets of platinum electrodes were fabricated using standard deposition techniques, and arranged in an opposing orientation. One electrode is pulsed, while the opposing electrode is grounded. (B) Human embryonic stem cells were cultured over the electrodes (black bars) using a gelatin surface coating for up to six days. Cells appeared healthy over several days after stimulation from a 30 µA biphasic square wave.

voltage is applied on two electrodes on opposing sides of a cell culture, inter-digitated electrodes that are physically coupled with cells required a much smaller voltage and can thus maintain an electrochemically safe environment.

The stimulation electrodes consisted of a 100 nm thick platinum layer deposited over a glass substrate using a 10 nm titanium adhesion layer. Square-wave current pulses were applied to one set of electrodes while the opposing set of electrodes was grounded.

This new stimulation system is fully operational, and the supporting circuitry has been created to allow stimulation of up to eight samples simultaneously. Successful biocompatibility experiments have been performed using differentiating human embryonic stem cell (hESC) cultured for up to six days (Figure 7.3). Experiments are currently to pace differentiating hESCs under varying physiologically relevant conditions and examine their subsequent gene expression.

## 7.3. Conclusions

The associated risk of arrhythmia following stem cell transplantation in the heart is not a new concern, but it has largely been ignored due to the difficulty in

elucidating the mechanisms of integration. This project aimed at creating a set of tools to understand how the electrical environment influences stem cell transplantation.

Fully identifying the electrical risks related to stem cell transplantation would be a major accomplishment, leading to optimized methods of treatment. Although the studies carried out within this project focused entirely on the ability of transplanted stem cells to conduct an electrical signal, it is certainly not the only way stem cells can be used to improve cardiac function. In addition to cardiac differentiation, stem cells may participate in neovascularization of surrounding tissue, as shown by several researchers using hematopoietic stem cells [7,8]. As a result, tissue regeneration may result as a secondary effect following vascularization. However, the mechanism of regeneration does not change the fact that a non-cardiomyocyte graft cells may severely disrupt electrical conduction in the heart.

Ideally, graft cells should possess the plasticity to both differentiate into cardiomyocytes that match the electrical properties as the host tissue, and participate in secondary processes that aid in tissue regeneration. Such complex processes are not likely to occur spontaneously *in vivo*, and there has been little evidence of graft stem cells self-differentiating and self-assembling to fully regenerate a damaged heart. Active intervention following transplantation may be needed to ensure successful integration. One idea presented in Chapters 5 and 6 of this work is to use an implantable pacemaker in combination with stem cell therapy to maximize cardiac differentiation and guide the structural orientation of graft cells. Underlying this idea is a sense of optimism that it is possible for stem cells to truly repair a damaged heart. While it may take considerably more time to unlock the full potential of stem cells, it is reasonable to expect new graft candidates in the future that are capable of cardiac regeneration without an arrhythmogenic risk.

# References


[1] G. Schram, M. Pourrier, P. Melnyk, and S. Nattel, "Differential distribution of cardiac ion channel expression as a basis for regional specialization in electrical function," *Circulation Research*, vol. 90, pp. 939-950, 2002.

[2] L. Roblee and T. L. Rose, "Electrochemical guidelines and selection of protocols and electrode materials for nerual stimulation," in *Neural Prosthesies: Fundamental Studies*, W.F.Agnew and D. B. McCreery, Eds. Englewood Cliffs: Prentice Hall, 1990.

[3] S. J. Morrison, N. M. Shah, and D. J. Anderson, "Regulatory mechanisms in stem cell biology," *Cell*, vol. 88, pp. 287-298, 1997.

[4] G. T. A. Kovacs, "Enabling Technologies for Cultured Neural Networks," in *Introduction to the Theory, Design, and Modeling of Thin-Film Microelectrodes for Neural Interfaces*, D. A. Stenger and T. M. McKenna, Eds. San Diego: Academic Press, Inc., 1994, pp. 121-165.

[5] H. Harris, *The Birth of the Cell*. New Haven, CT: Yale University Press, 1999.

[6] A. J. Becker, E. A. McCulloch, and J. E. Till, "Cytological demonstration of the clonal nature of spleen colonies derived from transplanted mouse marrow cells," *Nature*, vol. 197, pp. 452-454, 1963.

[7] J. A. Thomson, J. Itskovitz-Eldor, S. S. Shapiro, M. A. Waknitz, J. J. Swiergiel, V. S. Marshall, and J. M. Jones, "Embryonic stem cell lines derived from human blastocyts," *Science*, vol. 282, pp. 1145-1147, 1998.

[8] I. Weissman, "Stem Cells: Units of development, units of regeneration, and units in evolution," *Cell*, vol. 100, 2000.

[9] M. Pfeffer and E. Braunwald, "Ventricular remodelig after myocardial infarction. Experimental observations and clinical implications," *Circulation*, vol. 81, pp. 1161-1172, 1990.

[10] S. A. Hunt, "ACC/AHA 2005 Guideline Update for the Diagnosis and Management of Chronic Heart Failure in the Adult: A Report of the American College of Cardiology/American Heart Association Task Force on Practice Guidelines (Writing Committee to Update the 2001 Guidelines for the Evaluation and Management of Heart Failure)," *Journal of the American College of Cardiology*, vol. 46, pp. e1-e82, 2005.

[11] E. Braunwald and M. Pfeffer, "Ventricular enlargement and remodeling following acute myocaridal infarction: mechanisms and management," *Am J Cariol*, vol. 68, pp. 1D-6D, 1991.

[12] S. Hunt, "Current status of cardiac transplantation," *J Am Med Assoc*, vol. 280, pp. 1692-1698, 1998.

[13] S. Hughes, "Cardiac Stem Cells," *Journal of Pathology*, vol. 197, pp. 468-468, 2002.

[14] M. Scorsin, F. Marotte, A. Sabri, O. LeDref, M. Demirag, J. Samuel, L. Rappaport, and P. Menasche, "Can grafted cardiomyocytes colonize peri-infarct myocardial areas?," *Circulation*, vol. 94, pp. I1337-I1340, 1996.

[15] P. Menasché, A. A. Hagège, M. Scorsin, B. Pouzet, M. Desnos, D. Duboc, K. Schwartz, J.-T. Vilquin, and J.-P. Marolleau, "Myoblast transplation for heart failure," *The Lancet*, vol. 357, pp. 279-280, 2001.

[16] J.-Y. Min, Y. Yang, M. F. Sullivan, Q. Ke, K. L. Converso, Y. Chen, J. P. Morgan, and Y.-F. Xiao, "Long-term improvement of cardiac function in rats after infarction by transplantation of embryonic stem cells," *Journal of Thoracic and Cardiovascular Surgery,* vol. 125, pp. 361-369, 2003.

[17] C. Toma, M. Pittenger, K. Cahill, B. Byrne, and P. Kessler, "Human messenchymal stem cells differentiate to a cardiomyocyte phenotype in the adult murine heart," *Circulation,* vol. 2002, pp. 93-98, 2002.

[18] D. Orlic, J. Kajstura, S. Chimenti, F. Limana, I. Jakoniuk, F. Quaini, B. Nadal-Ginard, D. M. Bodine, A. Leri, and P. Anversa, "Mobilized bone marrow cells repair the infarcted heart, improving function and survival," *Proc Natl Acad Sci,* vol. 98, pp. 10344-10349, 2001.

[19] K. A. Jackson, S. M. Majka, H. Wang, J. Pocius, C. J. Hartley, M. W. Majesky, M. L. Entman, L. H. Michael, K. K. Hirschi, and M. A. Goodell, "Regeneration of ischemic cardiac muscle and vascular endothelium by adult stem cells," *Journal of Clinical Investigation,* vol. 107, 2001.

[20] J. A. Michael, I. G. Stiell, S. Agarwal, and D. P. Mandavia, "Cardioversion of Paroxysmal Atrial Fibrillation in the Emergency Department," *Annals of Emergency Medicine,* vol. 33, pp. 379-387, 1999.

[21] F. Morady, "Radio-frequency alation as treatment for cardiac arrhythmias," *NEJM,* vol. 340, pp. 534-544, 1999.

[22] S. Nattel and L. Carlsson, "Innovative approaches to anti-arrhythmic drug therapy," *Nature,* vol. 5, pp. 1034-1049, 2006.

[23] P. Menasche, A. A. Hagege, J.-T. Vilquin, M. Desnos, E. Abergel, B. Pouzet, A. Bel, S. Sarateanu, M. Scorsin, K. Schwartz, P. Bruneval, M. Benbunan, J.-P. Marolleau, and D. Duboc, "Autologous Skeletal Myoblast Transplantation for Severe Postinfarction Left Ventricular Dysfunction," *Journal of the American College of Cardiology,* vol. 41, pp. 1078-1083, 2003.

[24] S. Rohr, A. G. Kleber, and J. P. Kucera, "Optical recording of impulse progation in designer cultures. Cardiac tissue architecture inducing ultra-slow conduction," *TCM,* vol. 9, pp. 173-179, 1999.

[25] T. J. Ebner and G. Chen, "Use of voltage-sensitive dyes and optical recordings in the central nervous system," *Progress in Neurobiology,* vol. 46, 1995.

[26] A. Matiukas, B. G. Mitrea, A. M. Pertsov, J. P. Wuskell, M. Wei, J. Watras, A. C. Millard, and L. M. Loew, "New near-infrared optical probes of cardiac electrical activity," *Am J Physiol Heart Circ Physiol,* vol. 290, 2006.

[27] K. H. Gilchrist, V. N. Barker, L. E. Fletcher, B. D. DeBusschere, P. Ghanouni, L. Giovangrandi, and G. T. A. Kovacs, "General purpose, field portable cell-based biosensor platform," *Biosens. Bioelectron.,* vol. 16, pp. 557-564, 2001.

[28] R. H. Whittington, L. Giovangrandi, and G. T. A. Kovacs, "A closed-loop electrical stimulation system for cardiac cell cultures," *IEEE Transactions on Biomedical Engineering,* vol. 52, pp. 1261-1270, 2005.

[29] M. Q. Chen, R. H. Whittington, P. W. Day, B. R. Kobilka, L. Giovangrandi, and G. T. A. Kovacs, "A device for separated and reversible co-culture of cardiomyocytes," *Biotechnology Progress,* vol. *In Press*, 2010.

[30] M. G. Chang, L. Tung, R. B. Sekar, C. Y. Chang, J. Cysyk, P. Dong, E. Marban, and R. Abraham, "Proarrhythmic potential of mesenchymal stem cell transplantation revealed in an in vitro coculture model," *Circulation,* vol. 113, pp. 1832-1842, 2006.

[31] S. Rohr, D. Scholly, and A. Kleber, "Patterned growth of neonatal rat heart cells in culture. Morphological and electrophysiological characterization," *Circulation Research,* vol. 68, pp. 114-130, 1991.

[32] G. Gaudesius, M. Miragoli, S. P. Thomas, and S. Rohr, "Coupling of cardiac electrical over extended distances by fibroblasts of cardiac origin," *Circulation Research,* vol. 93, pp. 421-428, 2003.
[33] W. Bian and L. Tung, "Structure-Related Initiation of Reentry by Rapid Pacing in Monolayers of Cardiac Cells," *Circulation Research,* vol. 98, pp. e29-e38, 2006.
[34] Q.-D. Wang and P.-O. Sjoquist, "Myocardial regeneration with stem cells: Pharmacological possibiliites for efficacy enhancement," *Pharmacological Research,* vol. 53, pp. 331-340, 2006.
[35] W.-H. Zimmerman, K. Schneiderbanger, P. Schubert, M. Didie, F. Munzel, J. F. Heubach, S. Kostin, W. L. Neuhuber, and T. Eschenhagen, "Tissue engineering of a differentiated cardiac muscle construct," *Circulation Research,* vol. 90, pp. 223-230, 2002.
[36] W. R. Giles and Y. Imaizumi, "Comparison of potassium currents in rabbit atrial and ventricular cells," *J Physiol,* vol. 405, pp. 123-145, 1988.
[37] M. R. Boyett, H. Honjo, M. Yamamoto, M. R. Mikmaram, R. Niwa, and I. Kodama, "Downward gradient in action potential duration along conduction path in and around the sinoatrial node," *Am J Physiol,* vol. 276, pp. H686-H698, 1999.
[38] S. Abraham, G. N. Beatch, B. A. MacLeod, and M. J. Walker, "Antiarrhythmic properties of tetrodotoxin against occlusion-induced arrhythmias in the rat: a novel approach to the study of the antiarrhythmic effects of ventricular sodium channel blockade," *The Journal of Pharmacology,* vol. 251, pp. 1166-1173, 1989.
[39] B. Hille, *Ion Channels of Excitable Membranes*. Sunderland, MA: Sinauer Associates Inc., 2001.
[40] C. Murry, V. Richard, K. Reimer, and R. Jennings, "Ischemic preconditioning slows energy metabolism and delays ultrastructural damage during a sustained ischemic episode," *Circulation Research,* vol. 66, pp. 913-931, 1990.
[41] A. G. Kleber and Y. Rudy, "Basic machanisms of cardiac impulse propagation and associated arrhythmias," *Physiol Rev,* vol. 84, pp. 431-488, 2004.
[42] A. Marthur and J. Martin, "Stem cells and repair of the heart," *The Lancet,* vol. 364, pp. 183-192, 2004.
[43] M. Soonpaa and L. Field, "Survey of studies examining mammaliam cardiomyocyte DNA synthesis," *Circulation Research,* vol. 83, pp. 15-26, 1998.
[44] A. P. Beltrami, K. Urbanek, J. Kajstura, S.-M. Yan, N. Finato, R. Bussani, B. Nadal-Ginard, F. Silvestri, A. Leri, C. A. Beltrami, and P. Anversa, "Evidence That Human Cardiac Myocytes Divide after Myocardial Infarction," *NEJM,* vol. 344, pp. 1750-1757, 2001.
[45] M. Laflemme, D. Myerson, J. Saffitz, and C. Murry, "Evidence for cardiomyocyte repopulation by extracardiac progenitors in transplated human hearts," *Circulation Research,* vol. 90, pp. 634-640, 2002.
[46] P. Müller, P. Pfeiffer, J. Koglin, H.-J. Schäfers, U. Seeland, I. Janzen, S. Urbschat, and M. Böhm, "Cardiomyocytes of Noncardiac Origin in Myocardial Biopsies of Human Transplanted Hearts," *Circulation,* vol. 106, pp. 31-35, 2002.
[47] B. Douglas, "Conservative management of guillotine amputation of the finger in children," *Aust Paediatr J,* vol. 8, pp. 468-478, 1972.
[48] L. Mullen, S. Bryant, M. Torok, B. Blumberg, and D. Gardiner, "Nerve dependency of regeneration: the role of Distal-less and FGF signaling in amphibiam limb regeneration," *Development,* vol. 122, pp. 3487-3497, 1996.
[49] C. D'Jamoos, G. McMahon, and P. Tsonis, "Fibroblast growth factor receptors regulate the ability for hindlimb regeneration in *Xenopus laevis*," *Would Repair Regen,* vol. 6, pp. 388-397, 1998.

[50] P. Tsonis, "Effects of carcinogens on regenerating and non-regenerating limbs in amphibia " *Anticancer Res,* vol. 3, pp. 195-202, 1983.
[51] J. Yu, M. A. Vodyanik, K. Smuga-Otto, J. Antosiewicz-Bourget, J. L. Frane, S. Tian, J. Nie, G. A. Jonsdottir, V. Ruotti, R. Stewart, I. I. Slukvin, and J. A. Thomson, "Induced pluripotent stem cell lines derived from human somatic cells," *Science,* vol. 318, pp. 1917-20, 2007.
[52] K. Okita, T. Ichisaka, and S. Yamanaka, "Generation of germline-competent induced pluripotent stem cells," *Nature,* vol. 448, pp. 313-317, 2007.
[53] N. Sun, N. J. Panetta, D. M. Gupta, K. D. Wilson, A. Lee, F. Jia, S. Hu, A. M. Cherry, R. C. Robbins, M. T. Longaker, and J. C. Wu, "Feeder-Free Derivation of Induced Pluripotent Stem Cells from Adult Human Adipose Stem Cells," *PNAS in press,* 2009.
[54] D. T. Scadden, "The stem-cell niche as an entity of action," *Nature,* vol. 441, 2006.
[55] C. Verfaillie, "Adult stem cells: assessing the case for pluripotency," *Trends Cell Biol,* vol. 12, pp. 502-508, 2002.
[56] S. Orkin and L. Zon, "Hematopoiesis and stem cels: plasticity versus developmental heterogeneity," *Nat Immunol,* vol. 3, pp. 323-328, 2002.
[57] H. Reinecke, V. Poppa, and C. E. Murry, "Skeletal muscle stem cells do not transdifferentiate into cardiomyocytes after cardiac grafting," *J. Mol. Cell Cardiol.,* vol. 34, pp. 241-249, 2002.
[58] A. J. Wagers and I. L. Weissman, "Plasticity of adult stem cells," *Cell,* vol. 116, pp. 629-648, 2004.
[59] A. Wurmser and F. Gage, "Stem cells: cell fusion causes confusion," *Nature,* vol. 422, pp. 823-825, 2002.
[60] J. Isner, "Myocardial gene therapy," *Nature,* vol. 415, pp. 234-239, 2002.
[61] J. Müller-Ehmsenb, P. Whittaker, R. A. Kloner, J. S. Dow, T. Sakoda, T. I. Long, P. W. Laird, and L. Kedes, "Survival and Development of Neonatal Rat Cardiomyocytes Transplanted into Adult Myocardium " *Journal of Molecular and Cellular Cardiology,* vol. 34, pp. 107-116, 2002.
[62] F. Cao, S. Lin, X. Xie, P. Ray, M. Patel, X. Zhang, M. Drukker, S. Dylla, A. J. Connolly, X. Chen, I. L. Weissman, S. S. Gambhir, and J. C. Wu, "In-vivo visualization of embryonic stem cell survival, proliferation, and migration after cardiac delivery," *Circulation,* vol. 113, pp. 1005-1014, 2006.
[63] K. R. Boheler, J. Czyz, D. Tweedie, H.-T. Yang, S. V. Anisimov, and A. M. Wobus, "Differentiation of pluripotent embryonic stem cells into cardiomyocytes," *Circulation Research,* vol. 91, pp. 189-201, 2002.
[64] P. W. Burridge, D. Anderson, H. Priddle, M. D. B. Muñoz, S. Chamberlain, C. Allegrucci, L. E. Young, and C. Denning, "Improved Human Embryonic Stem Cell Embryoid Body Homogeneity and Cardiomyocyte Differentiation from a Novel V-96 Plate Aggregation System Highlights Interline Variability," *Stem Cells,* vol. 25, pp. 929-938, 2006.
[65] A. M. Wobus, G. Kaomei, J. Shan, M.-C. Wellner, J. Rohwedel, J. Guanju, B. Fleischmann, H. A. Katus, J. Hescheler, and W.-M. Franz, "Retinoic Acid Accelerates Embryonic Stem Cell-Derived Cardiac Differentiation and Enhances Development of Ventricular Cardiomyocytes," *Journal of Molecular and Cellular Cardiology,* vol. 29, pp. 1525-1539, 1997.
[66] C. Mummery, D. Oostwaard, P. Doevendans, R. Spijker, S. v. d. Brink, R. Hassink, M. v. d. Heyden, T. Opthof, M. Pera, A. d. l. Riviere, R. Passier, and L. Tertoolen, "Differentiation of Human Embryonic Stem Cells to Cardiomyocytes: Role of Coculture With Visceral Endoderm Like Cells," *Circulation,* vol. 107, pp. 2733-2740, 2007.

[67] H. Sauer, G. Rahimi, J. Hescheler, and M. Wartenberg, "Effects of electical fields on cardiomyocyte differentiation of embryonic stem cells," *Journal of Cellular Biochemistry*, vol. 75, pp. 710-723, 1999.

[68] R. H. Whittington, "Real-time control of electrical stimulation: A novel tool for compound screening and electrophysiological analysis," in *Electrical Engineering* Stanford: Stanford University, 2006.

[69] G. Ling and R. W. Gerard, "The membrane potential and metabolism of muscle fibers," *Journal of Cellular Physiology*, vol. 34, pp. 413-438, 1949.

[70] G. Ling and R. W. Gerard, "The normal membrane potential of frog sartorious fibers," *Journal of Cellular Physiology*, vol. 34, pp. 383-396, 1949.

[71] A. L. Hodgkin and A. F. Huxley, "A quantitative description of membrane current and its application to conduction and excitation in nerve," *J Physiol*, vol. 117, pp. 500-544, 1952.

[72] E. Neher, J. Sakmann, and H. Steinbach, "The extracellular patch clamp: a method for resolving currents through individual open channels in biological membranes," *Pflugers Arch*, vol. 375, pp. 219-228, 1978.

[73] O. P. Hamill, A. Marty, E. Neher, B. Sakmann, and F. J. Sigworth, "Improved patch-clamp techniques for high-resolution current recording from cells and cell-free membrane patches," *Pflugers Arch*, vol. 391, pp. 85-100, 1981.

[74] C. A. Thomas, P. A. Springer, G. E. Loeb, Y. Berwald-Netter, and L. M. Okun, "A miniature microelectrode array to monitor the bioelectric activity of cultured cells," *Exp Cell Res*, vol. 74, pp. 61-66, 1972.

[75] C. D. James, R. Davis, M. Meyer, A. Turner, S. Turner, G. Withers, L. Kam, G. Banker, H. Craighead, M. Isaacson, J. Turner, and W. Shain, "Aligned Microcontact Printing of Micrometer-Scale Poly-L-Lysine Structures for Controlled Growth of Cultured Neurons on Planar Microelectrode Arrays," *IEEE Trans. Biomed. Eng.*, vol. 47, pp. 17-21, 2000.

[76] B. DeBusschere and G. Kovacs, "Portable cell-based biosensor system using integrated CMOS cell-cartiges," *Biosensors and Bioelectronics*, vol. 16, pp. 543-556, 2001.

[77] K. Gilchirst, L. Giovangrandi, and G. Kovacs, "Sensitivity of cell-based biosensors to environmental variables," *Biosensors and Bioelectronics*, vol. 20, pp. 1397-1406, 2005.

[78] I. Kehat, A. Gepstein, A. Spira, J. Itskovitz-Eldor, and L. Gepstein, "High-resolution electrophysiological assessment of human embryonic stem cell-derived cardiomyocytes," *Circulation Research*, vol. 91, pp. 659-661, 2002.

[79] M. S. Spach, R. C. Barr, G. A. Serwer, J. M. Kootsey, and E. A. Johnson, "Extracellular potentials related to intracellular action potentials in the dog Purkinje system.," *Circulation Research*, vol. 30, pp. 505-519, 1972.

[80] R. Plonsey, "Action potential sources and their volume conductor fields," *Proceedings of the IEEE*, vol. 65, pp. 601-611, 1977.

[81] M. Grattarola and S. Martinoia, "Modeling the neuron-microtransducer junction: from extracellular to patch recording," *IEEE Trans. Biomed. Eng.*, vol. 40, pp. 35-41, 1993.

[82] E. C. Beyer, D. L. Paul, and D. A. Goodenough, "Connexin family gap junction proteins," *J Membr Biol*, vol. 116, pp. 187-194, 1990.

[83] M. A. Allessie, "Reentrant mechanisms underlying atrial fibrillation," in *Cardiac Electrophysiology: From Cell to Bedside*, D. P. Zipes and J. Jalife, Eds. Philadelphia, PA: Saunders, 1995.

[84] P. V. Bayly, B. H. KenKnight, J. M. Rogers, R. E. Hillsley, R. E. Ideker, and W. M. Smith, "Estimation of conduction velocity vector fields from epicardial mapping data," *IEEE Transactions on Biomedical Engineering,* vol. 45, pp. 563-571, 1998.

[85] W. H. Press, B. P. Flannery, S. S. Teukolsky, and W. T. Vetterling, *Numerical Recipes in C*. Cambridge, U.K.: Cambridge University Press, 1986.

[86] E. T. McAdams, A. Lackermeier, J. A. McLaughlin, and D. Macken, "The linear and non-linear electrical properties of the electrode-electrolyte interface," *Biosens. Bioelectron.,* vol. 10, pp. 67-74, 1995.

[87] Y. Sun, K. Bruce-Jacobson, and V. Golovlev, "Label-free detection of biomolecules on microarrays using surface-colloid interaction," *Anal Biochem,* vol. 361, pp. 244-252, 2007.

[88] P. J. Scales, F. Grieser, T. W. Healy, L. R. White, and D. Y. C. Chan, "Electrokinetics of the silica-solution interface: A flat plate streaming potential study," *Langmuir,* vol. 8, pp. 965-974, 1992.

[89] I. Y. Wong, M. J. Footer, and N. A. Melosh, "Dynamic control of biomolecular activity using electrical interfaces," *Soft Matter,* vol. 3, pp. 267-274, 2007.

[90] I. Borukhov, D. Andelman, and H. Orland, "Steric effects in electrolytes: A modifed Poisson-Boltzman equation," *Physical Review Letters,* vol. 79, pp. 435-438, 1997.

[91] J. Newman, "Resistance of flow of current to a disk," *Journal of Electrochemistry,* vol. 113, pp. 501-502, 1966.

[92] D. R. Merrill, M. Bikson, and J. G. Jefferys, "Electrical stimulation of excitable tissue: design of efficacious and safe protocol," *Journal of Neuroscience Methods,* vol. 141, pp. 171-198, 2005.

[93] R. H. Whittington and G. T. A. Kovacs, "A discrete-time control algorithm applied to closed-loop pacing of HL-1 cardiomyocytes," *IEEE Transactions on Biomedical Engineering,* vol. 55, pp. 21-30, 2008.

[94] R. H. Whittington, M. Q. Chen, L. Giovangrandi, and G. T. A. Kovacs, "Temporal resolution of stimulation threshold: A tool for electrophysiologic analysis," in *IEEE EMBC*. vol. 28 New York City: IEEE, 2006.

[95] W. C. Claycomb, J. Nicholas A. Lanson, B. S. Stallworth, D. B. Egeland, J. B. Delcarpio, A. Bahinski, and J. Nickolas J. Izzo, "HL-1 cells: A cardiac muscle cell line that contracts and retains phenotype characterisitcs of the adult cardiomyocyte," *Proc. Natl. Acad. Sci. USA,* vol. 95, pp. 2979-2984, 1998.

[96] D. A. Rubinson, C. P. Dillon, A. V. Kwiatkowski, C. Sievers, L. Yang, J. Kopinja5, D. L. Rooney, M. Zhang, M. M. Ihrig, M. T. McManus, F. B. Gertler, M. L. Scott5, and L. V. Parijs, "A lentivirus-based system to functionally silence genes in primary mammalian cells, stem cells and transgenic mice by RNA interference," *Nature Genetics,* vol. 33, pp. 401-406, 2003.

[97] B. Julesz, "Visual pattern discrimination," *IRE Trans. Inform. Theory,* vol. 8, pp. 84-92, 1962.

[98] R. M. Haralick, "Statistical and structural approaches to texture," *Proceedings of the IEEE,* vol. 67, pp. 786-804, 1979.

[99] S. Goktepe and E. Kuhl, "Computational modeling of cardiac electrophysiology: A novel finite element approach," *Int. J. Numer. Meth. Engng,* vol. 00:1-6, 2000.

[100] M. Lieberman, A. E. Roggeveen, J.E. Purdy, and E. A. Johnson, "Synthetic strands of cardiac muscle: Growth and physiological implication," *Science,* vol. 175, pp. 909-911, 1972.

[101] S. N. Bhatia, U. J. Balis, M. L. Yarmush, and M. Toner, "Microfabrication of Hepatocyte/Fibroblast Co-cultures: Role of Homotypic Cell Interactions," *Biotechnol. Prog.,* vol. 14, pp. 378-387, 1998.

[102] G. Y. Koh, M. G. Klug, M. H. Soonpaa, and L. J. Field, "Differentiation and long-term survival of C2C12 myoblast grafts in heart," *J. Clin. Invest.*, vol. 92, pp. 1548-1554, 1993.

[103] H. Reinecke, G. H. MacDonald, S. D. Hauschka, and C. E. Murry, "Electromechanical coupling between skeletal and cardiac muscle: implications for infarct repair," *Journal of Cell Biology*, vol. 149, pp. 731-740, 2000.

[104] H. Reinecke, E. Minami, V. Poppa, and C. E. Murry, "Evidence for fusion between cardiac and skeletal muscle cells," *Circulation Research*, vol. 94, pp. e56-e60, 2004.

[105] E. Devic, Y. Xiang, D. Gould, and B. Kobilka, "Beta -Adrenergic Receptor Subtype-Specific Signaling in Cardiac Myocytes from beta 1 and beta 2 Adrenoceptor Knockout Mice," *Molecular Pharmacology*, vol. 60, pp. 577-583, 2001.

[106] V. A. Maltsev, A. M. Wobus, J. Rohwedel, M. Bader, and J. Hescheler, "Cardiomyocytes differentiated in vitro from embryonic stem cells developmentally express cardiac-specific genes and ionic currents," *Circulation Research*, vol. 75, pp. 233-244, 1994.

[107] M. Yamada, K. Tanemura, S. Okada, A. Iwanami, M. Nakamura, H. Mizuno, M. Ozawa, R. Ohyama-Goto, N. Kitamura, M. Kawano, K. Tan-Takeuchi, C. Ohtsuka, A. Miyawaki, A. Takashima, M. Ogawa, Y. Toyama, H. Okano, and T. Kondo, "Electrical Stimulation Modulates Fate Determination of Differentiating Embryonic Stem Cells," *Stem Cells*, vol. 25, pp. 562-570, 2007.

[108] J. He, Y. Ma, Y. Lee, J. Thompson, and T. Kamp, "Human embryonic stem cells develop into multiple types of cardiac myocytes: action potential characterization," *Circulation Research*, vol. 93, pp. 32-39, 2003.

[109] I. Kehat, D. Kenyagin-Karsenti, M. Snir, M. Segev, M. Amit, A. Gepstein, E. Livne, O. Binah, J. Itskovitz-Eldor, and L. Gepstein, "Human embryonic stem cells can differentiate into myocytes with structural and functional properties of cardiomyocytes," *Journal of Clinical Investigation*, vol. 108, pp. 407-414, 2001.

[110] T. Xue, H. C. Cho, F. G. Akar, S.-Y. Tsang, S. P. Jones, E. Marban, G. F. Tomaselli, and R. A. Li, "Functional integration of electrically active cardiac derivatives from genetrically engeineered human embryonic stem cells with quiescent recipient ventricular cardiomyocytes. Insights into the development of cell-based pacemakers," *Circulation*, vol. 111, pp. 11-20, 2005.

[111] I. Kehat, L. Khimovich, O. Caspi, A. Gepstein, R. Shofti, G. Arbel, I. Huber, J. Satin, J. Itskovitz-Eldor, and L. Gepstein, "Electromechanical integration of cardiomyocytes derived from human embryonic stem cells," *Nature Biotechnology*, vol. 22, pp. 1282-1289, 2004.

[112] M. Rubart, K. B. S. Pasumarthi, H. Nakajima, M. H. Soonpaa, H. O. Nakajima, and L. J. Field, "Physiological coupling of donor and host cardiomyocytes after cellular transplantation," *Circulation Research*, vol. 92, pp. 1217-1224, 2007.

[113] Z. Li, Y. Suzuki, M. Huang, F. Cao, X. Xie, A. J. Connolly, P. C. Yang, and J. C. Wu, "Comparison of reporter gene and iron particle labeling for tracking fate of human embryonic stem cells and differentiated endothelial cells in living subjects," *Stem Cells*, vol. 26, pp. 864-873, 2008.

[114] R. Swijnenburg, S. Schrepfer, J. A. Govaert, F. Cao, K. Ransohoff, A. Y. Sheikh, M. Haddad, A. J. Connolly, M. M. Davis, R. C. Robbns, and J. C. Wu, "Immunosuppressive therapy mitigates immunological rejection of human embryonic stem cell xenografts," *PNAS*, vol. 105, pp. 12991-12996, 2008.

[115] H. Gelband, H. L. Bush, M. R. Rosen, R. J. Myerburg, and B. F. Hoffman, "Electrophysiologic properties of isolated preparations of human atrial myocardium," *Circulation Research*, vol. 30, pp. 292-300, 1972.

[116] M. K. Walton and H. A. Fozzard, "The conducted action potential. Models and comparison to experiments," *Biophysical Journal,* vol. 44, pp. 9-26, 1983.
[117] J. P. Fahrenbach, R. Majia-Alzarez, and K. Banach, "The relevance of non-excitable cells for cardiac pacemaker," *J.Physiol,* vol. 585, pp. 565-578, 2007.
[118] F. Cao, R. A. Wagner, K. D. Wilson, X. Xie, J.-D. Fu, M. Drukker, A. Lee, R. A. Li, S. S. Sambhir, I. L. Weissman, R. C. Robbins, and J. C. Wu, "Transcriptional and Functional Profiling of Human Embryonic Stem Cell-Derived Cardiomyocytes," *Plos One,* vol. 3, p. e3474, 2008.
[119] M. Radisic, H. Park, H. Shing, T. Consi, F. J. Schoen, R. Langer, L. E. Freed, and G. Vunjak-Novakovic, "Functional assembly of engineered myocardium by electrical stimulation of cardiac myocytes cultured on scaffolds," *PNAS,* vol. 101, pp. 18129-18134, 2004.
[120] T. L. Rose and L. S. Roblee, "Electrical stimulation with Pt electrodes. VII. Electrochemically safe charge injection limits with 0.2 ms pulses," *IEEE Transactions on Biomedical Engineering,* vol. 37, pp. 1118-1120, 1990.
[121] M. Q. Chen, X. Xie, K. D. Wilson, N. Sun, J. C. Wu, L. Giovangrandi, and G. T. A. Kovacs, "Current-Controlled Electrical Point-Source Stimulation of Embryonic Stem Cells," *Cellular and Molecular Bioengineering,* vol. 2, pp. 625-635, 2009.
[122] G. E. Loeb, C. J. Zamin, J. H. Schulman, and P. R. Troyk, "Injectable microstimulator for functional electrical stimulation " *Medical and Biological Engineering and Computing,* vol. 29, pp. NS13-NS19, 1991.
[123] N. d. N. Donaldson and P. E. K. Donaldson, "When are actively balanced biphasic ('Lilly') stimulating pulses necessary in a neurological prosthesis? I Historical background; Pt resting potential;Q studies " *Medical and Biological Engineering and Computing,* vol. 24, pp. 41-49, 1986.
[124] M. Q. Chen, X. Xie, R. H. Whittington, G. T. A. Kovacs, J. C. Wu, and L. Giovangrandi, "Cardiac Differentiation of Embryonic Stem Cells with Point-Source Electrical Stimulation," in *IEEE EMBC* Vancouver: IEEE, 2008.
[125] L. J. Leon and F. A. Roberge, "A model study of extracellular stimulation of cardiac cells," *IEEE Transactions on Biomedical Engineering,* vol. 40, pp. 1307-1319, 1993.
[126] A. Beqqali, J. Kloots, D. W.-w. Oostwaard, C. Mummery, and R. Passier, "Genome-wide transcriptional profiling of human embryonic stem cells differentiating to cardiomyocytes," *Stem Cells,* vol. 24, pp. 1957-1967, 2006.
[127] Y.-H. Loh, Q. Wu, J.-L. Chew, V. B. Vega, W. Zhang, X. Chen, G. Bourque, J. George, B. Leong, J. Liu, K.-Y. Wong, K. W. Sung, C. W. H. Lee, X.-D. Zhao, K.-P. Chiu, L. Lipovich, V. A. Kuznetsov, P. Robson, L. W. Stanton, C.-L. Wei, Y. Ruan, B. Lim, and H.-H. Ng, "The Oct4 and Nanog transcription network regulates pluripotency in mouse embryonic stem cells," *Nature genetics,* vol. 38, pp. 431-40, 2006.
[128] L. A. Hanna, R. K. Foreman, I. A. Tarasenko, D. S. Kessler, and P. A. Labosky, "Requirement for Foxd3 in maintaining pluripotent cells of the early mouse embryo," *Genes & development,* vol. 16, pp. 2650-61, 2002.
[129] D. H. Yang and E. G. Moss, "Temporally regulated expression of Lin-28 in diverse tissues of the developing mouse," *Gene expression patterns,* vol. 3, pp. 719-26, 2003.
[130] K.-L. Laugwitz, A. Moretti, L. Caron, A. Nakano, and K. R. Chien, "Islet1 cardiovascular progenitors: a single source for heart lineages?," *Development,* vol. 135, pp. 193-205, 2008.
[131] C.-L. Cai, X. Liang, Y. Shi, P.-H. Chu, S. L. Pfaff, J. Chen, and S. Evans, "Isl1 identifies a cardiac progenitor population that proliferates prior to differentiation and

contributes a majority of cells to the heart," *Developmental cell,* vol. 5, pp. 877-89, 2003.

[132] O. Karlsson, S. Thor, T. Norberg, H. Ohlsson, and T. Edlund, "Insulin gene enhancer binding protein Isl-1 is a member of a novel class of proteins containing both a homeo- and a Cys-His domain," *Nature,* vol. 344, pp. 879-82, 1990.

[133] E. N. Olson, "Gene regulatory networks in the evolution and development of the heart," *Science,* vol. 313, pp. 1922-7, 2006.

[134] L. Yang, M. H. Soonpaa, E. D. Adler, T. K. Roepke, S. J. Kattman, M. Kennedy, E. Henckaerts, K. Bonham, G. W. Abbott, R. M. Linden, L. J. Field, and G. M. Keller, "Human cardiovascular progenitor cells develop from a KDR+ embryonic-stem-cell-derived population," *Nature,* vol. 453, pp. 524-8, 2008.

[135] T. Toyofuku, H. Zhang, A. Kumanogoh, N. Takegahara, M. Yabuki, K. Harada, M. Hori, and H. Kikutani, "Guidance of myocardial patterning in cardiac development by Sema6D reverse signalling," *Nature cell biology,* vol. 6, pp. 1204-11, 2004.

[136] Y. Yoshida, B. Han, M. Mendelsohn, and T. M. Jessell, "PlexinA1 signaling directs the segregation of proprioceptive sensory axons in the developing spinal cord," *Neuron,* vol. 52, pp. 775-88, 2006.

[137] M. Eiraku, A. Tohgo, K. Ono, M. Kaneko, K. Fujishima, T. Hirano, and M. Kengaku, "DNER acts as a neuron-specific Notch ligand during Bergmann glial development," *Nature neuroscience,* vol. 8, pp. 873-80, 2005.

[138] J. Honold, D. Assmus, R. Lehman, A. M. Zeiher, and S. Dimmeler, "Stem cell therapy of cardiac disease: an update," *Nephrol Dial Transplant,* vol. 19, pp. 1673-1677, 2004.

[139] S. Roy, M. Q. Chen, G. T. Kovacs, and L. Giovangrandi, "Conduction analysis in mixed cardiomyocytes-fibroblasts cultures using microelectrode arrays.," in *IEEE EMBC*. vol. 31 Minneapolis, MN, USA, 2009.

[140] M. Q. Chen, J. Yu, R. H. Whittington, J. C. Wu, G. T. A. Kovacs, and L. Giovangrandi, "Modeling conduction in host-graft interactions between stem cell grafts and cardiomyocytes," in *IEEE EMBC* Minneapolis, MN, USA, 2009.

[141] T. Asahara, T. Murohara, A. Sullivan, M. Silver, R. v. d. Zee, T. Li, B. Witzenbichler, G. Schatteman, and J. M. Isner, "Isolation of putative progenitor endothelial cells for angiogenesis," *Science,* vol. 275, pp. 964-966, 1997.

[142] Q. Shi, S. Rafii, M. H. Wu, E. S. Wijelath, C. Yu, A. Ishida, Y. Fujita, S. Kothari, R. Mohle, L. R. Sauvage, M. A. S. Moore, R. F. Storb, and W. P. Hammond, "Evidence for Circulating Bone Marrow-Derived Endothelial Cells " *Blood,* vol. 92, pp. 362-367, 1998.

# Appendix: Cell Culture Protocols

## Cultivation of Cell Lines: HL-1 Cardiomyocytes, 3T3 Murine Fibroblasts, C2C12 Murine Skeletal Myoblasts, and IMR90 Human Fibroblasts

Murine HL-1 cardiomyocytes were cultured in Claycomb media (Sigma-Aldrich) supplemented with 10% fetal bovine serum (Hyclone), 100 mM norepinephrine (Sigma-Aldrich), 100 units/ml penicillin-streptomycin (Invitrogen), and 4 mM L-glutamine (Invitrogen). Cells were cultured to confluency before passaging every three to four days.

Murine 3T3 fibroblasts, murine C2C12 skeletal myoblasts, and human IMR90 fibroblasts were all cultured under the same conditions. Culture medium consisted of a solution containing 89% DMEM (Invitrogen), 10% FBS (Hyclone), and 1% penicillin–streptomycin (Invitrogen).

## Murine Ventricular Cardiac Myocytes

Ventricular cardiac myocytes were isolated from 1 to 2 day old neonatal WT or DKO mice as described previously [1,2]. Hearts were excised, atria were removed, and the remaining ventricles were minced and digested with collagenase type 2 (500 units/ml; Worthington Biochemical Corporation, Lakewood, NJ) in calcium and bicarbonate free Hanks solution with HEPES at 37˚C with rocking. After 35 minutes, the tissue/enzyme solution was triturated to break up any remaining tissue and cells were filtered through a 40 µM cell strainer (BD Biosciences, San Jose, CA). Cells were pre-plated to remove fibroblasts and re-suspended in Dulbecco's Modified Eagle's Medium (DMEM; Invitrogen, Carlsbad, CA), 10% Nu Serum IV (BD Biosciences, San Jose, CA), 5% certified fetal bovine serum (FBS; Hyclone, Logan, UT), 1 mM glutamine (Invitrogen), and 1x ITS media supplement (Sigma-Aldrich, St. Louis, MO). Cardiomyocytes were plated onto laminin-coated (10 µg/µl; Invitrogen) dishes or MEAs.

## Murine Embryonic Stem cells

Murine ES-D3 cell line (CRL-1934) was obtained from the American Type Culture Collection (ATCC; Manassas, VA). The ES cells were cultured to keep them in an undifferentiated, pluripotent state using 1000 IU leukemia inhibitory factor (LIF; Millipore, Billerica, MA), and grown over a layer of murine embryonic fibroblast feeder cells. The fibroblasts were inactivated using 10 μg/mL mitomycin C (Sigma-Aldrich, St. Louis, MO). The surfaces of the culture dishes were coated with 0.1% gelatin. Cells were cultured in ES medium containing Dulbecco's Modified Eagle Medium supplemented with 15% fetal calf serum, 0.1 mmol/L β- mercaptoethanol, 2 mmol/L glutamine, and 0.1 mmol/L nonessential amino acids as described previously[3]. The culture medium for the ES cells was changed on a daily basis, and cultures were passaged every one to two days. To develop the ES cells into embryoid bodies, the "hanging drop" method was used as described previously.[4] LIF was withdrawn from the medium, and a cultivation of about 400 cells was suspended in 18 μL hanging drops to form an aggregate of cells termed embryoid bodies (EB). At this point, the differentiation stage of the EB was noted as Day 0. After two days, each EB was transferred into its own well in an ultra-low attachment 96-well plate (Corning Life Sciences, Lowell, MA) for two days, after which they were further seeded onto 48-well plates. At the desired differentiation stage, whole EBs were dissociated with collagenase B (Worthington, Lakewood, NJ) and cells were plated onto an MEA surface.

## Human Embryonic Stem cells

The hESCs used for the graft model are from the H9 lineage (WiCell Research Institute, Madison,WI) and underwent the differentiating process using Iscove's modified Dulbecco's medium and 20% defined fetal bovine serum (FBS; HyClone), 0.1 mM nonessential amino acids, 2 mM L-glutamine, 450 M monothioglycerol (Sigma-Aldrich), 50 U/ml penicillin, and 50 g/ml streptomycin, in ultralow-attachment

plates for the formation of suspended embryoid bodies (EB) for six days as previously described [5]. At Day 7, floating EBs were gathered and seeded to 0.1% gelating coated 10cm Petri dishes for further differentiation. At Day 14, EBs were dissociated in collagenase IV (Sigma-Aldrich).

To isolate hESC-derived cardiomyocytes, Percoll purification was performed as previously described [6]. Differentiated hESC cultures were washed with phosphate buffered saline (PBS) and incubated with 0.56 units/ml Liberase Blendzyme IV (Roche, Indianapolis, IN) at 37°C for 25 min. After dissociation, the cell suspension was separated by Percoll density centrifugation (58.5% and 40.5%) at 1500 g for 30 minutes at room temperature.

# References


[1] E. Devic, Y. Xiang, D. Gould, and B. Kobilka, "beta -Adrenergic receptor subtype-specific signaling in cardiac myocytes from beta 1 and beta 2 adrenoceptor knockout mice," *Molecular Pharmacology*, vol. 60, pp. 577-583, 2001.

[2] E. Devic, Y. Xiang, D. Gould, and B. Kobilka, "Beta-adrenergic receptor subtype-specific signaling in cardiac myocytes from beta(1) and beta(2) adrenoceptor knockout mice," *Mol Pharmacol*, vol. 60, pp. 577-83, Sep 2001.

[3] K. R. Boheler, J. Czyz, D. Tweedie, H.-T. Yang, S. V. Anisimov, and A. M. Wobus, "Differentiation of pluripotent embryonic stem cells into cardiomyocytes," *Circulation Research*, vol. 91, pp. 189-201, 2002.

[4] V. A. Maltsev, A. M. Wobus, J. Rohwedel, M. Bader, and J. Hescheler, "Cardiomyocytes differentiated in vitro from embryonic stem cells developmentally express cardiac-specific genes and ionic currents," *Circulation Research*, vol. 75, pp. 233-244, 1994.

[5] T. Chen, H. Bai, Y. Shao, M. Arzigian, V. Janzen, E. Attar, Y. Xie, D. T. Scadden, and Z. Z. Wang, "Stromal Cell-Derived Factor-1/CXCR4 Signaling Modifies the Capillary-Like Organization of Human Embryonic Stem Cell-Derived Endothelium In Vitro," *Stem Cells*, vol. 25, pp. 392-401, 2007.

[6] F. Cao, R. A. Wagner, K. D. Wilson, X. Xie, J.-D. Fu, M. Drukker, A. Lee, R. A. Li, S. S. Sambhir, I. L. Weissman, R. C. Robbins, and J. C. Wu, "Transcriptional and Functional Profiling of Human Embryonic Stem Cell-Derived Cardiomyocytes," *Plos One*, vol. 3, p. e3474, 2008.